

Acquisitions and Bibliographic Services Branch

395 Wellington Street Ottawa, Ontario K1A 0N4 Bibliothèque nationale du Canada

Direction des acquisitions et des services bibliographiques

395, rue Wellington Ottawa (Ontario) K1A 0N4

Your life. Votre relevence

Our No Notre reference

NOTICE

The quality of this microform is heavily dependent upon the quality of the original thesis submitted for microfilming. Every effort has been made to ensure the highest quality of reproduction possible.

La qualité de cette microforme dépend grandement de la qualité de la thèse soumise au microfilmage. Nous avons tout fait pour assurer une qualité supérieure de reproduction.

AVIS

If pages are missing, contact the university which granted the degree.

S'il manque des pages, veuillez communiquer avec l'université qui a conféré le grade.

Some pages may have indistinct print especially if the original pages were typed with a poor typewriter ribbon or if the university sent us an inferior photocopy. La qualité d'impression de certaines pages peut laisser à désirer, surtout si les pages originales ont été dactylographiées à l'aide d'un ruban usé ou si l'université nous a fait parvenir une photocopie de qualité inférieure.

Reproduction in full or in part of this microform is governed by the Canadian Copyright Act, R.S.C. 1970, c. C-30, and subsequent amendments.

La reproduction, même partielle, de cette microforme est soumise à la Loi canadienne sur le droit d'auteur, SRC 1970, c. C-30, et ses amendements subséquents.



AN ANALYTICAL STUDY OF THE LOAD FLOW PROBLEM

by

MARGARET TOUSSAINT

B.Sc (Eng), University of the West Indies, Trinidad

Department of Electrical Engineering McGill University, Montreal September, 1994

A Thesis submitted to the Faculty of Graduate Studies and Research in partial fulfilment of the requirements of the degree of Master of Engineering

© Margaret Toussaint 1994



Acquisitions and Bibliographic Services Branch

395 Wellington Street Ottawa, Ontario K1A 0N4 Bibliothèque nationale du Canada

Direction des acquisitions et des services bibliographiques

395, rue Wellington Ottawa (Ontario) K1A 0N4

Your file Votte relétence

Our file Notre référence

THE AUTHOR HAS GRANTED AN IRREVOCABLE NON-EXCLUSIVE LICENCE ALLOWING THE NATIONAL LIBRARY OF CANADA TO REPRODUCE, LOAN, DISTRIBUTE OR SELL COPIES OF HIS/HER THESIS BY ANY MEANS AND IN ANY FORM OR FORMAT, MAKING THIS THESIS AVAILABLE TO INTERESTED PERSONS.

L'AUTEUR A ACCORDE UNE LICENCE IRREVOCABLE ET NON EXCLUSIVE PERMETTANT A LA BIBLIOTHEQUE NATIONALE DU CANADA DE REPRODUIRE, PRETER, DISTRIBUER OU VENDRE DES COPIES DE SA THESE DE QUELQUE MANIERE ET SOUS QUELQUE FORME QUE CE SOIT POUR METTRE DES EXEMPLAIRES DE CETTE THESE A LA DISPOSITION DES PERSONNE INTERESSEES.

THE AUTHOR RETAINS OWNERSHIP OF THE COPYRIGHT IN HIS/HER THESIS. NEITHER THE THESIS NOR SUBSTANTIAL EXTRACTS FROM IT MAY BE PRINTED OR OTHERWISE REPRODUCED WITHOUT HIS/HER PERMISSION.

L'AUTEUR CONSERVE LA PROPRIETE DU DROIT D'AUTEUR QUI PROTEGE SA THESE. NI LA THESE NI DES EXTRAITS SUBSTANTIELS DE CELLE-CI NE DOIVENT ETRE IMPRIMES OU AUTREMENT REPRODUITS SANS SON AUTORISATION.

ISBN 0-612-05480-2



ABSTRACT

Some analytical properties of the load flow problem are examined in this work. In order to facilitate this, the load flow equations are expressed in rectangular co-ordinates.

Each load flow equation is formulated as a fully quadratic form and the nature of these quadratic forms is studied in detail. The eigenvalues and eigenvectors of the matrix in each equation are derived and their significance to the nature and existence of load flow solutions is discussed.

An experimental study is also done on the load flow feasibility region which is defined, in the space of net real and reactive powers as well as the voltage magnitudes squared, for a general power network. The network is assumed to consist of a slack bus, voltage control buses and load buses. This region is characterised by all injections for which there is a real voltage solution to the load flow equations. The geometric nature of the region and its relationship to the number of load flow solutions are examined.

RESUMÉ

Cette thèse se concentre sur certaines propriétés analytiques du problème d'écoulement de puissance. Afin de faciliter l'analyse, les équations d'écoulement de puissance sont exprimées en coordonnées rectangulaires.

Chaque équation d'écoulement de puissance est formulée de façon quadratique complète et la nature de ces équations quadratiques est étudiée en détail. Les valeurs et vecteurs propres de la matrice de chaque équation sont dérivés et leur signification quant à la nature et l'existence de solutions au problème d'écoulement de puissance est abordé.

Une étude expérimentale est également effectuée sur la région de faisabilité du problème d'écoulement de puissance qui est définie, dans l'espace des puissances réelles et réactives ainsi que du carré des grandeurs de tension, pour un réseau de puissance quelconque. Il est entendu que le réseau est constitué d'une barre d'oscillation, de barres à tension contrôlée et de barres à charge. Cette région est caractérisée par toutes injections pour lesquelles il y a une solution réelle de tension aux équations d'écoulement de puissance. La nature géométrique de la région et sa relation avec le nombre de solutions du problème d'écoulement de puissance sont analysés.

ACKNOWLEDGEMENTS

I wish to express my sincere gratitude to Prof. F.D. Galiana for his guidance and advice during the course of this work. His enthusiasm and constant encouragement as well as his kind and friendly disposition were sources of motivation.

I would also like to thank - Mr. D. McGillis, for his general interest; my colleagues in the Power Group, for their friendship and good-natured company; Mrs. P. Hyland and Mrs. R. Russo, for being always willing to help; Ms. Julie Griffin and Mr. Djordje Atanackovic, for kindly translating the abstract; some of the students from the Caribbean, for being a good support group and everyone else who may have contributed to the successful completion of this thesis.

I am also grateful to my parents and my brother and sister for always being there for me and in particular to my brother, who strongly encouraged me to undertake Graduate Studies. Their support helped to make it possible.

Finally, I wish to express my appreciation for the financial support of the Canadian Commonwealth Fellowship and Scholarship Plan.

TABLE OF CONTENTS

		ABSTRACT	i
		RESUME	ii
		ACKNOWLEDGEMENTS	iii
		TABLE OF CONTENTS	iv
		LIST OF SYMBOLS	viii
		LIST OF TABLES	x
		LIST OF FIGURES	xii
CHAPTER	I	INTRODUCTION	1
	1.1	General	
	1.2	Background and Motivation	1
	1.3	Definition of the Load Flow Problem	2
		1.3.1 General	2
		1.3.2 Load Flow Equations	
		1.3.3 Classification of Variables	4
	1.4	Scope of Work	5
	1.5	Outline of Thesis	5
CHAPTER	II	REVIEW OF LITERATURE	7
	2.1	Introductory Remarks	7
	2.2	Multiple Load Flow Solutions	8
		2.2.1 General	
		2.2.2 Methods for Finding Multiple Load Flow	
		Solutions	8
		2.2.3 Analytical Approaches to the Multiplicity	
		of Load Flow Solutions	11

		2.2.4 Number of Solutions	13
	2.3	Voltage Stability and Flow Solutions	14
	2.4	Existence of Load Flow Solutions	15
CHAPTER	III	ANALYTICAL PROPERTIES OF THE	
		LOAD FLOW EQUATIONS	T
	2.1	Dealissinson, Demosts	1-
	3.1	Preliminary Remarks	
	3.2	Power System Model	1
	3.3	Formulation of the Load Flow Equations in	10
		Rectangular Co-ordinates	10 10
		3.3.1 2N Equations	10
	3.4	3.3.2 2N-1 Equations	23
	3.4	Eigenvalues and Eigenvectors of the J _i Matrices	23
		F1	مير
		3.4.1.2 J_{Qi} 3.4.1.3 J_{Vi}^2	2420
			20
		3.4.2 The (2N-1) Matrix	2: 20
			23
		QI VIZ	34
			22
	3.5	the (2N-1) x (2N-1) matrices	53
	3.3	Nature of the Quadratic Surfaces Defined by the J _i Matrices	22
	26		3
	3.6	Load Flow Solutions and Intersection	24
	3.7	of Quadratic Surfaces	:د دد
	3.7 3.8	Load Flow Convergence and Quadratic Surfaces	، د
		Bounds on the Real and Reactive Powers	ەد
	3.9	Illustrative 2-Bus Network	3
	3.10	Additional Properties of the Load Flow	40
		Equations	42
CHAPTER	IV	EXPERIMENTAL STUDIES ON THE	
		LOAD FLOW FEASIBILITY REGION	4
	4.1	Introductory Remarks	4
	4.2	Definition and Properties of R,	45
		4.2.1 Definition of R ₂	4
		4.2.2 General Properties of R	40

	4.3	Feasibility Surface P_{z0}	.4/
		4.3.1 Definition	.47
		4.3.2 Finding z ₀	.48
	4.4	Illustrative Example	
	4.5	Supporting Hyperplanes of R,	
	4.6	Security Considerations Involving R _z	53
		4.6.1 Security Region	
		4.6.2 Effect of Contingencies on R,	54
		4.6.3 Example	
	4.7	Structure of the Voltage Space	
		4.7.1 Solution of the Generalised	
		Eigenvalue Problem	56
		4.7.2 Singular Surfaces in the Voltage Space	
		4.7.3 Experimental Results	
		4.7.3.1 Magnitude of the Eigenvalues	
		4.7.3.2 Nullity of the Jacobian	
		4.7.3.3 Observations on the Right and	
		Left Eigenvectors	60
	4.8	Singular Surfaces in R _z	60
		4.8.1 Boundary of R	
		4.8.2 Experimental Results	
		4.8.3 Interior Surfaces of R ₂	63
		4.8.4 Experimental Results	
		4.8.4.1 5-Bus Network	
		4.8.4.2 2 and 3-Bus Examples	
		4.8.5 Classification of Singular Points in R ₂	
	4.9	Convexity of R _z	
	4.10	Multiple Load Flow Solutions and Singular	,
		Surfaces of R _z	72
		4.10.1 Nature of Multiple Solutions	72
		4.10.2 Numerical Results	
		4.10.3 Number of Solutions	
		4.10.3.1 Position of Injection in R ₂	
		4.10.3.2 Example	
		4.10.3.3 Structure of R ₂	o. หว
		7.10.3.3 Structure of Tympanianianianianianianianianianianianiania	00
CHAPTER	V	CONCLUSIONS AND RECOMMENDATIONS FOR	
		FURTHER RESEARCH	84
	5.1	Conclusions	86
	5.2	Recommendations for Further Research	

Table	of	Contents

SELECTED BIBLIOGRAPHY	87
APPENDIX A	96
APPENDIX B	100
APPENDIX C	109

LIST OF SYMBOLS

N	Number of buses in the system
Y	Complex N x N bus admittance matrix
G	Real part of Y
g	ith column of G
В	Imaginary part of Y
b	ith column of B
V	N x 1 vector of complex voltages
е	N x 1 vector of the real part of V
f	N x 1 vector of the imaginary part of V
x_r	2N x 1 vector of the real and imaginary parts of V
x	(2N-1) x 1 vector of the real and imaginary parts of V
I	N x 1 vector of complex currents
0	N x N null matrix
S	N x 1 vector of complex bus powers
P	Vector of net real power injections
Q	Vector of net reactive power injections
V^2	Vector of voltage magnitude squared at PV buses
$\mathbf{z_i}$	Any specified injection at bus i
J_i	Real symmetric matrix describing the network structure
S	Reference bus number
β	N x 1 vector of zeroes except for a "1" at position s
$\lambda_{\mathrm{p1}},~\lambda_{\mathrm{p2}}$	Eigenvalues of 2N x 2N J _{Pi} matrix
λ_{pa1} , λ_{pa2}	Eigenvalues of (2N-1) x (2N-1) J _{Pi} matrix

 λ_{q1} , λ_{q2} Eigenvalues of 2N x 2N J_{Qi} matrix

 λ_{qa1} , λ_{qa2} Eigenvalues of (2N-1) x (2N-1) J_{Qi} matrix

v Eigenvector

 α N x 1 vector with one non-zero element (1) in the ith position

γ N x 1 arbitrary vector

 α_s 2N x 1 vector containing two non-zero elements (tan δ_s and -1) at the

sth and (N+s)th positions

m 2N x 1 vector of zeroes except for a "1" at position (N+s)

 δ_s Reference angle

z = F(x) Load flow equations

L(x) One half the load flow jacobian

J(a) $\Sigma a_i J_i$ i = 1, 2, ... 2N-1

 λ_{max} Maximum eigenvalue λ_{min} Minimum eigenvalue

 R_z Load flow feasibility region ϵR^{2N-1}

 z_0 (2N-1) x 1 vector such that $J(z_0)$ is positive definite

 P_{z0} Intersection of R_z and the plane $z_0^T z = k$

z₁ Arbitrary search direction in the injection space

a (2N-1) x 1 vector

x_s Point in the voltage space where jacobian is singular

r Right eigenvector of singular load flow jacobian

l Left eigenvector of singular load flow jacobian

 z_s Injection defined by x_s

z_b Injection on the boundary of R_z

z_r Injection defined by r

 a_{\max} $\lambda_{\max} z_0 - z_1$

 a_{min} $z_1 - \lambda_{min} z_0$

x* Any solution of the load flow equations

X Transmission line reactance

LIST OF TABLES

3.1	Eigenvalues of J _{Pi} and J _{Qi} for an 8-Bus System	34
3.2	Eigenvalues and Eigenvectors of J _{P2}	39
3.3	Eigenvalues and Eigenvectors of J _{Q2}	10
3.4	Load Flow Solutions for 2-Bus System	10
4.1	Eigenvalues and Eigenvectors of A	50
4.2	Various Search Directions, z ₁	55
4.3	Eigenvalues, Singular Points	
	Right and Left Eigenvectors of L(x _s)	59
4.4	Angle Between Boundary Injection, z _{min} of R _z	
	5-Bus Network	62
4.5	Eigenvalues, Eigenvectors and Boundary Injections	
	of 2-Bus Network	63
4.6a	Angle Between Boundary Injection, z _{min} and	
	Injections on Other Singular Surfaces of R _z	65
4.6b	Angle Between Boundary Injection, z _{max} and	
	Injections on Other Singular Surfaces of R _z	65
4.7a	Angle Between the Vector, amin and Other Vectors	
	Perpendicular to Hyperplanes which are Tangent to	
	the Singular Surfaces of R _z	66
4.7b	Angle Between the Vector, a _{max} and Other Vectors	
	Perpendicular to Hyperplanes which are Tangent to	
	the Singular Surfaces of R _z	66
4.8	Summary of the Eigenvalue Analysis of a 3-Bus System	70
4.9	Injections on the Singular Surfaces of R _z	.76

4.10	The Ten Solutions of a 5-Bus System	77	
4.11	Real Part of the Eigenvalues and Determinant of the		
	Jacobian Matrices Formed from the Sum of	Two Load Flow	
	Solutions	79	
4.12	Specified Injection as the Sum of two		
	Injections on the Singular Surfaces of R.	80	

LIST OF FIGURES

3.1	8-Bus Network
3.2	Intersection of 2-Dimensional Quadratic Forms
3.3	2-Bus Network
3.4	Surface Representing P_2 : $XP_2 = e_1 f_2$
3.5a	Surface Representing Q_2 : $XQ_2 = e_2^2 + f_2^2 - e_1e_2$ ($e_2 = F(e_2, f_2)$
3.5b	Surface Representing Q_2 : $XQ_2 = e_2^2 + f_2^2 - e_1e_2$ ($f_1 = F(e_1, e_2)$
3.6	Projection of Surfaces in Co-ordinate Planes
3.7	Intersection of Surfaces - Two Solutions
3.8	Intersection of Surfaces - One Solution
3.9a	Points of Maximum Power Transfer - Voltage Space
3.9b	Points of Maximum Power Transfer - Injection Space
4.1	Arbitrary R _z
4.2	Supporting Hyperplanes of R _z
4.3a	2-Bus Network
4.3b	Feasibility Network of 2-Bus Network
4.4a	Feasibility Region with z ₀
4.4b	Feasibility Surface in the Plane $z_0 = 1$
4.5	Intersection of P_{z0} and the Plane $z_1^T z = c$
4.6	5-Bus Network54
4.7	Angle Between Supporting Hyperplanes of R _z -
	Base Case and Single Line Outage55
4.8	Boundary Injections of R _z and Vectors Perpendicular to them61
4.9	Angle Between The Hyperplanes Tangent
	to the Singular Surfaces of R _z
4.10a	3-Bus AC Network
4.10b	Feasibility Region of 3-Bus AC Network
4.11	3-Bus Resistive Network

List of Figures

4.12	Surfaces of the Feasibility Region of a 3-Bus Resistive Network	
4.13	Complete Feasibility Region of a 3-Bus Resistive Network	
4.14	Feasibility Surface Pzo of a 3-Bus Resistive Network	
4.15	Projection of Feasibility Region in the V ₂ ² -V ₃ ² Plane	
4.16	Illustration of Convexity Argument	71
4.17	Relationship Between Multiple Load Flow Solutions	73
4.18	5-Bus Network	76
4.19	Feasibility Surface Showing Pairs, z_h and z_r	82

CHAPTER I

INTRODUCTION

1.1 General

A modern power system is a very complex electrical network which usually includes generation sites, transmission lines, substations, interconnections, distribution networks and a variety of loads. Its function is to convert non-electrical energy into electrical energy and make this electrical energy available to consumers. The increasing size and complexity of these systems have made their operation very challenging - a challenge that has been met, in part, by the use of sophisticated control and communications systems.

In recent years, the demand for a reliable and secure electric power supply has had to be balanced against dwindling natural resources, a depressed economic climate and growing environmental concerns about the electric power industry. These often conflicting factors have made the operation of large power networks even more challenging. As a result, in spite of an expected modest growth in the demand for electric energy over the next decade (in the U.S.A., only 1.3 to 1.9% annually up to 2010 [64]), people involved in power systems planning and operation must continue to devise ways of resolving these conflicting factors.

1.2 Background and Motivation

Several computational problems are associated with the planning and operation of power systems [28]. Among these are fault analysis, for selecting the protection equipment; transient stability studies, used in assessing the impact of disturbances on the system; state-estimation, to provide data for use in on-line monitoring and control; economic dispatch, which seeks to maximise the efficient use

of resources; and the load flow, which analyses the steady state performance of the power network.

The load flow is one of the most frequently used of the abovementioned tools. For a specified network and loading condition, the load flow analysis determines the complete state of the system. This information determines whether or not a specified power demand can be met by the given network and, if it can, whether the operating conditions satisfy predetermined engineering and security constraints. These constraints include bounds on the system voltages as well as limits on the capacity of transmission lines and the reactive power sources. These constraints must be satisfied for both the intact system and the system resulting from any probable contingency.

The importance of load flow studies in power system analysis is underscored by the volume of research that has been done in this area. A sample of these works can be found in references [1-27,29,33-35,37-59]. Although there is a sentiment that not many new contributions can be made to such a widely researched field of study, new insights can always be gained from approaching the same problem in a different way.

Therefore, this study has been undertaken with the purpose of expanding our basic knowledge about the nature of the load flow problem.

1.3 Definition of the Load Flow Problem

1.3.1 General

The components of an interconnected power system include numerous transmission lines and "buses". At such buses, power is being injected into the

network by generators or is being drawn from the network by the system loads. The transmission lines serve as a route for the flow of power from one bus to another. A constant system frequency indicates that a balance is kept between the generated real power and the real power demand as well as the system losses [36].

Power flow or load flow analysis is concerned with determining how a given set of loads can be supplied by a given set of generators. The load flow problem involves the formulation of a suitable mathematical model of the network, the specification of power and voltage constraints at the buses and the numerical computation of the power flow equations subject to the specified constraints [36].

1.3.2 Load Flow Equations

The load flow equations express the net injected bus powers as a function of various bus voltages and, as such, are non-linear. In addition, since they describe the behaviour of a static system, they are algebraic. The equations are developed using network theory and full details are given in Chapter III. A brief introduction is now provided.

The complex power, S_i, injected into bus i of the network is given by

$$S_i = (P_{gi} - P_{di}) + j(Q_{gi} - Q_{di})$$
 (1.1)

where P_{gi} and Q_{gi} are the generated real and reactive powers, while P_{di} and Q_{di} are the real and reactive load powers. Equation (1.1) can also be written as

$$P_{i} + jQ_{i} = V_{i} I_{i}^{*}$$

$$= V_{i} \sum_{k=1}^{N} V_{k}^{*} Y_{ki}^{*}$$
(1.2)

where V_i is the complex voltage at bus i, V_k^* is the complex conjugate of the voltage at bus k and Y_{ik} is the (i,k)th element of the bus admittance matrix. Separating (1.2) into its real and imaginary parts yields, in polar coordinates,

$$P_{i} = |V_{i}| \sum_{k=1}^{N} |Y_{ik}| |V_{k}| \cos(\delta_{k} - \delta_{i} + \theta_{ik})$$
 (1.3)

$$Q_i = |V_i| \sum_{k=1}^N |Y_{ik}| |V_k| \sin(\delta_k - \delta_i + \theta_{ik})$$
 (1.4)

where δ_i is the voltage phase angle at bus i and θ_{ik} is the angle of the (i,k)th element of the admittance matrix. In rectangular coordinates, these equations are expressed by

$$P_{i} = e_{i} \sum_{k=1}^{N} (e_{k}G_{ik} - f_{k}B_{ik}) + f_{i} \sum_{k=1}^{N} (f_{k}G_{ik} + eB_{ik})$$
 (1.5)

$$Q_{i} = f_{i} \sum_{k=1}^{N} (e_{k}G_{ik} - f_{k}B_{ik}) - e_{i} \sum_{k=1}^{N} (f_{k}G_{ik} + eB_{ik})$$
 (1.6)

where e_i and f_i are the real and imaginary parts of the complex voltage and G_{ik} and B_{ik} are the real and imaginary parts of the (i,k)th element of Y.

There are therefore 2N such relations for an N-bus system.

1.3.3 Classification of Variables

Each of the above load flow equations contains six variables, P_{gi} , Q_{gj} , P_{di} , Q_{di} , V_{i} and δ_{i} . The classification of these variables as given and unknowns is

dictated by the different buses in the system. In general, there will be different known and unknown quantities associated with each bus. For a given set of these quantities, the load flow calculation determines the remaining unknown variables. This is discussed in more detail in Section 3.2.

1.4 Scope of Work

The work in this thesis addresses itself to an investigation of some basic analytical properties of the load flow equations. To this end, each equation is formulated as a fully quadratic form in rectangular co-ordinates. The nature of this quadratic form is examined as well as its relationship to the multiplicity and the existence of load flow solutions.

In addition, an experimental study is done on the nature of the *load* flow feasibility region. This region characterises all the possible injections for which there is a real voltage solution to the load flow equations. The study is based on concepts presented in [9,25,26]. Special emphasis is placed on how the structure of this region determines the general nature and the number of multiple load flow solutions.

1.5 Outline of the Thesis

The thesis is organised as follows:

Chapter II

This chapter contains a review of some of the work that has been done on the analytical aspects of the load flow equations. Included in this review are algorithms to find multiple load flow solutions, the relationship between multiple load flow solutions and voltage stability and conditions for the existence of load flow solutions.

Chapter III

The formulation of the load flow equations in rectangular co-ordinates is presented in this chapter. The quadratic nature of this formulation is examined in detail and the way in which this property impacts on the solution of the load flow equations is examined.

Chapter IV

In this chapter, general properties of the load flow feasibility region are presented and the structure of this region is examined. The relationship between the structure of this region and the nature as well as the number of load flow solutions is also studied. The results of numerical simulations are provided.

Chapter V

This chapter contains the conclusions of the research and recommendations for further study.

CHAPTER II REVIEW OF LITERATURE

2.1 Introductory Remarks

The load flow problem has been an active field of research for more than three decades and numerous contributions have been made to this important area of power systems analysis. The research effort can be classified broadly into two areas - the development of numerical tools required to solve the load flow equations and the comprehensive understanding of some of the analytical properties of these equations.

The work on these two aspects of the load flow problem has often complimented each other. More efficient numerical algorithms have been conceived as a result of a better understanding of the analytical properties of the load flow equations [43] and also observations on the behaviour of numerical procedures for solving these equations have been the motivation for work on theoretical explanations for certain load flow phenomena [5].

Foremost among the analytical properties of the load flow equations are the non-uniqueness and existence of solutions. There is an abundance of literature on this subject and in this chapter, a brief review of some of the work that has been done on these two important questions in load flow studies is presented. The evolution of the numerical procedures is outlined in Appendix A.

2.2 Multiple Load Flow Solutions

2.2.1 General

The load flow equations are a set of simultaneous nonlinear equations and in general, such equations will have more than one solution. Very often, for a given set of operating parameters, only one of the solutions of the load flow equations corresponds to a practical stable equilibrium point in the sense that the solution will persist even when the system is subjected to small perturbations [6]. Such a solution is usually referred to as a "valid" operating point.

The other solutions are more than just a mathematical curiousity and their engineering significance has been confirmed by studies done on voltage stability, for example the work reported in [6]. One interpretation of multiple load flow solutions is that they represent all the possible states through which a network may pass in response to a disturbance [17]. It is important to note that the load flow equations satisfy the fundamental laws (namely Ohm's and Kirchoff's) of circuit theory and as such, all the states described by the multiple solutions can be physically realised [1]. Of course, most of them can exist only under abnormal operating conditions.

2.2.2 Methods for Finding Multiple Load Flow Solutions

In this section, some of the numerical techniques for finding multiple load flow solutions are discussed. It must be mentioned that most of these methods were developed as a result of a sound understanding of some of the basic properties of the load flow equations. The rectangular version of these equations highlights some of these properties and was used in one of the earliest algorithms to find the multiple solutions [1]. Since then, this formulation of the load flow equations has been used in numerous other numerical schemes [2,3,4].

One of these numerical procedures [2] has been designed specifically to locate a pair of solutions which are close to each other. Such a situation arises when the operating point is near to a point at which the load flow jacobian is singular. The authors use, as the basis of their algorithm, the interesting fact that these two solutions and the singular point lie approximately in a straight line.

The more general methods described by Tamura et al, [3,4], have been developed to find all the possible solutions. The success of these methods depends on the robustness of the numerical algorithm used and the availability of suitable initial guesses. The authors use the Newton-Raphson technique with the optimal multiplier [7] to make the algorithm more robust. In [8], it is argued that even this improvement is not enough to guarantee that the approach in [4] would find all the solutions.

The algorithm in [3] uses the fact that, in rectangular co-ordinates, each load flow equation describes a quadratic form. Based on the general solution of quadratic equations, it is assumed that any two solutions of the load flow can be represented by the sum and difference respectively, of two vectors. Conditions which these two vectors must satisfy are derived and those conditions are used to generate suitable initial guesses to find all the load flow solutions. Results are presented for a 3 and a 6 bus systems.

It is known that some load flow solutions are characterised by unusually low voltage magnitudes at various buses. Tamura et al [4] use this property as the basis of another algorithm. This approach is similar to the one proposed in [1]. Assuming that at least one solution is known, a local analysis is performed at each bus, again exploiting the properties of the rectangular load flow, in order to obtain an analytical expression for a guess of the low voltage solution at that bus. This

procedure provides a systematic way of obtaining 2^(N-1) initial guesses. The authors report the greatest success when the initial guess contains a low voltage guess at only one of the buses. This observation led to a simplified method which required the use of fewer initial guesses and found solutions which are similar to a "valid" operating point.

A different approach reported by Salam *et al* [10] uses a homotopy method to find the multiple solutions. An augmented form of the load flow equations and a polynomial with known solutions are used to construct an homotopy. The load flow solutions are found by tracing ^{2N}C_N homotopy curves, starting at the solutions of the polynomial. This method requires a fairly large computational effort.

One of the latest contributions in this area, by Thorp [8], uses a continuation method with a parameterised version of the load flow - a formulation which is similar to the one used in reference [11]. The theoretical foundation of the algorithm is based on the topological structure of the solution set of these parameterised equations. This solution set consists of a set of smooth curves which connect the load flow solutions to each other. All the solutions may therefore be found by tracing a number of these smooth curves which form a connected graph. The curves are traced by the continuation method using a known solution of the load flow as the initial and termination point.

The method is guaranteed to find all the solutions in a maximum of (Ns/2) steps, where s is the number of solutions and N, the number of buses in the system. The results from a 5-bus and a 7-bus system show that a smaller number of traces is required to find all the solutions when the reactive power is included in the parameter set that is used. The efficiency of the method would be even better if the number of solutions were known a priori.

There are other methods which, although not designed specifically for finding the multiple solutions, can do so. One such method [12], and a modification of it [11], are used to generate quasi steady-state load flow trajectories. A parameterised version of the load flow equations is also employed. This method was applied to small systems and in the course of producing the solution loci, all load flow solutions were found.

2.2.3 Analytic Approaches to the Multiplicity of Load Flow Solutions

The non-uniqueness of the load flow solutions has been analysed in many different contexts. The need to investigate this question first became evident in the course of transient stability studies [13]. The relationship between transient stability and multiple load flow solutions is due to the fact that the solutions of the load flow equations represent the equilibrium or singular points of the "swing" equations which describe the dynamic behaviour of the power network [15]. These equilibrium points are usually classified as either stable or unstable and are used to define a hypersurface enclosing the initial states for which transient stability is guaranteed [11].

Korsac [14] and Baillieul and Byrnes [15] showed that stable load flow solutions are not necessarily unique. The argument used is that the load flow equations define a topological manifold and the dynamic equations define a vector field on this manifold. The solutions of the load flow are therefore the critical points of this vector field on the manifold and may be studied by a global analysis of vector fields on manifolds. The stability of the solutions must be checked by methods such as Lyapunov functions. The stable solutions are defined as points at which the energy functions are at a minimum.

A less mathematical approach to the multiple solutions, in particular non-unique stable solutions, is presented by Johnson [16]. The physical characteristics of the system and the way in which reactive power limits are handled by system models are used to explain the occurrence of multiple solutions. Cases are cited where multiple solutions occur due to deficiencies in the representation of certain system components. It is also suggested that some physically realisable multiple solutions may not be found by the traditional load flow.

A novel method presented by Price [17] uses a numerical technique to produce a two-dimensional graphical display that predicts the occurrence, nature and number of multiple solutions, among other things. It also shows the effects of parameter variations and changes in system structure on the nature of the solutions and on the overall performance of the system. This method is a generalisation of the elementary circle diagram and uses a set of constraints which are different from the "bus-type" constraints employed in the conventional load flow. This is one instance where local geometry is used to obtain global information about power system behaviour [18].

Another approach to the study of the multiple solutions has focused on the role of the singular jacobian matrix. Tavora and Smith [19] reported results on such a study for a lossless three bus system with generators at all buses. They showed that the conditions which make the jacobian singular, define surfaces in the state space and that the maximum possible number of load flow solutions is equal to the number of "central" points in that space. The properties of these surfaces and their mapping into the parameter space are also examined. It was established that two solutions are introduced whenever a boundary of any surface in the parameter space is crossed.

In a recent work, Galiana and Zeng [5] provided a theoretical analysis of the mechanism producing multiple solutions in the vicinity of a jacobian singularity. It was established that the pair of solutions which was observed to occur close to such a point, is due to the fact that a change in the system parameters produces a corresponding change in the system variables which contains components in both the positive and negative directions of the null vector of the singular jacobian. This is an extension of the earlier results presented by Galiana [9] and Tamura et al [3] that solutions to the load flow are given by the sum and difference, respectively, of a point of jacobian singularity and a vector in the null space of the singular jacobian.

A more formal mathematical treatment of multiple load flow solutions has used bifurcation theory to analyse their existence and characteristics [20]. Conditions are derived which define the bifurcation points in the state space. At these points, the nature of the solution set changes and new solutions "appear" or "disappear". The bifurcation points correspond to points where the jacobian is singular.

2.2.4 Number of Solutions

It is known that the number of solutions of the load flow equations depends on the topology of the network and the position of the given injection in the injection space and also, for a given network, the number of solutions decreases as the load increases. However, there has been no reported method to pre-determine the number of solutions except for very small systems.

The number 2^(N-1), where N is the number of buses in the system, has been proposed as an upper bound on the maximum number of solutions. However, this is contradicted by a thorough analytical treatment of the subject for a lossless

three bus system consisting of three generator buses [11,15,19] which revealed that for certain injections and network structures, up to six solutions may exist. Baillieul and Byrnes [15] apply some results from intersection theory and algebraic geometry to establish an upper bound, $^{(2N-2)}C_{(N-1)}$, on the number of solutions for lossless system with generator buses. In their analysis, the $2^{(N-1)}$ solutions are considered to be *elementary* solutions and they show that other non-elementary solutions may exist.

2.3 Voltage Stability and Multiple Load Flow Solutions

No discussion on multiple load flow solutions is complete without a mention of their relationship to voltage stability. Voltage stability is itself a very complex phenomenon. It is generally agreed, that steady state methods cannot adequately explain all the observed phenomena and dynamic considerations must be included.

As mentioned previously, the multiple load flow solutions correspond to the equilibrium points of the dynamic equations of the network. As a result, there have been efforts to use the relationship between the load flow jacobian and the system state matrix [21] to analyse the characteristics of the various equilibrium points. This information is useful in explaining the different types of voltage instabilities.

In most cases, there is at least one stable equilibrium point (not always the case [20]). At this point, all the eigenvalues of the load flow jacobian have negative real parts. The other equilibrium points may be classified by the dimension of their unstable manifolds [15] or by the number of eigenvalues of the load flow jacobian that have positive real parts. At a "type one" solution the real part of only one of the eigenvalues is positive. The other unstable equilibrium points define

jacobian matrices having more than one eigenvalue with a positive real part and are regarded as being of type greater than one.

One type of voltage instability is voltage collapse which is characterised by a large drop in voltage magnitudes at some buses in the system with fairly insignificant changes in the phase angles [6]. This results in loss of steady state stability. For typical power system models, it has been shown [22] that such an instability is caused by a saddle-node bifurcation between a stable operating point and a "type one" equilibrium point.

In an approach to voltage collapse based on energy methods, Overbye and DeMarco [6] use the properties of these "type one" unstable equilibria to predict the most likely areas of voltage collapse in a given network. They report extensive numerical results which indicate that these "type one" equilibrium points are in fact the solutions found by the simplified method of reference [4].

Another type of voltage instability involves oscillation of the system voltage. This is usually referred to as angular instability and occurs as a result of Hopf bifurcations between a stable operating point and low voltage solutions of type greater than one. A more thorough discussion of bifurcation phenomena in power systems can be found in references such as [24].

2.4 Existence of Load Flow Solutions

The load flow equations describe a mapping of the entire voltage space into a subset of the injection or parameter space. Therefore, for any given network, there are some injections for which no inverse relation exists or in other words, no

physically realisable voltage can satisfy the given operating constraints. This fact may be deduced from physical as well as mathematical considerations.

Those injections for which a real solution of the load flow exists, characterise the load flow feasibility region. Points on the extreme boundary of this region define points of maximum power transfer of the network. The precise geometry of this region is unknown except in the simple case of a two-bus system. However, it has been proposed [9,25] that the boundaries of the region consist of a cone and a set of hyperplanes. A recent report [27] provides additional information on the radius of curvature of this region.

In [19], one of the earliest efforts is made to examine the characteristics of the load flow feasibility region. A conjecture is presented that this region may be totally enclosed by a set of hyperplanes. A method to systematically characterise this region was proposed by Galiana [25]. Jarjis, [26] expanded the method in [25] and developed necessary and sufficient conditions for the existence of a load flow solution. A method was devised, quite apart from the numerical approach, to determine whether a real voltage solution exists for any given injection.

The works reported in [11,17,19] all provide graphical methods of predicting the existence of load flow solutions and apart from [17], these methods are amenable only to very small systems. Not much has been presented on this subject for general power networks and very often, the existence (or lack thereof) of load flow solutions must be inferred from the divergence of the numerical procedure.

The challenge still remains to find a simple method, such as would be applicable to on-line security assessment, which would determine whether or not there is a solution to the load flow equations for any given operating conditions.

CHAPTER III

ANALYTICAL PROPERTIES OF THE LOAD FLOW EQUATIONS

3.1 Preliminary Remarks

The load flow equations describe conditions which must be satisfied so that a balance is kept between the power that is generated and consumed in an electric power network. These equations may formulated in either polar or rectangular co-ordinates and while the polar formulation appears to be well suited to numerical calculations [29], the rectangular version is more amenable to analytical studies.

In this chapter, the equations are formulated in rectangular coordinates in a way that specifically includes an equation for the specification on the reference bus. This makes all the equations fully quadratic and the analytical properties of these quadratic equations are analysed in detail.

3.2 Power System Model

The AC power network in its sinusoidal steady-state, is assumed to be a balanced three-phase system. As a result, it may be represented by its single-phase positive sequence network. The components of the network are usually modelled as follows: the generators are considered to be constant-voltage power sources, the loads are treated as power sinks and the transformers and transmission lines are represented by lumped pi-networks [36].

There are four quantities associated with each bus in the network - the net real power, the net reactive power, the voltage magnitude and the voltage phase angle. These are elements of the set of fixed constraints which must be satisfied and two of them have to be specified at each bus. The choice is usually dictated by the components which are connected to the particular bus.

The buses are classified according to the quantities that are specified. At a PV or voltage-control bus, those quantities are the net injected real power and voltage magnitude. At a PQ or load bus, the net injected real and reactive powers are both specified and at the reference bus the phase angle is specified. Because the system losses are not known a priori, the real power injected into at least one bus (one to which a generator is connected) cannot be specified. This bus is known as the slack or swing bus. Generally, the slack bus is also chosen as the reference bus.

These modelling assumptions form the basis for predicting the power flow on an electric power grid.

3.3 Formulation of the Load Flow Equations in Rectangular Co-ordinates

3.3.1 2N Equations

In an N-bus system, let z_i denote a specified quantity (P, Q or V^2) at bus i. This quantity can be expressed as the following quadratic form in x_*

$$z_i = x_r^T J_i x_r \tag{3.1}$$

where x_r is the 2N x 1 vector of the real and imaginary components of the node voltages,

Chapter III: Analytical Properties of the Load Flow Equations

$$x_{x} = \begin{bmatrix} e \\ f \end{bmatrix} \tag{3.2}$$

and where J_i is a 2N x 2N constant real symmetric matrix defined by the type of injection and the admittance matrix [25].

Equation (3.1) is derived as follows: the complex current injected into the buses of an N-bus network may be written as

$$I = YV \tag{3.3}$$

where I is an N x 1 vector of complex current injections, Y is the complex N x N bus admittance matrix and V is the N x 1 vector of complex bus voltages. In power systems however, complex *powers*, not currents are known. From circuit theory, the net injected bus powers are given by

$$S = diag(V) I^*$$

$$= diag(V) (Y V)^*$$

$$= P + jQ$$
(3.4)

where S is an N x 1 vector of complex bus powers, diag(V) is an N x N diagonal matrix of complex voltages and P and Q are N x 1 vectors of net real and reactive power injections respectively. If V is replaced by e + jf and Y by G + jB in equation (3.4) and the resulting expression is simplified, the real and imaginary parts of S become

$$P = diag(e) [Ge - Bf] + diag(f) [Gf + Be]$$
 (3.5)

and

$$Q = diag(e) [-Gf - Be] + diag(f) [Ge - Bf]$$
 (3.6)

where diag(e) and diag(f) are N x N diagonal matrices with diagonal elements equal to e and f respectively.

Chapter III: Analytical Properties of the Load Flow Equations

For any arbitrary N x 1 vector of real constants, γ , and an N x 1 vector, z, of specified injections, the following is true

$$\gamma^T z = \sum_{i=1}^N \gamma_i z_i \tag{3.7}$$

If z is a vector of real power injections, a linear combination of these injections is given by

$$\gamma^{T}P = x_{r}^{T} \frac{1}{2} \begin{bmatrix} diag(\gamma) G + Gdiag(\gamma) & Bdiag(\gamma) - diag(\gamma) B \\ -Bdiag(\gamma) + diag(\gamma) B & diag(\gamma) G + Gdiag(\gamma) \end{bmatrix} x_{r}$$
 (3.8a)

Similarly, if z consists of reactive power injections it follows that

$$\gamma^{T}Q = x_{r}^{T} \frac{1}{2} \begin{bmatrix} -diag(\gamma) B - Bdiag(\gamma) & Gdiag(\gamma) - diag(\gamma) G \\ -Gdiag(\gamma) + diag(\gamma) G & -diag(\gamma) B - Bdiag(\gamma) \end{bmatrix} x_{r}$$
(3.9a)

where diag(γ) is an N x N diagonal matrix with γ as the diagonal elements and x_r is as defined in equation (3.2).

If γ consists of zeroes everywhere except for a one at position i, $\gamma^T P$ and $\gamma^T Q$ are equal to P_i and Q_i respectively and equations (3.8a) and (3.9a) represent the real and reactive powers at bus i. This particular γ is now defined as α and (3.8a) and (3.9a) may be simplified to

$$\alpha^{T}P = x_{r}^{T} \frac{1}{2} \begin{bmatrix} \alpha g^{T} + g \alpha^{T} - \alpha b^{T} + b \alpha^{T} \\ \alpha b^{T} - b \alpha^{T} & \alpha g^{T} + g \alpha^{T} \end{bmatrix} x_{r}$$
 (3.8)

and

$$\alpha^{T}Q = x_r^{T} \frac{1}{2} \begin{bmatrix} -\alpha b^{T} - b\alpha^{T} - \alpha g^{T} + g\alpha^{T} \\ \alpha g^{T} - g\alpha^{T} - \alpha b^{T} - b\alpha^{T} \end{bmatrix} x_r$$
 (3.9)

where g and b are the ith column of G and B respectively.

The square of the voltage magnitude at bus i may also be written in a similar way as

$$\alpha^T V^2 = x_r^T \begin{bmatrix} diag(\alpha) & O \\ O & diag(\alpha) \end{bmatrix} x_r$$
 (3.10)

where V^2 is an N x 1 vector of voltage magnitudes squared, diag(α) is an N x N matrix with α as the diagonal elements and O is an N x N null matrix.

Recall that one of the voltage angles is usually specified to provide a reference for the other angles. The components of the reference bus voltage, V_s , are related to each other by [65]

$$f_s = e_s \tan \delta_s \tag{3.11}$$

where δ_s is the reference angle and bus s is the reference bus. This equation may be re-written as

$$e_s \tan \delta_s - f_s = 0 \tag{3.12a}$$

or as

$$\alpha_s^T x_r = 0 (3.12b)$$

where α_s is a 2N x 1 vector of zeroes except for its sth and (N+s)th entries which are equal to tan δ_s and -1, respectively. Note that (3.12b) describes a hyperplane through the origin.

At each of the PQ and PV buses in the system, therefore, there are two quadratic algebraic equations describing the specified injections. At the slack bus there is one quadratic equation describing the voltage magnitude squared while at the reference bus, there is an additional equation specifying conditions in equation (3.12). The specified injections form (2N-1) non-linear equations and along with

(3.12) constitute 2N load flow equations, in 2N unknowns, which characterise the static behaviour of the power system.

3.3.2 (2N-1) Equations

Equation (3.12) may be used to reduce the number of equations and unknowns by one. In most cases, however, the slack bus is taken as the reference bus and *two* unknowns are eliminated. The resulting (2N-2) equations are no longer fully quadratic but have a linear term in x describing the specification on the slack/reference bus [3,44].

The formulation here retains the equation for the slack bus and uses equation (3.12) to eliminate the variable \mathbf{f}_s which is the quadrature component of the voltage at the reference bus. A generator bus is usually chosen as the reference bus. This produces (2N-1) purely quadratic equations in (2N-1) unknowns. This implies that the dimension of the J_i matrices is reduced to (2N-1) x (2N-1). The reduced matrix may be obtained from the 2N x 2N matrix as follows:

First, define a new variable, $d = M x_r$, where

$$M = I - mm^T + m\alpha_s^T \qquad (3.13)$$

I is a $2N \times 2N$ identity matrix and m is a $2N \times 1$ vector of zeroes except for a "1" at the (N+s)th position. The matrix M is similar to the identity matrix but its (N+s)th row describes the condition in (3.12a). Equation (3.1) can then be re-written as

$$z_{i} = d^{T} (M^{-1})^{T} J_{i} M^{-1} d$$

= $d^{T} J_{s_{i}} d$ (3.14)

where J_i is as defined in (3.8), (3.9) or (3.10) and has dimension 2N x 2N and the definition of J_{S_i} is understood.

Since the (N+s)th element of \mathbf{d} ($\mathbf{e_s} \tan \delta_s - \mathbf{f_s}$) is equal to zero, it can be deleted. The resulting vector is identical to the $(2N-1) \times 1$ voltage vector, \mathbf{x} . The $(2N-1) \times (2N-1) \mathbf{J_i}$ matrix may be obtained by deleting the (N+s)th row and column from $\mathbf{Js_i}$. Note that the reduced matrix is also symmetric but its sth row and column now have elements containing the quantity $\tan \delta_s$. Consequently, the structure of the $(2N-1) \times (2N-1)$ matrices will be different for each different choice of reference bus. Examples of such $(2N-1) \times (2N-1)$ matrices are provided in Appendix C.

In most formulations of the load flow equations, the slack bus is chosen as the reference bus and the reference angle is set to zero, without loss of generality. This choice of reference angle ensures that the initial guess used in some numerical algorithms converges to the most stable load flow solution [11,29]. When $\delta_s = 0$, the (2N-1) x (2N-1) matrix can be obtained simply by deleting the (N+s)th row and column from the 2N x 2N J_i matrix.

3.4 Eigenvalues and Eigenvectors of the J_i Matrices

Some of the analytical properties of the load flow equations may be studied by expressing each quadratic equation in its canonical form and examining the characteristics of these quadratic forms. This involves the derivation of the eigenvalues and eigenvectors of the matrices defining each specified injection.

The special structure of the J_i matrix allows its characteristic eigenvalues and eigenvectors to be evaluated by direct non-iterative means, irrespective of the size of the matrix and consequently, of the size of the network. Furthermore, when the matrix defines a power injection, it has only *four* non-zero eigenvalues and four corresponding orthogonal eigenvectors [26,33]. Details of these

Chapter III: Analytical Properties of the Load Flow Equations derivations are provided in Appendix B. If the injection is a voltage magnitude

squared, then there are two non-zero eigenvalues and eigenvectors.

3.4.1 The 2N x 2N Matrix

The J_i matrix in equation (3.8), (3.9) or (3.10) is a sparse symmetric real matrix consisting of two non-zero rows and columns. When x_r is as defined in (3.2) and the dimension of the matrix is 2N x 2N, these non-zero elements are at rows i and N+i and similarly at columns i and N+i [3,9,44].

3.4.1.1 Eigenvalues and Eigenvectors of J_{Pi}

In this case, the matrix defining the quadratic form of the real power injection has two identical pairs of eigenvalues: λ_{p1} , λ_{p2} , λ_{p1} , λ_{p2} . Each pair is given by

$$\lambda_{p1} = \frac{g^T \alpha + \sqrt{-(\alpha^T b)^2 + g^T g + b^T b}}{2}$$
 (3.15a)

$$= \frac{G_{ii} + \sqrt{G_{ii}^2 + \sum_{\substack{k=1\\k \neq i}}^{N} (G_{ik}^2 + B_{ik}^2)}}{2}$$
 (3.15b)

and

$$\lambda_{p2} = \frac{g^T \alpha - \sqrt{-(\alpha^T b)^2 + g^T g + b^T b}}{2}$$
 (3.16a)

$$= \frac{G_{ii} - \sqrt{G_{ii}^2 + \sum_{\substack{k=1\\k \neq i}}^{N} (G_{ik}^2 + B_{ik}^2)}}{2}$$
 (3.16b)

One set of orthogonal eigenvectors corresponding to these eigenvalues

is

$$v = \begin{bmatrix} g + (2\lambda - \alpha^T g) \alpha \\ -b + (\alpha^T b) \alpha \end{bmatrix}$$
 (3.17a)

or equivalently

 $V = \begin{bmatrix} G_{1i} \\ \vdots \\ G_{i-1i} \\ 2\lambda \\ G_{i+1i} \\ \vdots \\ G_{Ni} \\ -B_{1i} \\ \vdots \\ -B_{i-1i} \\ 0 \\ -B_{j+1i} \\ \vdots \\ -B_{Ni} \end{bmatrix}$ (3.17b)

for the first pair $\lambda_{p1},~\lambda_{p2}$ and

$$v = \begin{bmatrix} b - (\alpha^T b) \alpha \\ g + (2\lambda - \alpha^T g) \alpha \end{bmatrix}$$
 (3.18a)

or

Chapter III: Analytical Properties of the Load Flow Equations

$$V = \begin{cases} B_{1i} \\ B_{2i} \\ \vdots \\ B_{i-1i} \\ 0 \\ B_{i+1i} \\ \vdots \\ B_{Ni} \\ G_{1i} \\ G_{2i} \\ \vdots \\ G_{i-1i} \\ 2\lambda \\ G_{i+1i} \\ \vdots \\ G_{Ni} \end{cases}$$
(3.18b)

for the second pair λ_{p1} , λ_{p2} . The vector \mathbf{x}_{r} is as defined in (3.2).

3.4.1.2 Eigenvalues and Eigenvectors of J_{Qi}

The matrix defining the reactive power injection at bus i also has two identical pairs of eigenvalues - λ_{q1} , λ_{q2} , λ_{q1} , λ_{q2} . Each pair can be defined as

$$\lambda_{q1} = \frac{-b^T \alpha + \sqrt{-(\alpha^T g)^2 + g^T g + b^T b}}{2}$$
 (3.19a)

$$= \frac{-B_{ii} + \sqrt{B_{ii}^2 + \sum_{\substack{k=1\\k \neq i}}^{N} (G_{ik}^2 + B_{ik}^2)}}{2}$$
 (3.19b)

and

$$\lambda_{q2} = \frac{-b^{T}\alpha - \sqrt{-(\alpha^{T}b)^{2} + g^{T}g + b^{T}b}}{2}$$
 (3.20a)

$$= \frac{-B_{ii} - \sqrt{B_{ii}^2 + \sum_{\substack{k=1\\k \neq i}}^{N} (G_{ik}^2 + B_{ik}^2)}}{2}$$
 (3.20b)

A corresponding set of orthogonal eigenvectors is

$$v = \begin{bmatrix} -b + (2\lambda + \alpha^T b) \alpha \\ -g + (\alpha^T g) \alpha \end{bmatrix}$$
 (3.21a)

or expressed differently

$$V = \begin{bmatrix} -B_{1i} \\ \vdots \\ B_{i-1i} \\ 2\lambda \\ -B_{i+1i} \\ \vdots \\ -B_{Ni} \\ -G_{1i} \\ \vdots \\ -G_{i-1i} \\ 0 \\ -G_{i+1i} \\ \vdots \\ -G_{Ni} \end{bmatrix}$$
(3.21b)

for the first pair of eigenvalues $\lambda_{q1},~\lambda_{q2}$ and

$$v = \begin{bmatrix} g^{-}(\alpha^{T}g) \alpha \\ -b + (2\lambda + \alpha^{T}b) \alpha \end{bmatrix}$$
 (3.22a)

or

Chapter III: Analytical Properties of the Load Flow Equations

$$V = \begin{bmatrix} G_{1i} \\ \vdots \\ G_{i-1i} \\ 0 \\ G_{i+1i} \\ \vdots \\ G_{Ni} \\ -B_{1i} \\ \vdots \\ -B_{i-1i} \\ 2\lambda \\ -B_{i+1i} \\ \vdots \\ -B_{Ni} \end{bmatrix}$$
(3.22b)

for the second pair. Again, x_r is as defined in (3.2).

3.4.1.3 Eigenvalues and Eigenvectors of J_{vi}²

The matrix describing the square of the voltage magnitude at bus i has two non-zero eigenvalues each of which is equal to one. The two eigenvectors corresponding to these eigenvalues are given by

$$v = \begin{bmatrix} 0 \\ 0 \\ \vdots \\ 1 \\ 0 \\ 0 \\ \vdots \\ 0 \end{bmatrix}$$
 (3.23)

where "1" is in the ith position and

Chapter III: Analytical Properties of the Load Flow Equations

$$v = \begin{bmatrix} 0 \\ 0 \\ \vdots \\ 0 \\ 1 \\ 0 \\ \vdots \\ 0 \end{bmatrix}$$
 (3.24)

where "1" is in the (N+i)th position.

3.4.2 The (2N-1) x (2N-1) Matrix

In the following analysis, the slack bus is taken as the reference bus and the reference angle is assumed to be zero, as is normally done in load flow studies. These assumptions hold for all future references to the $(2N-1) \times (2N-1) J_i$ matrices.

The (2N-1) x (2N-1) matrices describing the real and reactive power injections also have two pairs of eigenvalues. One of the pairs is identical to the pair found for the 2N x 2N matrices. However, the magnitude of the second pair is less than that of the first one. This is true for N>2. For N=2, the dimension of the J_i matrices are 3 x 3 and therefore each matrix has only three eigenvalues and eigenvectors.

3.4.2.1 Eigenvalues and Eigenvectors of $J_{\rm Pi}$

For real power injections, these eigenvalues are λ_{p1} , λ_{p2} , λ_{pa1} , λ_{pa2} . The pair λ_{p1} and λ_{p2} is the same as in the case already described. The other pair is given by

$$\lambda_{pa1} = \frac{g^{T}\alpha + \sqrt{-(\alpha^{T}b)^{2} + g^{T}g + b^{T}b - (\beta^{T}b)^{2} - (\beta^{T}g)^{2}}}{2}$$
 (3.25a)

$$= \frac{G_{ii} + \sqrt{G_{ii}^2 + \sum_{\substack{k=1\\k\neq i,s}}^{N} (G_{ik}^2 + B_{ik}^2)}}{2}$$
 (3.25b)

and

$$\lambda_{pa2} = \frac{g^{T}\alpha - \sqrt{-(\alpha^{T}b)^{2} + g^{T}g + b^{T}b - (\beta^{T}g)^{2} - (\beta^{T}b)^{2}}}{2}$$
(3.26a)

$$= \frac{G_{ii} - \sqrt{G_{ii}^2 + \sum_{\substack{k=1 \ k \neq i, s}}^{N} (G_{ik}^2 + B_{ik}^2)}}{2}$$
 (3.26b)

where β is an N x 1 vector of zeros except for a "1" at position s and bus s is the reference bus,

One set of eigenvectors corresponding to these eigenvalues is

$$V = \begin{bmatrix} g + (2\lambda - \alpha^T g + \alpha^T b \left(\frac{\beta^T g}{\beta^T b} \right)) \alpha - \left(\frac{\beta^T g}{\beta^T b} \right) b \\ -b + (\alpha^T b + \alpha^T g \left(\frac{\beta^T g}{\beta^T b} \right) - 2\lambda \left(\frac{\beta^T g}{\beta^T b} \right)) \alpha - \left(\frac{\beta^T g}{\beta^T b} \right) g \end{bmatrix}$$
(3.27a)

or equivalently

Chapter III: Analytical Properties of the Load Flow Equations

$$V = \begin{bmatrix} G_{1i} - \frac{B_{1i}G_{si}}{B_{si}} \\ G_{21} - \frac{B_{2i}G_{si}}{B_{si}} \\ \vdots \\ \vdots \\ G_{i-1i} - \frac{B_{i-1i}G_{si}}{B_{si}} \\ 2\lambda \\ G_{i+1i} - \frac{B_{i+1i}G_{si}}{B_{si}} \\ \vdots \\ \vdots \\ G_{Ni} - \frac{B_{Ni}G_{si}}{B_{si}} \\ -B_{1i} - \frac{G_{1i}G_{si}}{B_{si}} \\ -B_{2i} - \frac{G_{2i}G_{si}}{B_{si}} \\ \vdots \\ -B_{i-1i} - \frac{G_{i-1i}G_{si}}{B_{si}} \\ -B_{i+1i} - \frac{G_{i+1i}G_{si}}{B_{si}} \\ -B_{i+1i} - \frac{G_{i+1i}G_{si}}{B_{si}} \\ \vdots \\ -B_{N-1i} - \frac{G_{N-1i}G_{si}}{B_{si}} \\ \end{bmatrix}$$

for λ_{pa1} , λ_{pa2} and

$$V = \begin{bmatrix} b - (\alpha^T b + \alpha^T g \left(\frac{\beta^T g}{\beta^T b} \right) - 2\lambda \left(\frac{\beta^T g}{\beta^T b} \right)) \alpha + \left(\frac{\beta^T g}{\beta^T b} \right) g \\ g + (2\lambda - \alpha^T g + \alpha^T b \left(\frac{\beta^T g}{\beta^T b} \right)) \alpha - \left(\frac{\beta^T g}{\beta^T b} \right) b \end{bmatrix}$$
(3.28a)

or equivalently

Chapter III: Analytical Properties of the Load Flow Equations

$$V = \begin{bmatrix} B_{1i} + \frac{G_{1i}G_{is}}{B_{is}} \\ B_{2i} + \frac{G_{2i}G_{is}}{B_{is}} \\ \vdots \\ B_{i-1i} + \frac{G_{i-1i}G_{is}}{B_{is}} \\ \frac{2\lambda G_{is}}{B_{is}} \\ B_{i+1i} + \frac{G_{i+1i}G_{is}}{B_{is}} \\ \vdots \\ \vdots \\ B_{Ni} + \frac{G_{Ni}G_{is}}{B_{is}} \\ G_{2i} - \frac{B_{2i}G_{is}}{B_{is}} \\ G_{2i} - \frac{B_{i-1i}G_{is}}{B_{is}} \\ \vdots \\ \vdots \\ G_{N-1i} - \frac{B_{i-1i}G_{is}}{B_{is}} \\ G_{i+1i} - \frac{B_{N-1i}G_{is}}{B_{is}} \\ \vdots \\ \vdots \\ G_{N-1i} - \frac{B_{N-1i}G_{is}}{B_{is}} \end{bmatrix}$$

for λ_{p1} and λ_{p2} . When bus i is not connected to the reference bus, the term G_{is} / B_{is} in equations (3.27b) and (3.28b) is set to zero.

3.4.2.2 Eigenvalues and Eigenvectors of J_{0i} and J_{vi}^2

The eigenvalues and eigenvectors of the matrix describing the reactive power injection can be obtained from the expressions of those for the real power by replacing G with -B and B with G respectively in equations (3.27b) and (3.28b).

Those of the matrix describing the voltage magnitude squared are unchanged.

3.4.3 Comparison of 2N x 2N and (2N-1) x (2N-1) J_i Matrices

A close scrutiny of the eigenvalues and eigenvectors of the $2N \times 2N$ matrix and those of the $(2N-1) \times (2N-1)$ matrix reveals that the two sets of eigenvalues are *identical* except when the matrices define power injections at buses connected to the reference bus. This is also true for the eigenvectors if the (N+s)th element is deleted from the $2N \times 1$ eigenvectors.

3.5 Nature of the Quadratic Surfaces Defined by the J. Matrices

The four orthonormal eigenvectors of each (2N-1) x (2N-1) J_i matrix represent a set of principal axes of the particular quadratic surface [30]. It is worthwhile to note that these eigenvectors or principal axes are in general not unique. In Appendix B, it is shown that for buses not connected to the reference/slack bus, two components of the eigenvectors (e_k and f_k , for an injection specified at bus k) are completely arbitrary. In cases where the bus at which the injection is specified is connected to the slack/reference bus, only one component of the eigenvector is arbitrary.

The hypersurfaces representing the real and reactive power injections are hyperbolic because the matrices describing them have eigenvalues of different signs. The positive eigenvalues of the matrix describing the reactive power injection are larger than those of the matrix describing the real power. Also, the ratio of the magnitudes of the positive to negative eigenvalues is a lot larger for the matrix

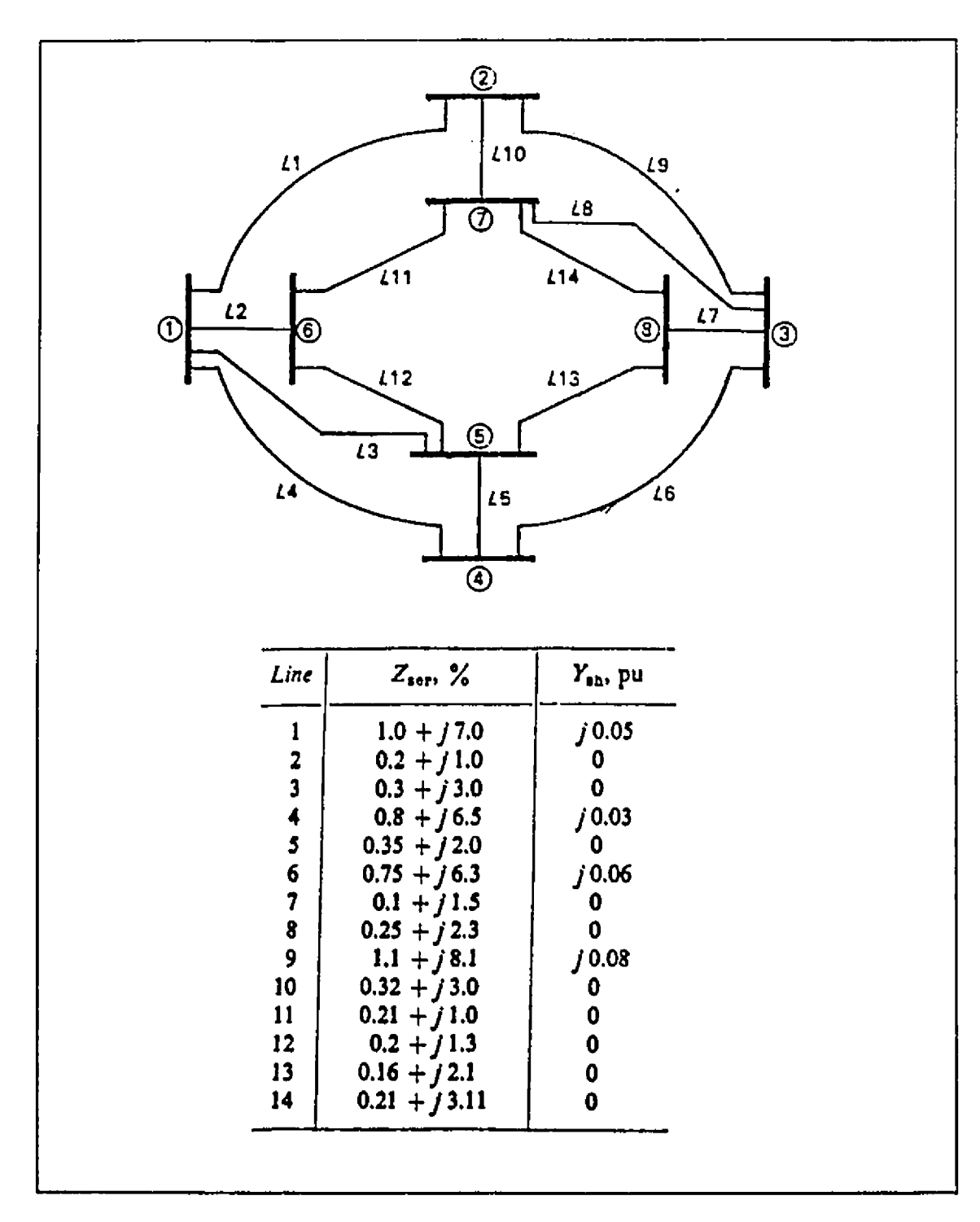


Figure 3.1. 8-Bus System

describing the reactive power than for the one describing the real power. Since reactive power injections are specified at load buses, they are negative. This indicates that the surfaces describing the reactive power injections are "narrower" than those representing the real power.

Table 3.1 shows the positive and negative eigenvalues of the (2N-1) x (2N-1) matrices of the 8-bus example in Figure (3.1).

Table 3.1.	Eigenvalues	of Jp; and	Joi for an	8-Bus Network
------------	-------------	------------	------------	---------------

	λ,	λ.
P ₂	21,60 22,94	-14.44 -15.78
P ₃	47.68 47.68	-35.08 -35.08
P ₄	32,67 33,75	-20.46 -21.53
P_{s}	66.36 68.90	-39.40 -41.94
P ₆	92.44 108.46	-41.53 -57.56
P ₇	75.44 75.44	-44.98 -44.98
P ₈	49,29 49.29	-39.10 -39.10
\mathbf{Q}_{S}	216.11 217.31	-12,10 -13,30
Q_6	280.75 288.70	-13.67 -21.62
Q_7	219.19 219.19	-15.48 -15.48
Q_8	157.92 157.92	-12.20 -12.20

The extreme points of these hypersurfaces may be found by determining their intercepts on the principal axes. This is done by first expressing J_i in its canonical form and rewriting equation (3.1) as

$$z_i = \sum_{k=1}^4 \lambda_k (v_k^T x)^2$$
 (3.29)

where z_i is any power injection and λ_k and v_k are the eigenvalue and normalised eigenvector respectively of the J_i matrix. The points of intersection of the hypersurfaces and their principal axes, c, are then given by

$$C = \pm \sqrt{\frac{z_i}{\lambda}} \tag{3.30}$$

Evidently, z_i and λ must both be of the same sign and so, the hypersurface representing a power injection can intersect only two of the four principal axes.

The hypersurfaces are all symmetrical about their principal axes and principal planes and each has a centre at the origin.

3.6 Load Flow Solutions and Intersection of Quadratic Surfaces

The load flow equations may be solved by finding the intersection of 2N quadratic hypersurfaces and one hyperplane in a 2N-dimensional space or by finding the intersection of (2N-1) quadratic surfaces in a (2N-1)-dimensional space. A knowledge of the nature of the intersection of high-dimensional quadratic surfaces can therefore be useful in providing information on the characteristics of load flow solutions. However, the nature of this intersection is fully understood only for low-dimensional surfaces. It has been stated [34] that this factor has restricted the full exploitation of the quadratic formulation of the load flow equations.

The simple case of two quadratic surfaces in a 3-dimensional space indicates how varied these intersections can be. This intersection can produce a plane curve, a skew curve, two curves in different planes or a single point [31]. Nonetheless, authors [1,2,3,44] have, in different ways, extended what is known about

Chapter III: Analytical Properties of the Load Flow Equations the simple quadratic equation in one unknown to the multi-variable quadratic load flow equations.

In [3], conditions are derived for the existence of multiple load flow solutions based on the fact that the solutions of a quadratic equation can be expressed as the sum and difference of two points. It is also shown if a matrix is defined as the sum of the J_i matrices in each load flow equation, then the eigenvectors of that matrix satisfy at least one of those conditions. All the possible combinations of the sums and differences of these eigenvectors are then used as the initial guesses in the Newton-Raphson algorithm to find all the solutions of the load flow equations.

During the course of this research, an attempt was made to utilise the principal axes and principal planes of the quadratic hypersurfaces to develop an algorithm to find the load flow solutions. The hypothesis was that since the load flow solutions are given by the intersection of these quadratic hypersurfaces, then any load flow solution must lie in a region enclosed by the principal axes and principal planes of the quadratic surfaces. Conversely, any principal axis or plane must lie between two load flow solutions. Figure (3.2) illustrates the idea in two dimensions.

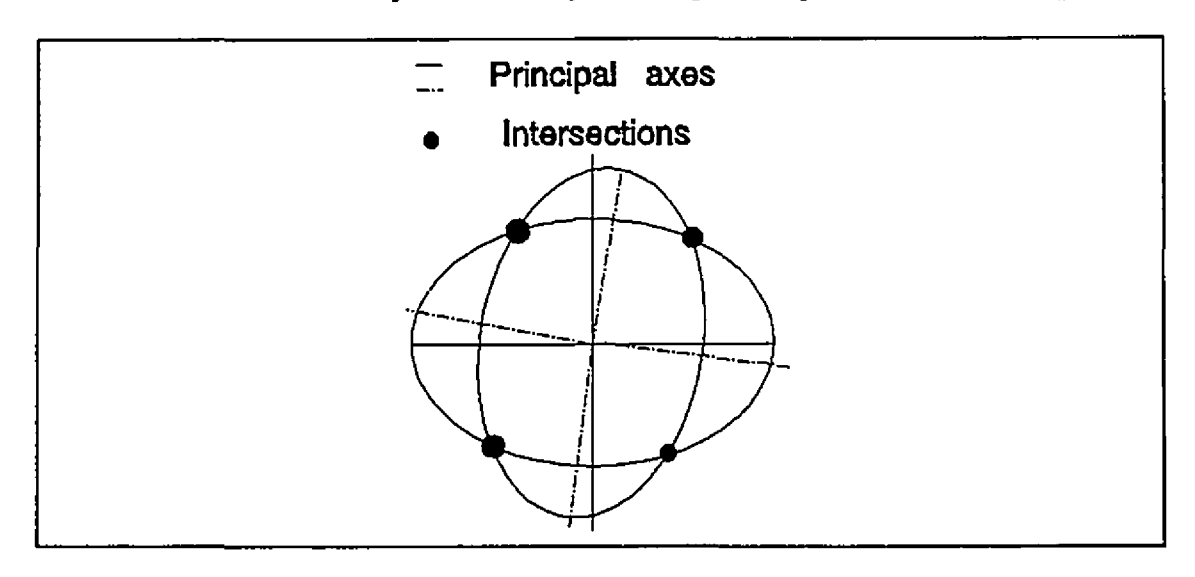


Figure 3.2. Intersection of 2-Dimensional Quadratic Forms

There was not much success in this regard, however. The challenge was to systematically select one of the four eigenvectors from each of the matrices describing the specified injections and find a way of expressing the solution as a linear combination of the selected (2N-1) eigenvectors.

3.7 Load Flow Convergence and Quadratic Surfaces

It is known that factors such as choice of slack bus and the ratio of line resistance to reactance affect the convergence of the load flow algorithms. These factors may be considered in light of the nature of the hypersurfaces described by the load flow equations. Recall that the reference angle is assumed to be zero and the slack bus is taken as the reference bus.

Equations (3.27b) and (3.28b) show that for buses connected to the slack/reference bus, the components of the eigenvectors of the matrices describing the power injections depend on the ratio G_{is} / B_{is} . This indicates that the ratio of

the admittance to susceptance of the line between the reference bus and the bus at which the injection is specified, as well as the location of the slack/reference bus, determines the orientation of some of the hypersurfaces in the voltage space. As a result, these factors will also affect the nature of the intersection of these surfaces since the position of each hypersurface has a direct bearing on the nature of the intersection.

It was also established that at buses not connected to the slack/reference bus, two components of the eigenvectors of matrices describing those specified injections are completely arbitrary. These components are $\mathbf{e_k}$ and $\mathbf{f_k}$ and bus k is where the injection is specified.

These facts are consistent with reports in the literature that:

- (i) Load flow convergence varies for different choices of slack/reference bus [35] and
- (ii) The convergence of the load flow may be improved by having a *distributed* slack/reference bus [46].

3.8 Bounds on the Real and Reactive Power Injections

The expression for the eigenvalues and eigenvectors of the J_i matrices was presented in reference [33]. However, only the J_i matrix of dimension 2N x 2N was considered. Using the properties of symmetric quadratic forms and assuming the voltage is known at a particular bus, the author derived expressions for the maximum and minimum power injections that are possible at that bus. It is shown that these limits depend on the difference between the positive and negative eigenvalues of the J_i matrices describing the power injections. Potential applications in expansion

planning, contingency analysis and determination of load flow feasibility were proposed.

3.9 Illustrative 2-Bus Network

The two-bus system in Figure 3.3 is used to illustrate some of the ideas presented. It consists of a PQ bus and a slack bus and although it is by no means representative of a general power network, it allows a visualisation of the concepts introduced in the preceding sections.

Figures 3.4 and 3.5 depict the quadratic surfaces defined by the real and reactive power respectively. The surface representing Q_2 is a hyperboloid of two sheets and that representing P_2 is a hyperbolic cylinder. The surface representing V_1^2 is obviously a pair of parallel planes and is not shown. The J_i matrices defining P_2 and Q_2 as well as their corresponding eigenvalues and eigenvectors are given in Tables 3.2 and 3.3.

Table 3.2. Eigenvalues And Eigenvectors of J_{P2}

J_{P2}	λ	0	0.94	-0.94
0 0 0.94	v	0	0.7071	0.7071
0 0 0.94		0	0	0
0.94 0 0		0	0.7071	-0.7071

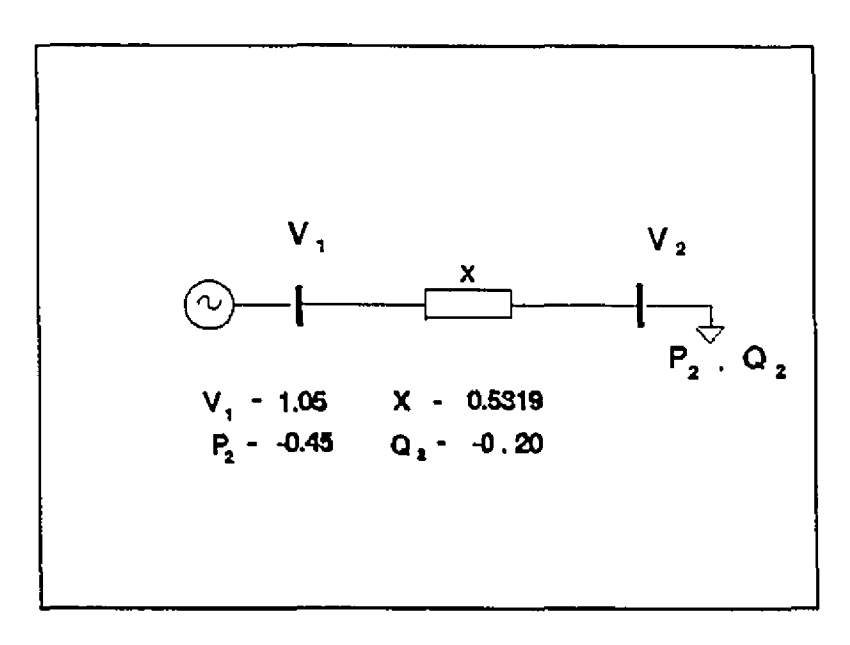


Figure 3.3. 2-Bus Network (p.u. system)

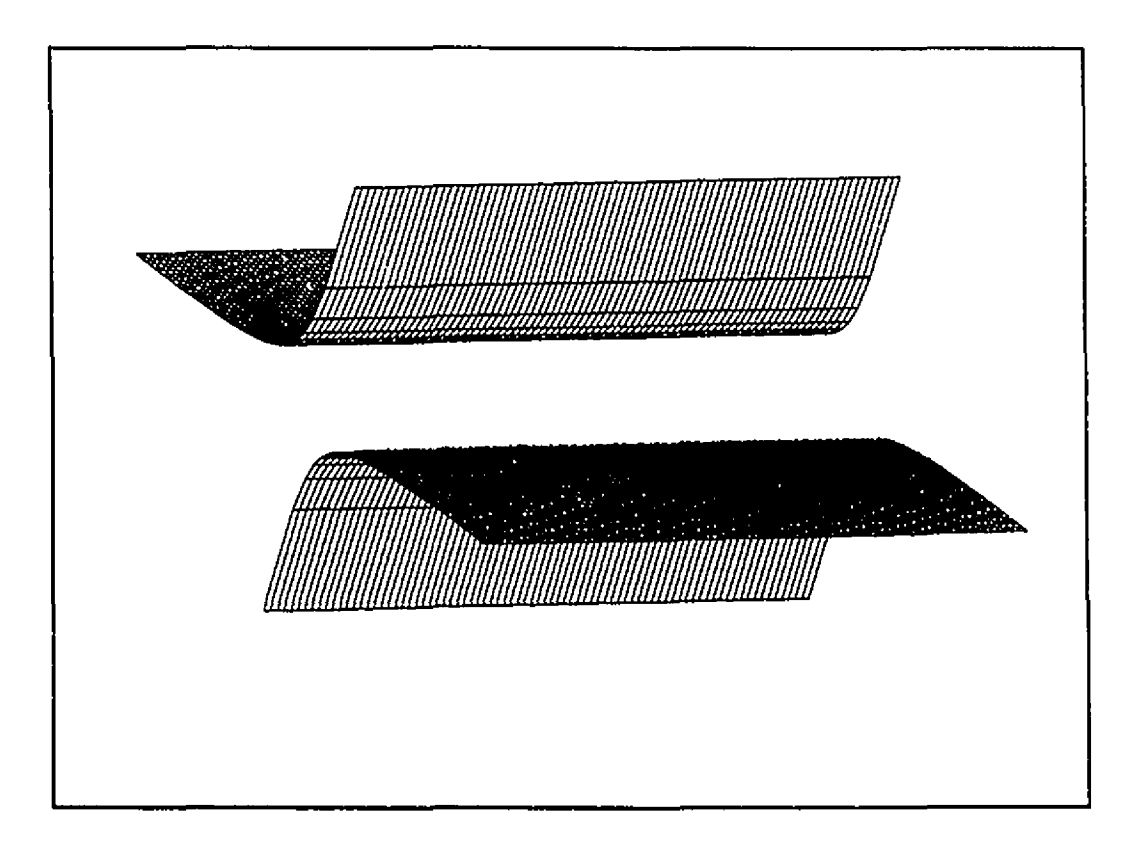
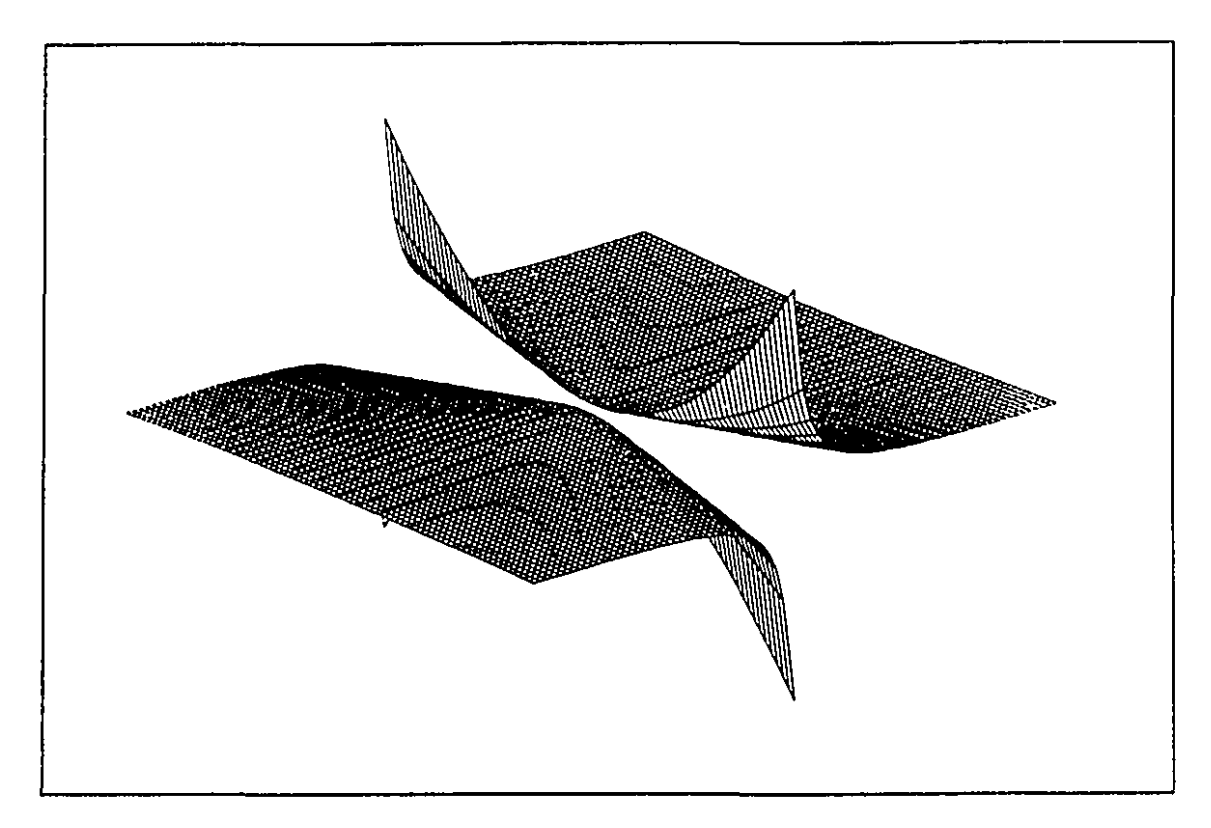
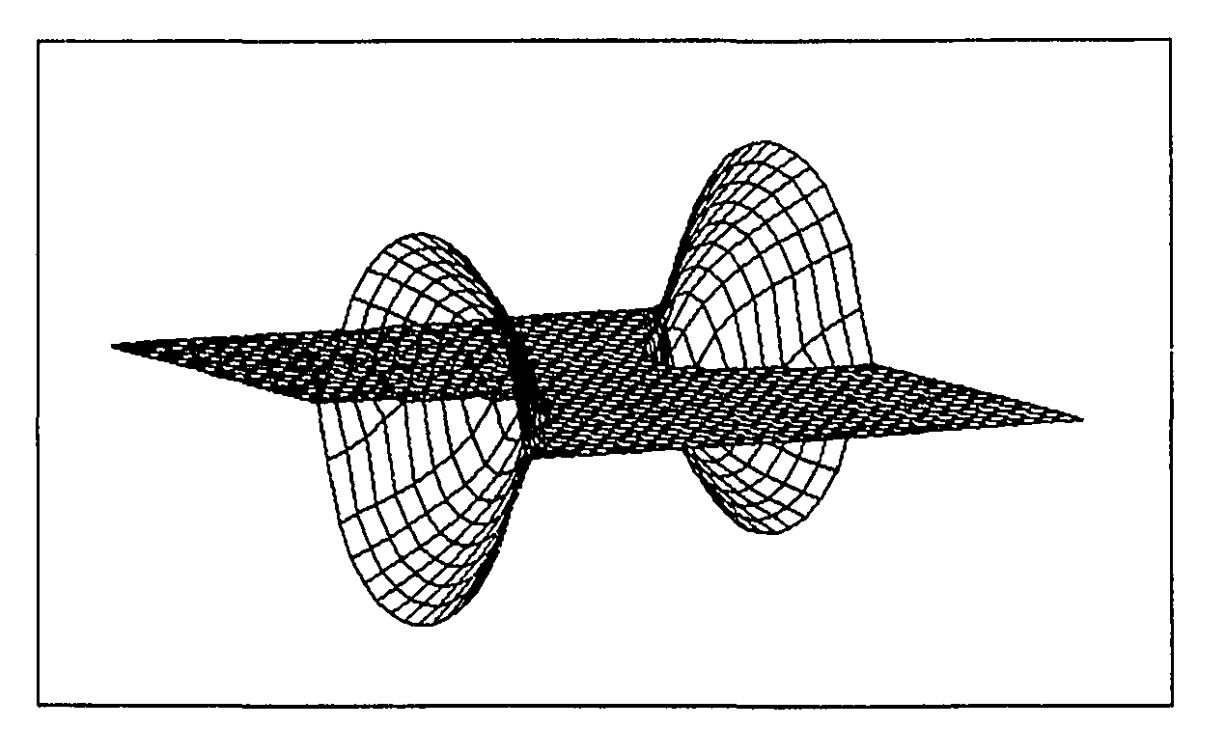


Figure 3.4. Surface Representing P_2 : $X P_2 = e_1 f_2 (e_1 = F(f_2))$

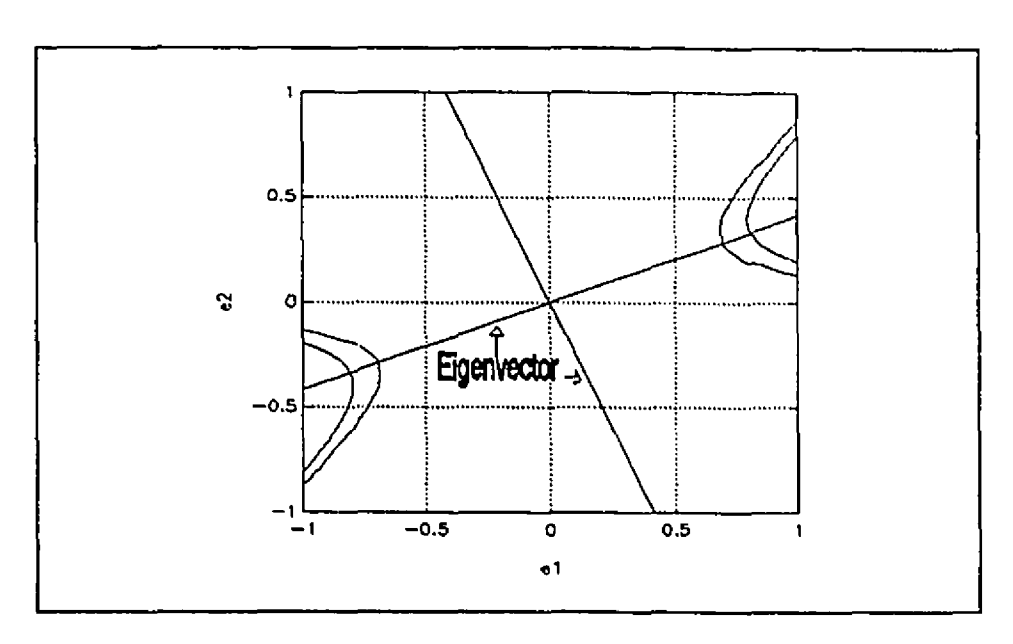


(a)
$$e_1 = F(e_2, f_2)$$

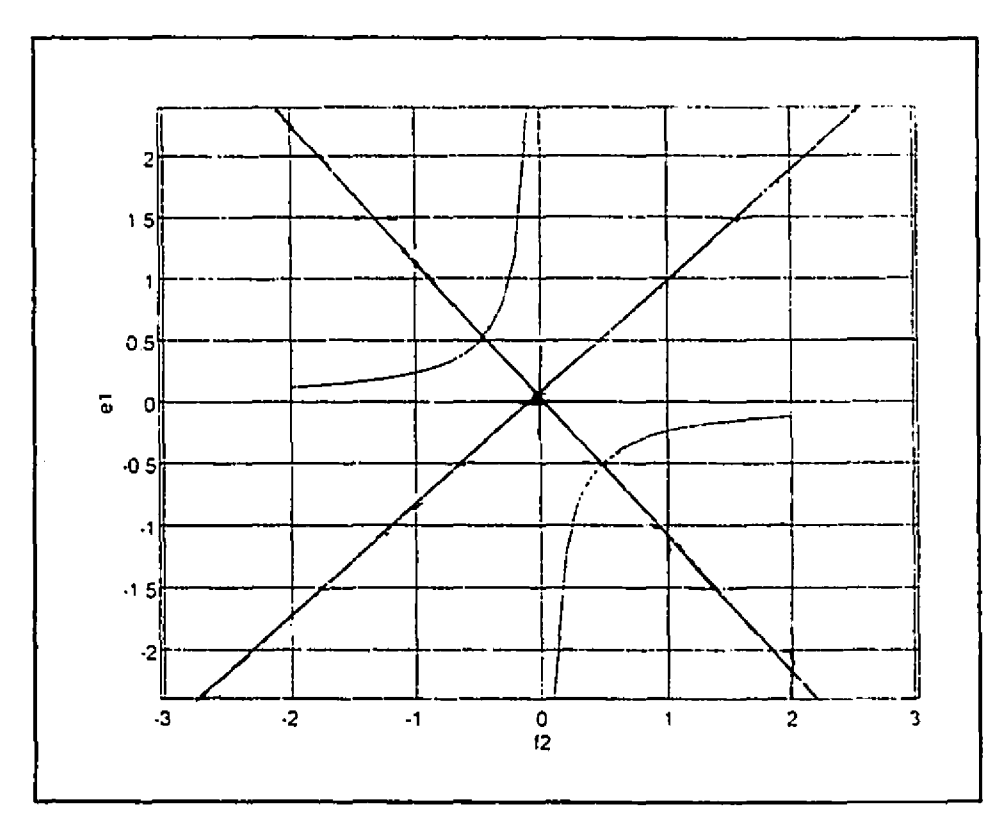


(b) $f_2 = F(e_1, e_2)$

Figure 3.5. Surface Representing Q_2 : $X Q_2 = e_2^2 + f_2^2 - e_1 e_2$



(a) Projection of 3.5b onto $e_1 - e_2$ plane



(b) Projection of 3.4 onto e_1 - f_2 plane

Figure 3.6. Projection of Surfaces Onto Co-ordinate Planes

Table 3.3. Eigenvalues and Eigenvectors of J_{Q2}

J_{Q2}	λ	1.88	2.2693	-0.3894
0 -0.94 0	v	0	-0.3827	-0.9239
-0.94 1.88 0		0	0.9239	-0.3827
0 0 1.88		1	0	0

Figures (3.6a) and (3.6b) show the projection of these surfaces onto the planes containing the eigenvectors.

The intersection of the three surfaces is shown in the $\mathbf{e_2}$ - $\mathbf{f_2}$ plane for values of $\mathbf{e_1}$ equal to 0 and 1.05. The circle in Figure 3.7 is the projection of the hyperboloid describing $\mathbf{Q_2}$ and the straight line is the projection of the hyperbolic cylinder describing $\mathbf{P_2}$. The intersection of the circle and straight line are therefore the intersection of the three surfaces and consequently, the two solutions of the load flow equations for this system.

Table 3.4. Load Flow Solutions for 2-Bus System

Solutions		Sum and Difference of Solutions		
1	2	(1 + 2)/2	(1 - 2)/2	
1.05	1.05	1.05	0	
0.8674	0.1825	0.5249	0.3421	
-0.228	-0.228	-0.228	0	

Although this example is rather simplistic, it provides a good insight into the general nature of the load flow solutions for more complex systems. For instance, Figure (3.7) demonstrates that the two solutions may be written as

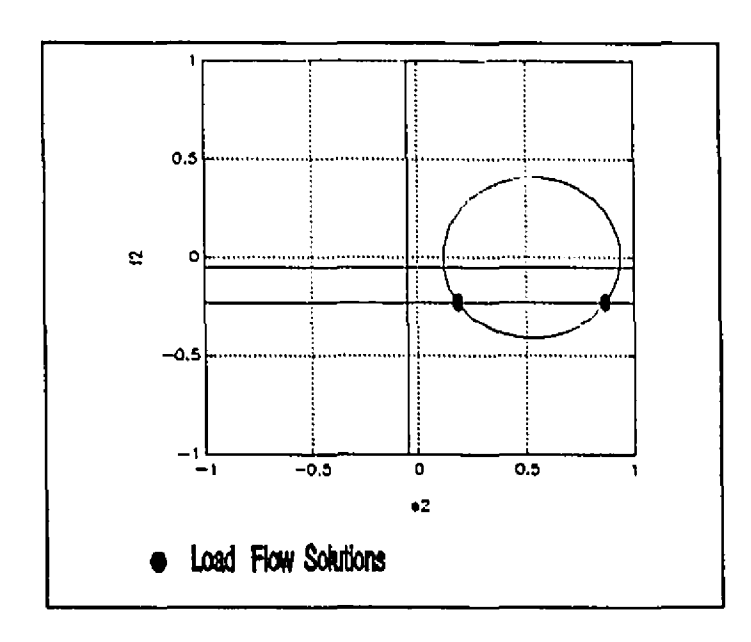


Figure 3.7. Intersection of Surfaces - Two Solutions

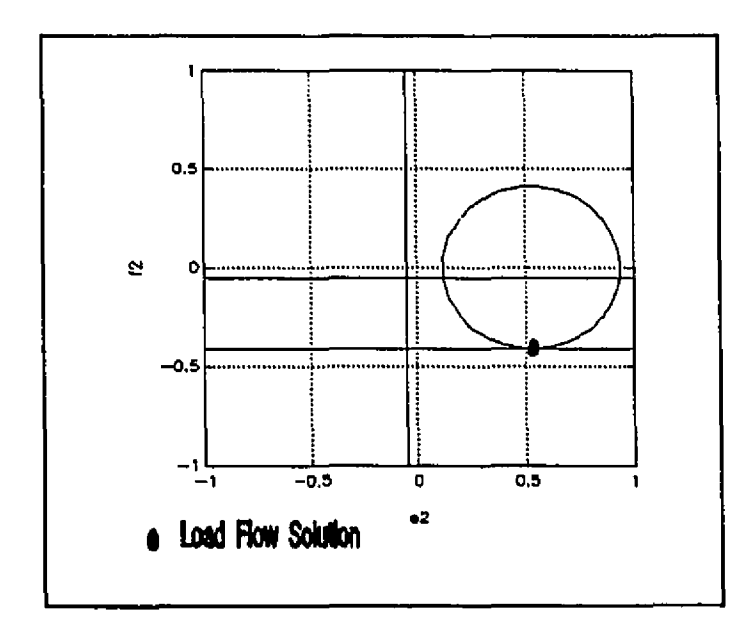


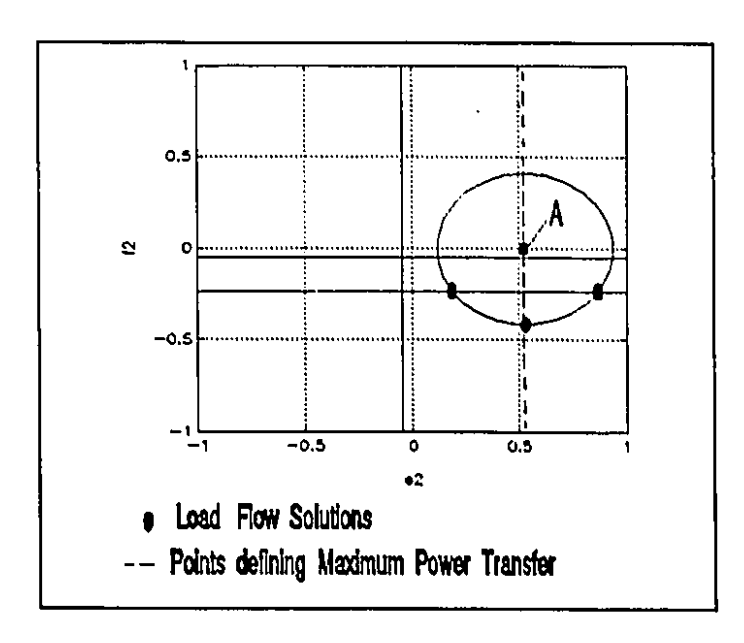
Figure 3.8. Intersection of Surfaces - One Solution

 $x_1 \pm x_2$. It is assumed that the multiple solutions for the multi-dimensional load flow problem are of the same form [3,9]. Note that x_1 is equal to one half the sum of the two solutions. The sum and difference of the two solutions each lie on a principal plane of the surface describing the reactive power.

Figure (3.8) shows how the solutions change when the real power demand is increased while the reactive power demand and slack bus voltage are assumed to remain constant. The point at which the solutions coincide determines the maximum real power that can be supplied for that level of reactive power demand and the given slack bus voltage. If the real power demand is increased further, the solution "disappears" and the load flow is said to be unfeasible.

At the point where there is only one solution (Figure 3.8), the surfaces describing the power injections share a common tangent. At the absolute maximum power transfer limit (A in Figure 3.9b), the surface describing the reactive power injection is tangent to the plane describing the voltage at the slack bus. Note that this point is also the centre of all the circles which represent the reactive power in the $\mathbf{e_2}$ - $\mathbf{f_2}$ plane (Figure 3.9a).

There are several such points in the voltage space, all lying on the midpoint of the segment connecting any two solutions (Figure 3.9a). Note that these points also lie on one of the principal planes of the surface describing the reactive power (Figure 3.5b). These points define different injections corresponding to maximum power transfer for various levels of real and reactive power. The injections are on a surface in the injection space that divides that space into a region where a real load flow solution is possible and another region where no real solutions can exist (Figure 3.9b).



(a) Voltage Space $(e_1 = 0, 1.05)$

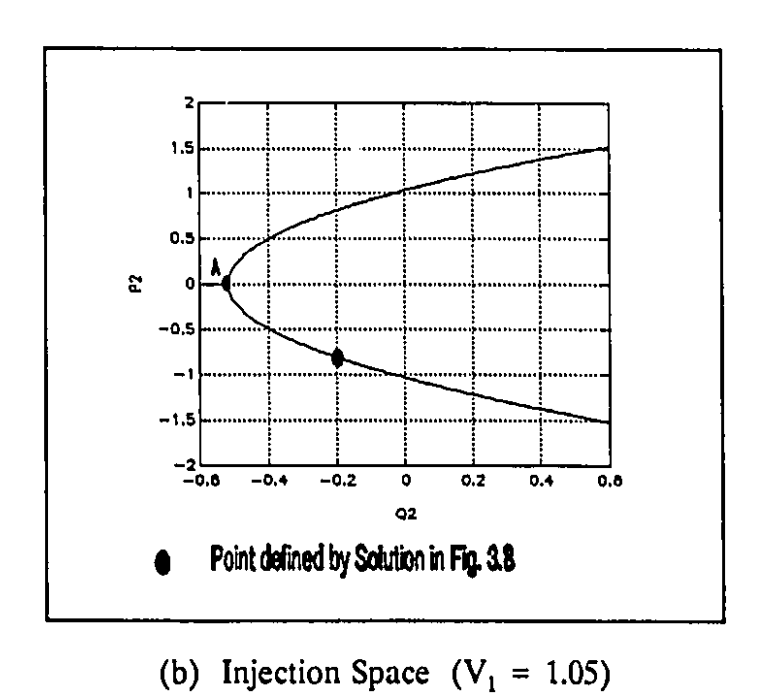


Figure 3.9. Points of Maximum Power Transfer

In a large practical system, the load may be increased in any number of ways. However, irrespective of the direction of load increase, a point will be reached where one or more of the power injections reach a maximum in that direction. That point is on a hypersurface in the injection space. At the corresponding point in the voltage space, at least two of the load flow solutions coincide and the jacobian matrix is singular.

3.10 Additional Properties of the Load Flow Equations

The load flow equations in rectangular co-ordinates are quite suited to analytical studies. Some of their properties will be used in the next chapter and they are summarised below.

Denote the load flow equations by

$$z = L(x) x \tag{3.31}$$

where z is a (2N-1) x 1 vector of specified injections and x is as previously defined and

$$L(x) = \begin{bmatrix} x^T J_1 \\ x^T J_2 \\ \vdots \\ x^T J_{2N-1} \end{bmatrix}$$
 (3.32)

Note that L(x) is also equal to one half of the load flow jacobian matrix and since the J_i matrices are symmetric

$$L(x_1) x_2 = L(x_2) x_1 (3.33)$$

for any two arbitrary vectors, x_1 and x_2 .

Any linear combination of the specified injections may be defined as

$$a^{T}Z = a^{T}L(x)x$$

$$= \left[\sum_{i=1}^{2N-1} (a_{i}x^{T}J_{i})\right]x$$

$$= x^{T}\sum_{i=1}^{2N-1} (a_{i}J_{i})x \qquad (3.34)$$

where a is an arbitrary (2N-1) x 1 vector. This expression can be written more compactly as

$$a^T L(x) x = x^T J(a) x (3.35)$$

where the meaning of J(a) is understood from (3.34).

CHAPTER IV

EXPERIMENTAL STUDIES ON THE LOAD FLOW FEASIBILITY REGION

4.1 Introductory Remarks

In order for power systems to operate normally, they must satisfy a number of constraints. The *load flow feasibility* constraints are, by far, the most restrictive of these because they define conditions on the specified injections (generations and loads) for which a system state (voltages) corresponding to these injections may be physically realised. In other words, the load flow feasibility constraints describe the relationship among the specified injections which guarantees a real voltage solution to the load flow equations. Such constraints arise because there are limits imposed on the specified injections by the system structure (as described by the bus admittance matrix and the bus types) and by the non-linear relationship between the power and voltage [9,25]. If these limits are violated, there would be no real solution to the load flow equations.

Load flow feasibility was first studied through the concept of feasibility regions by Tavora and Smith [19]. Since then, other authors [9,25,60,61] have used a variety of approaches to examine the question of feasibility. The pioneering works in [9,25,26] studied the load flow feasibility constraints through a load flow feasibility region defined in the space of real and reactive powers and voltage magnitude injections for a general power network. This was done using an analysis based on the generalised eigenvalue problem. More recent works [60,61] have used a power system model which includes the dynamic equations of the system in addition to the

Chapter IV: Experimental Studies on the Load Flow Feasibility Region load flow equations and have employed concepts from bifurcation theory to study feasibility conditions. In [60,61], feasibility regions are defined for fixed parameter values. In [60], the feasibility regions are defined in a space consisting of system components and operating parameters and in [61], the feasibility regions are considered in the space of real and reactive power demands.

The approach in [9,25,26] is adopted as the basis of the material presented in this chapter. Therefore, a load flow feasibility region is defined, in the space of power and voltage magnitude injections, for a power network consisting of a slack bus as well as load and voltage control buses. The methods of [9,25,26] will then be employed to conduct an empirical study of the characteristics of this region and their relationship to the multiple load flow solutions.

4.2 Definition and General Properties of R₂

4.2.1 Definition of R₂

The non-linearity of the load flow equations (z = L(x)x) limits the range of power injections that a power system can sustain. The load flow feasibility region, R_z , is then defined as the set of all injections, z, for which there is a real voltage solution, x, to these equations [9, 25,26]. The set R_z can therefore be described as

$$R_z = \{ z : z = L(x) x, (z, x) \in \mathbb{R}^{2N-1} \}$$
 (4.1)

Alternatively, R_z can be viewed as a mapping of the entire voltage space, x, into a subset of the injection space, z, through the function defined by the load flow equations [25,57]. Any injection, z, in R_z is said to be a feasible injection. As a result, the entire injection space may be considered to contain two regions: R_z , which

Chapter IV: Experimental Studies on the Load Flow Feasibility Region contains all feasible injections and another region of infeasible injections. The hypersurface separating these two regions is now defined as the boundary of R₂.

4.2.2 General Properties of R,

Using some characteristics of the load flow equations in rectangular coordinates, two general properties of the load flow feasibility region have been proposed [9,25]:

- (i) R₂ is a cone stretching to infinity with its vertex at the origin of the injection space
- (ii) R_z lies on or above a set of hyperplanes passing through the origin.

The first property is justified by the fact that if z is a vector of feasible injections, then ρz must also be feasible if ρ is a positive scalar. This is so because each injection can be written as

$$\rho z_i = (\pm \sqrt{\rho} x)^T J_i (\pm \sqrt{\rho} x) \qquad (4.2)$$

where J_i has dimension (2N-1) x (2N-1) and x is a solution of the load flow equations with z as the specified injections. Equation (4.2) implies that the feasibility of a vector z is independent of the length of the vector and as such R_z stretches to infinity. This property is important because it suggests that the characteristics of the load flow feasibility region may be determined by studying any "cross-section" of R_z that is representative of the entire region.

The second property stems from an assumption usually made in load flow studies, that at least one of the specified quantities is the voltage magnitude at the slack bus. In rectangular co-ordinates, this corresponds to specifying an injection which is the square of the voltage magnitude. Assume that z is of the form

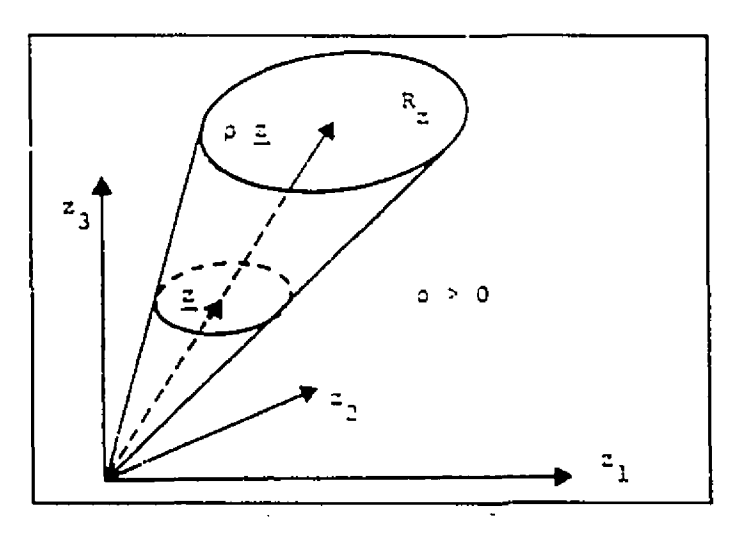


Figure 4.1. R_z is a cone of infinite length

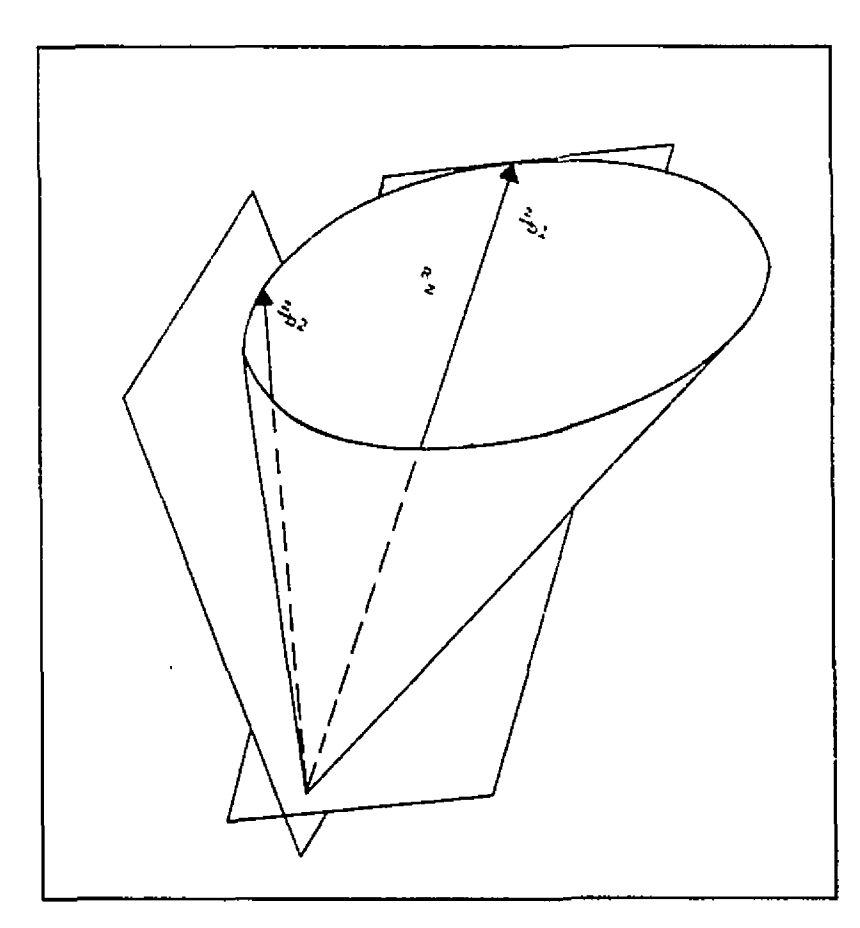


Figure 4.2. R_z lies on or above a set of supporting hyperplanes

Chapter IV: Experimental Studies on the Load Flow Feasibility Region

$$z = \begin{bmatrix} P \\ Q \\ V^2 \end{bmatrix} \tag{4.3}$$

where P, Q and V^2 are column vectors of the specified net real powers, net reactive powers and voltage magnitudes squared, respectively. Then for any feasible z, the following is true

$$a^T z \ge 0 \tag{4.4}$$

where a is a (2N-1) x 1 vector of zeroes except for a "1" in the position multiplying the component of z corresponding to the slack bus voltage squared. Equation (4.4) represents a hyperplane through the origin of the injection space which is tangent to R_z and is such that all vectors $z \in R_z$ lie on or "above" it.

There exist similar hyperplanes, one for each of the PV buses in the system, such that R_z lies on or above them. These hyperplanes characterise part of the boundary of R_z . The more interesting hyperplanes, though, are the ones which describe the feasibility constraints on the voltage magnitude as well as the real and reactive power injections.

4.3 Feasibility Surface P₂₀

4.3.1 Definition

It was mentioned that since R_z is a cone, its properties may be determined by studying a "cross-section" that characterises the whole region. If a hyperplane that cuts the entire boundary of R_z can be found, then the resulting intersection will constitute a valid "cross-section". The desired "cross-section", defined as the feasibility surface P_{z0} , is the intersection of R_z and the plane

Chapter IV: Experimental Studies on the Load Flow Feasibility Region

$$z_0^T z = k \quad \forall z \in R_z, z \neq 0, k < \infty$$
 (4.5)

where k is a positive constant and \mathbf{z}_0 is a constant vector perpendicular to the hyperplane. More precisely

$$P_{z0} = \{z : z \in R_z, z_0^T z = k, 0 < k < \infty\}$$
 (4.6)

It is important that all $z \in R_z$ satisfy (4.5) because this ensures that the feasibility surface, P_{z0} , is bounded in every direction. If some z do not satisfy (4.5), then the intersection of R_z and the hyperplane will be an open surface.

Using (3.35), equation (4.5) can be re-written in terms of x as

$$x^T J(z_0) x = k \qquad \forall x \in \mathbb{R}^{2N-1}$$
 (4.7)

4.3.2 Finding z_0

In order to define P_{z0} , a vector \mathbf{z}_0 as described in the preceding section must be found. The existence of such a vector for a general power network (though not for the lossless case) has been proven and the following heuristic method to find \mathbf{z}_0 has been developed [26].

Since the square of the voltage magnitude is always positive, the components of z_0 multiplying those injections are made equal to one. It remains, therefore, to find suitable constants to multiply the real and reactive power injections such that (4.5) is satisfied.

Numerical experience indicates that a positive constant multiplying the reactive power injections and zero multiplying the real power injections will satisfy

Chapter IV: Experimental Studies on the Load Flow Feasibility Region

(4.5). For system sizes ranging from 2 buses to 118 buses, the following z_0 satisfy (4.5)

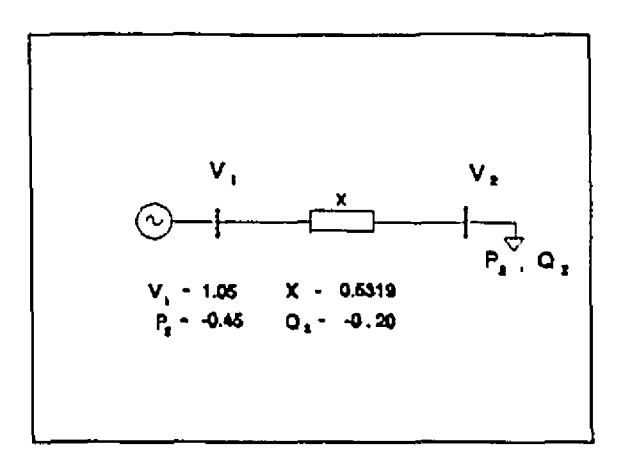
$$z_0 = \begin{bmatrix} 0 \\ 0.01 \\ 1 \end{bmatrix} \tag{4.8}$$

where the dimension of z_0 is the same as that of z as defined in (4.3). From equation (4.7), it can be deduced that when the matrix $J(z_0)$ is positive definite, the hyperplane in (4.5), will cut the entire boundary of R_z . The requirement that $J(z_0)$ be positive definite provides a means of verifying that z_0 is suitable.

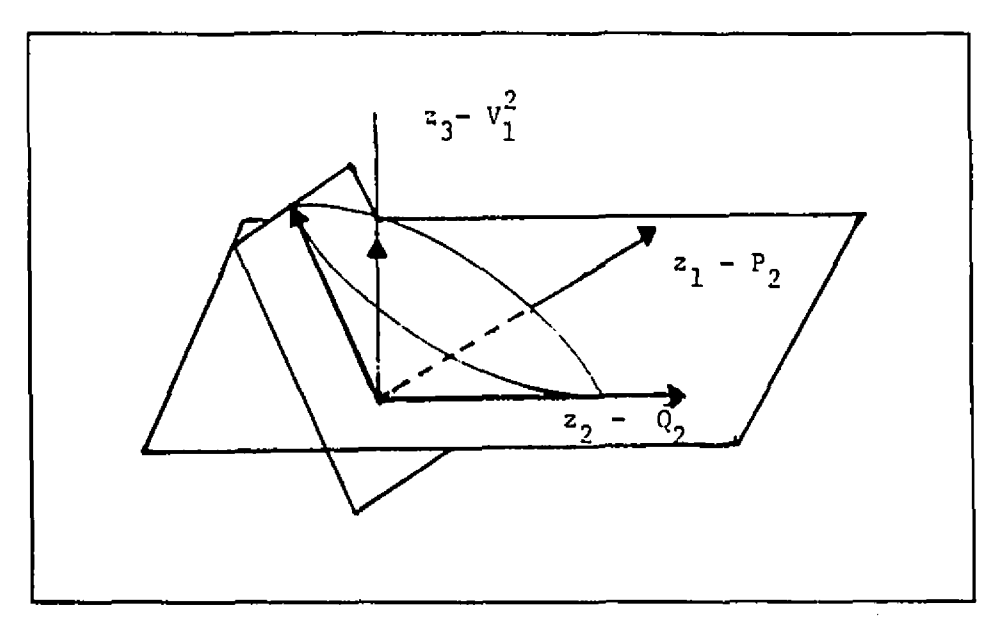
The rationale for choosing z_0 as defined in (4.8) is that in load flow studies, the constraints on the reactive power injections are usually the most prohibitive and very often load flow feasibility is violated when reactive power sources exceed their limits. Also, keeping in mind the definition of $J(z_0)$ (3.34), (3.35) and comparing the magnitude of the ratio λ_+ / λ_- where λ_+ , λ_- are the positive and negative eigenvalues of J_i , it is evident that this ratio is much larger for J_Q than for J_P . It seems reasonable to assume, then, that the proposed z_0 would prove to be satisfactory.

4.4 Illustrative Example

Given the fact that the load flow feasibility region is defined in a (2N-1)-dimensional space where N is the number of buses in the system, it is impossible to obtain a visualisation of the concepts discussed above except for 2- and 3-bus networks. In this section, a system consisting of a lossless transmission line connected by a slack bus and a load bus (Figure 4.3) will be used to illustrate some of the main ideas.



(a) 2-Bus Network



(b) Feasibility Region of a Lossless 2-Bus Network

Figure 4.3.

The load flow feasibility constraints are well understood for such a simple system. In fact, analytical expressions describing R_z can be obtained and are given by

$$(V_1^2)^2 + 4XQ_2V_1^2 - 4X^2P_2^2 \ge 0 (4.9a)$$

and

$$V_1^2 \ge 0$$
 (4.9b)

The nature of this load flow feasibility region can be studied by rewriting (4.9a) as

$$[P_2 \quad Q_2 \quad V_1^2]^T \begin{bmatrix} -4X^2 & 0 & 0 \\ 0 & 0 & 2X \\ 0 & 2X & 1 \end{bmatrix} \quad [P_2 \quad Q_2 \quad V_1^2] \quad \geq \quad 0 \quad (4.10)$$

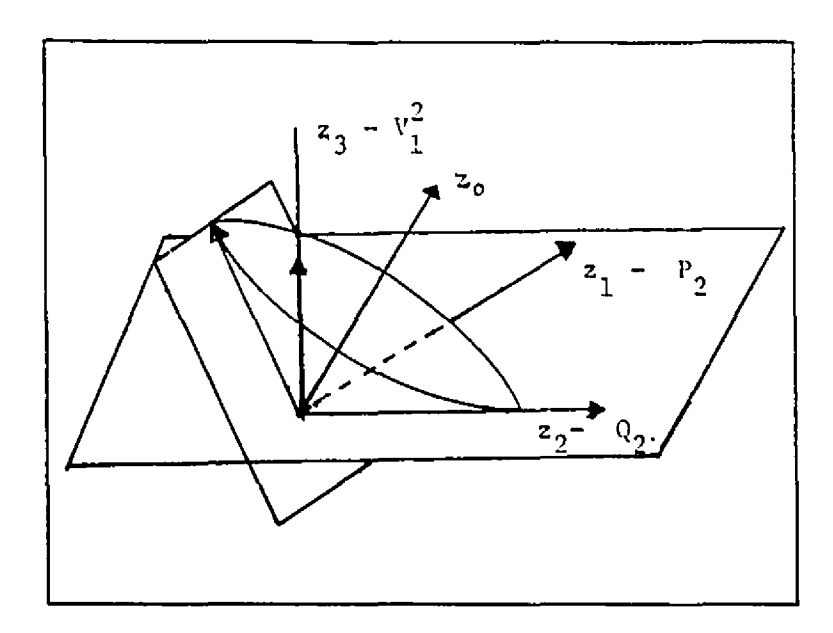
and by examining the eigenvalues and eigenvectors of the matrix in (4.10).

Equation (4.10) is re-written for the system in Fig. (4.3a) and the eigenvalues and eigenvectors of the matrix, referred to as A, are found.

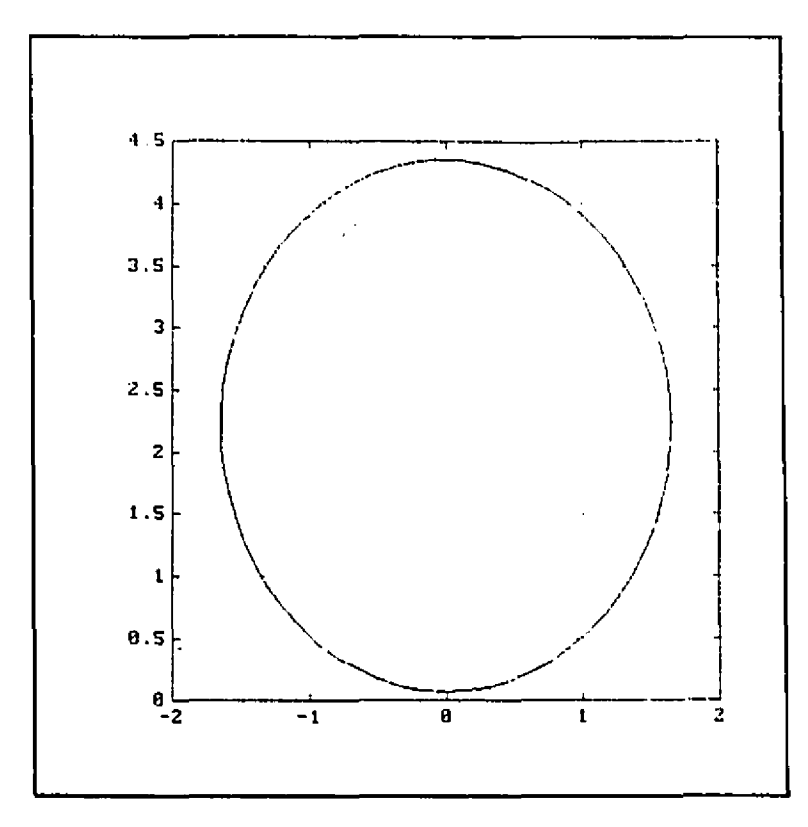
$$z^{T} \begin{bmatrix} -1.132 & 0 & 0 \\ 0 & 0 & 1.064 \\ 0 & 1.064 & 1 \end{bmatrix} z \ge 0$$
 (4.11)

Table 4.1. Eigenvalues and Eigenvectors of A

λ	-1.1318	-0.6755	1.6755
v	1	0	0
	0	-0.8442	0.5360
	. 0	0.5360	0.8442



(a) Feasibility Region with z_0



(b) Feasibility Surface P_{z0} in the Plane $z_0 = 1$

Figure 4.4.

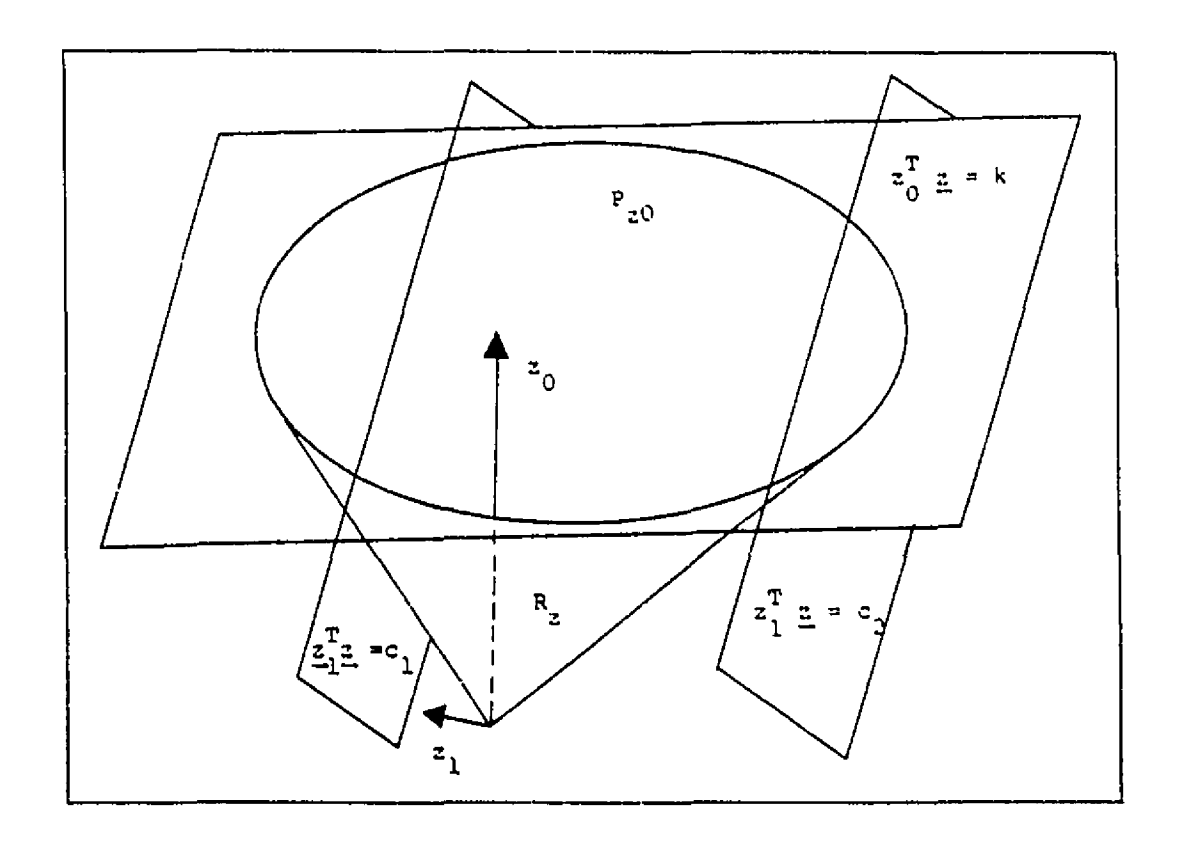
Using well-known properties of 3-dimensional quadratic surfaces, it is seen that the surface described by (4.11) is a hyperboloid of two sheets, centred at the origin. The restriction on $(V_1)^2$ limits the feasibility region to the intersection of only one of the sheets of the hyperboloid and the plane $(V_1)^2 = 0$ (Figure 4.3b).

In this simple example, $\mathbf{z_0}$ can be chosen intuitively as the eigenvector corresponding to the positive eigenvalue (Figure 4.4a). This eigenvector is a principal axis of the surface and is also the only principal axis that the surface intersects. Any plane to which this eigenvector is perpendicular will therefore cut the entire boundary of $\mathbf{R_z}$. Note that this rather obvious choice of $\mathbf{z_0}$ i.e. [0 0.5360 0.8442]^T, has the same form as would a $\mathbf{z_0}$ found by the heuristic method. The corresponding matrix $\mathbf{J}(\mathbf{z_0})$ is positive definite.

The feasibility surface, P_{z0} can also be determined analytically for this example. Taking $\mathbf{z_0}^T \mathbf{z} = 1$ and changing to a new co-ordinate system defined by the eigenvectors of A, P_{z0} is shown (Figure 4.4b) to be an ellipse in the plane $\mathbf{z_0} = 1$.

4.5 Supporting Hyperplanes of R.

In the ensuing discussion, the feasibility surface, P_{z0} , is assumed to be representative of the load flow feasibility region, R_z , and is used in a systematic procedure to locate the supporting hyperplanes of R_z . These hyperplanes are of the form $\mathbf{a}^T \mathbf{z} = 0$ and may be found by searching over the feasibility surface, P_{z0} in any arbitrary direction \mathbf{z}_1 provided \mathbf{z}_1 is not parallel to \mathbf{z}_0 . The vector \mathbf{z}_1 defines another hyperplane $\mathbf{z}_1^T \mathbf{z} = \mathbf{c}$ which will intersect the feasibility surface for different values of \mathbf{c} (Figure 4.5).



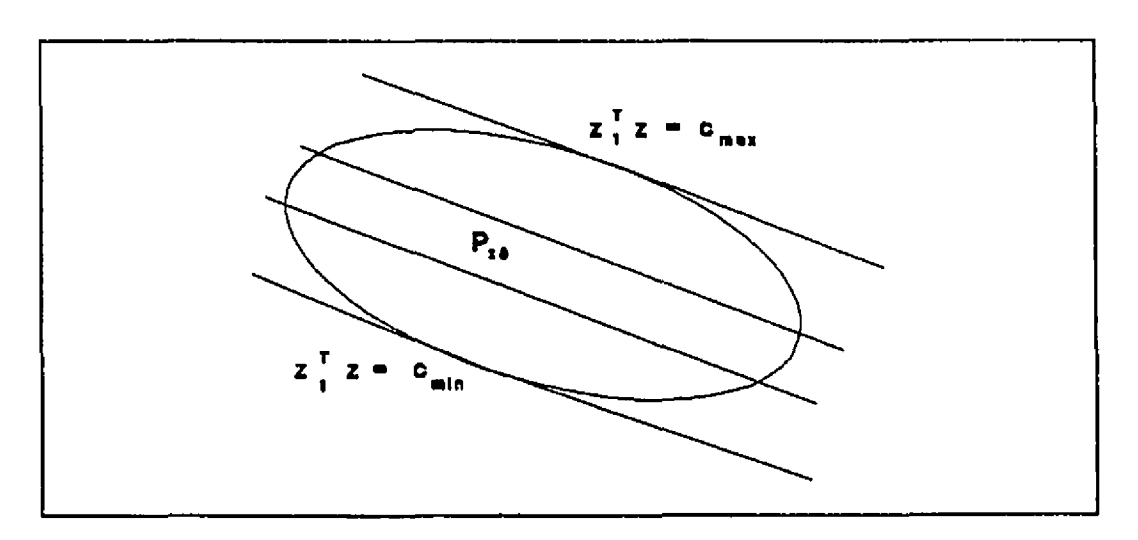


Figure 4.5. Intersection of P_{z0} and the Plane $z_0^T z = c$

At the minimum and maximum possible values of c, the plane,

 $\mathbf{z_1}^T \mathbf{z} = \mathbf{c}$ will be tangent to the feasibility surface, P_{z0} . Using this fact, the hyperplanes tangent to R_z can be found by solving the following optimisation problem [9,25,26]

$$\begin{array}{llll}
\max \\
z \in R_z & z_1^T z = c \\
s.t. & z_0^T z = k
\end{array}$$
(4.12)

The problem can be re-formulated in terms of x by using (3.34) and (3.35). This formulation has an advantage in that it guarantees that z will be in R_z . Equation (4.12) becomes

$$\begin{array}{llll}
\max_{\boldsymbol{x} \in \mathbb{R}^{2N-1}} & \boldsymbol{x}^T J(\boldsymbol{z}_1) & \boldsymbol{x} = \boldsymbol{C} \\
s.t. & \boldsymbol{x}^T J(\boldsymbol{z}_0) & \boldsymbol{x} = \boldsymbol{k}
\end{array} \tag{4.13}$$

Forming the Lagrangian [62] of (4.13) and differentiating with respect to x results in

$$\frac{\partial L}{\partial x} = 2 \left[J(z_1) x - \lambda J(z_0) x \right] \tag{4.14}$$

The optimisation problem then reduces to finding the solution to

$$[J(z_1) - \lambda J(z_0)]x = 0 (4.15)$$

which is the equation of the generalised eigenvalue problem [63].

The eigenvalues of (4.15) are all real and finite because the matrices are real and symmetric and $J(z_0)$ is positive definite [63]. Let the maximum and minimum these eigenvalues be λ_{max} and λ_{min} respectively. Then for λ_{max} and λ_{min}

$$X^{T} \left[J(z_{1}) - \lambda_{\max} J(z_{0}) \right] X \leq 0$$
 (4.16)

$$x^{T}[J(z_{1}) - \lambda_{\min}J(z_{0})] x \ge 0$$
 (4.17)

This implies that the matrix in (4.16) is negative definite and the one in (4.17) is positive definite.

Re-writing the equations in terms of z (3.35), the following expressions are obtained

The condition in (4.18) may be written more compactly as

$$a^T z \ge 0 \quad \forall z \in R_z$$
 (4.19)

where $\mathbf{a} = \lambda_{\text{max}} \mathbf{z_0} - \mathbf{z_1}$ or $\mathbf{z_1} - \lambda_{\text{min}} \mathbf{z_0}$. This is a necessary condition for load flow feasibility and the equality defines two supporting hyperplanes of R_z for each direction $\mathbf{z_1}$.

4.6 Security Considerations Involving R.

4.6.1 Security Region

Some of the supporting hyperplanes of R_z can be used to define a security region around R_z since injections which fail to satisfy (4.19) are not feasible. For a particular network structure, several vectors a can be calculated and for any injection $\mathbf{z_g}$, if $\mathbf{a^T} \mathbf{z_g} > 0$, then $\mathbf{z_g}$ is not feasible. This security region would be best suited to a very heavily-loaded system which has an operating point close to the boundary of R_z because usually, other operating constraints become active before load flow feasibility is violated.

4.6.2 Effect of Contingencies on R,

The supporting hyperplanes can also be used to approximate the "size" of R_z [9]. The angle between the two vectors defining a, can be considered as a measure of the "width" R_z in the given direction z_i . It is reasonable to assume that network contingencies will reduce the load flow feasibility region and it is expected that this will be reflected in the angle between the supporting hyperplanes of the new region.

4.6.3 Example

The 5-bus network in Figure 4.6 will be used to show the effect of a single line outage on the angles between the supporting hyperplanes of R_z . Line #1-3 is removed. The different search directions are given in Table 4.2.

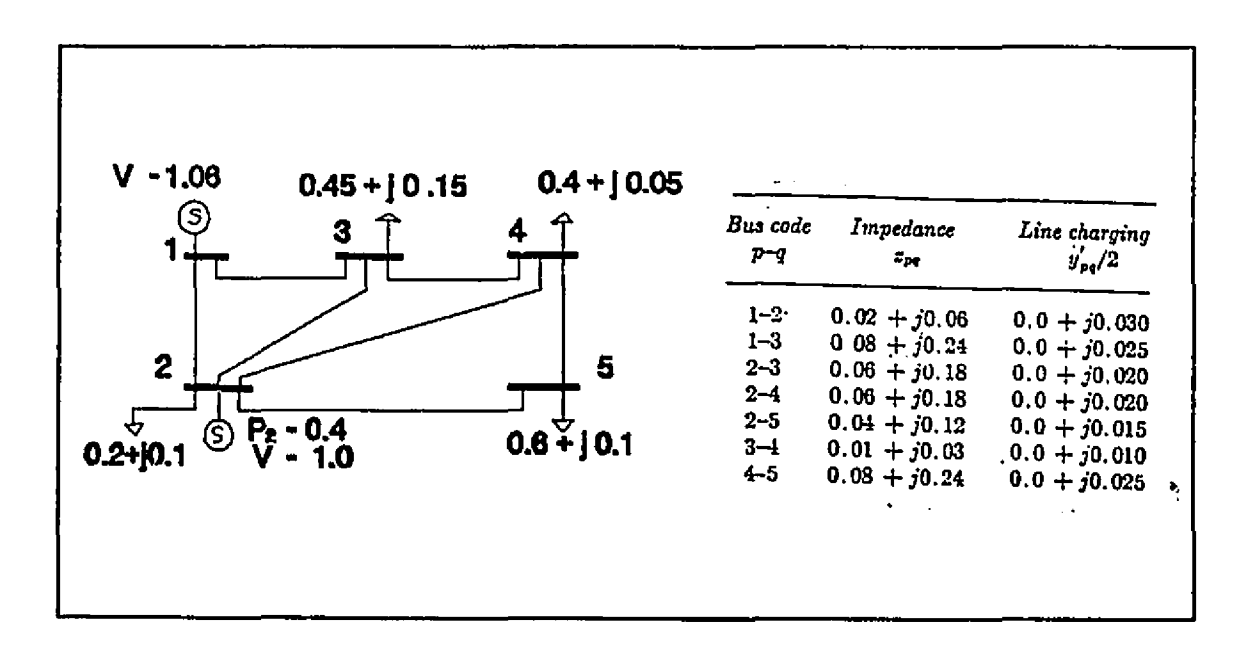


Figure 4.6. 5-Bus Network

Table 4.2. Various Search Directions z_1

	$\mathbf{z_1} = [P_2 \ P_3 \ P_4 \ P_5 \ Q_3 \ Q_4 \ Q_5 \ V_2^2 \ V_1^2]^T$									
A	-0.1	-0.1	-0.1	-0.1	-0.1	-0.1	-0.1	0	0	· · -
В	0.2	-0.45	-0.40	0.6	60 -0.	15 -0.	05 -0	.10	1 1.1236	
С	1	1	1	1	0	0	0	1	1	
D	1	1	1	1	1	1	1	1	1	
Е	0.01	5 -2.1	53 -2.4	177 -1	.568 -	2.325	-2.665	-1.3	34 7.934 -5.79	1
F	0	0	0	0	-2	-2	-1	0	0	
G	1	1	1	1	0	0	0	0	0	
Н	0	0	0	0	0	0	0	1	1	
I	0.20	-0.45	5 -0.4	0 -0.	60 -0	.16 -0	.06 -	0.11	0 0.1236	

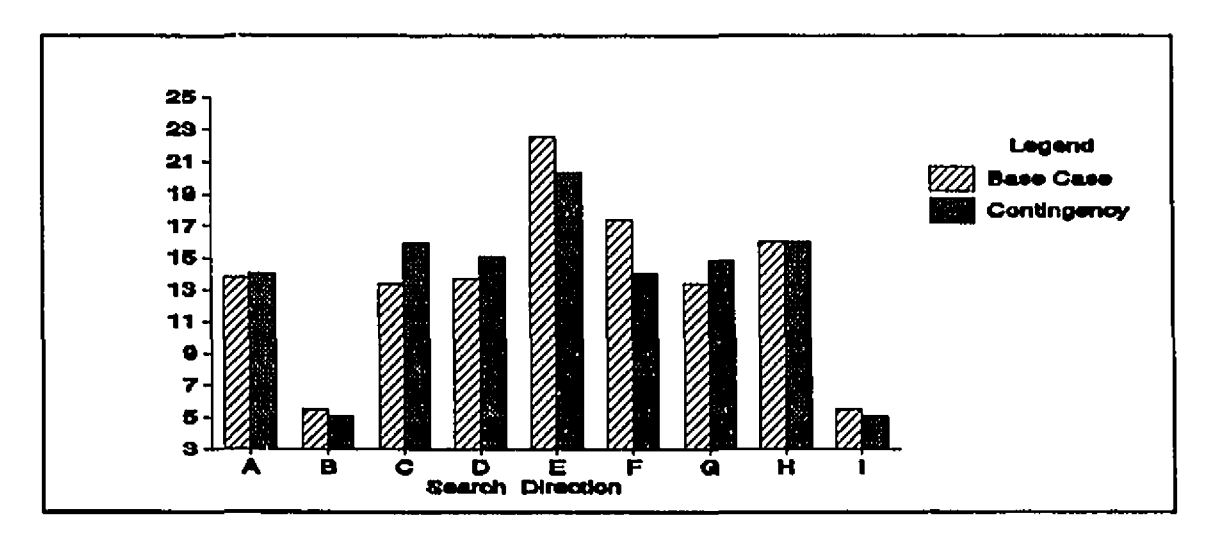


Figure 4.7. Angle between Extreme Supporting Hyperplanes of $R_{\rm z}$ - Base Case and Single Line Outage

Since the size of the feasibility region is expected to decrease with the removal of the line, the angle between \mathbf{a}_{max} and \mathbf{a}_{min} should be larger in the case of the contingency than in the base case. This is seen to be true for some of the search directions. The opposite is true when the direction includes reactive power demand (B,E,F,I). It is also evident that this is not a very severe contingency because the angles for the base case and the contingency are almost equal.

4.7 Structure of the Voltage Space

4.7.1 Solution of the Generalised Eigenvalue Problem

Recall that the dimension of the J_i matrices is (2N-1) x (2N-1) and the reference angle has been assumed, without loss of generality, to be equal to zero. As a result, the solution of the generalised eigenvalue problem of (4.15) yields (2N-1) real eigenvalues and their corresponding eigenvectors. These eigenvalues may or may not be distinct depending on z_0 , z_1 and the topology of the network.

The maximum and minimum of these eigenvalues, λ_{max} and λ_{min} , have been used to define hyperplanes which are tangent to R_z (4.19). The eigenvalues in between these two extremes will be referred to as *intermediate eigenvalues* and the focus of this section is to examine how they can be used to obtain a better understanding of the nature of the load flow feasibility region.

4.7.2 Singular Surfaces in the Voltage Space

Each eigenvector defines a point in the voltage space, x_s , at which the load flow jacobian is singular. This can be seen from the following: For any arbitrary vectors z_1 and z_2 ,

$$J(z_1) + J(z_2) = J(z_1 + z_2)$$
 (4.20)

Thus, using (4.20), equation (4.15) can be re-written as

$$J(z_1 - \lambda z_0) x_s = 0 (4.21)$$

which implies that $J(z_1-\lambda z_0) = J(a)$ is singular. But from (3.35),

$$J(a) x_s = [L(x_s)]^T a$$
 (4.22)

This means that $[L(x_s)]^T$ is also singular and the vector a lies in its null space. Since $[L(x_s)]^T$ is singular, so are L(x) and the load flow jacobian which is equal to one half of $L(x_s)$.

For a fixed z_0 , each different search direction z_1 produces a different set of eigenvalues and their associated eigenvectors, x_s . The set of all vectors, x_s , describe a collection of points in the voltage space where the load flow jacobian is singular. These points will be referred to as singular surfaces. Of course, the existence of these surfaces is well known and their characteristics have been documented [15,19,60]. The approach presented here facilitates the experimental study of these surfaces.

Consider the singular matrix $L(x_s)$. Then, there exist vectors r, such that

$$L(x_s) r = 0 (4.23)$$

as well as vectors I such that

$$[L(x_s)]^T I = 0 (4.24)$$

The vectors \mathbf{r} and \mathbf{l} are known as the right and left eigenvectors, respectively, of $L(\mathbf{x}_s)$. Note that the vector \mathbf{a} defined in (4.19) is just a scalar multiple of \mathbf{l} . The vectors \mathbf{r} and \mathbf{l} are unique when the nullity of $L(\mathbf{x}_s)$ is equal to one.

Since L(x)r = L(r)x, it is clear that r also defines a singular matrix L(r) and as a result, r is also a singular point. The singular surfaces in the voltage space can therefore be considered to consist of the set of all singular points, x_s , and their associated right eigenvectors, r.

4.7.3 Experimental Results

The results of numerical simulations done on the 5-bus system in Figure 4.6 are now presented. Due to space restrictions, results from only one search direction, $\mathbf{z}_1 = [-0.1 \ -0.1 \ -0.1 \ -0.1 \ -0.1 \ -0.1 \ -0.1 \ 0]^T$, are shown. The vector \mathbf{z}_0 is defined as $[0\ 0\ 0\ 0\ 0.01\ 0.01\ 0.01\ 1\ 1]^T$. The eigenvalues, λ , and their associated eigenvectors, \mathbf{x}_s along with the corresponding right eigenvectors, \mathbf{r} , and left eigenvectors, \mathbf{l} , of the matrices $\mathbf{L}(\mathbf{x}_s)$ are given in Table 4.3.

4.7.3.1 Magnitude of the Eigenvalues

In the simulations carried out for different search directions, z_1 , the magnitudes of six of the nine eigenvalues were approximately equal to each other and larger than the other three. This is illustrated in Table 4.3 for one direction. In simulations done on larger systems (14, 30, 57 and 118 bus), it was also found that approximately two-thirds of the (2N-1) eigenvalues had very similar magnitudes.

Table 4.3. Eigenvalues, Singular Points, Right and Left Eigenvectors of L(x,)

1 aute 4.5.	cigenvaiues,	amania ,	omes, regne and		nicators or D(xg)				
λ	0.813	-1.064	-0.294	-13.405	-13.393	-13.351	-13.346	-13.336	-13.337
								1	
x ₁ =	0.6234	-0.5357	0.0000	-0.0089	0.0000	0.0066	0.0000	0.0000	0.0050
e ₁	0.0234	0.2517	0.6764	-0.0043	-0.135	-0.0018	-0.0017	-0.0002	-0.0004
e ₂	0.2243	0.1066	0.2918	-0.0036	0.5521	0.0007	-0.4766	0.6925	0.0001
C₃ C₄	0.2183	0.1321	0.3117	-0.0035	0.5860	0.0004	-0.4230	-0.7203	-0.0003
II .	0.2019	0.2001	0.3642	-0.0028	0.5930	-0.9014	0.7707	0.0401	0.0001
e ₅ f ₂ f ₃	-0.4869	-0.6035	0.2871	0.0125	-0.0046	0.0053	-0.0006	-0.0001	0.0011
f_	-0.2414	-0.2257	0.1981	-0.6190	-0.0026	0.4039	0.0005	-0.0002	0.3127
f ₄	-0.2483	-0.2516	0.2116	-0.6086	-0.0028	0.2134	0.0005	0.0002	-0.8971
f_s	-0.2660	-0.3201	0.2473	-0.4961	-0.0028	-0.8895	-0.0009	0.0000	0.3122
r =	0.0000	0.0000	0.7720 0.244	0.0000	-0.985 -0.002	0.0000	-0.991 0.005	0.9991 -0.018	0.0000
C ₁	-0.6321	0.4083	0.0506 -0.285	0.0125	0.000 0.005	-0.0053	0.0000 0.001	0.0000 0.000	-0.0011
c_2 c_3	-0.4167	0.1216	0.4176 -0.076	-0.6191	-0.144 0.002	-0.4039	-0.114 0.000	0.0374 -0.001	-0.3127
e ₄	-0.4164	0.1183	0.3863 -0.099	-0.6086	-0.097 0.003	-0.2134	-0.068 0.000	0.0106 -0.000	0.8971
	-0.3996	0.1539	0.2476 -0.181	-0.4961	-0.019 0.003	0.8895	-0.011 0.001	0.0004 0.000	-0.3122
e ₅ f ₂ f ₃	-0.2750	0.1703	-0.119 0.672	0.0043	-0.000 -0.013	-0.0018	0.0000 -0.002	0.0000 -0.000	-0.0004
l ĉ	-0.0282	0.5557	0.0342 0.317	0.0024	-0.001 0.552	0.0000	-0.002 -0.477	0.0121 0.692	0.0000
l Ē.	-0.0465	0.5360	0.0322 0.337	0.0027	-0.001 0.586	-0.0002	-0.002 -0.423	-0.013 -0.720	-0.0004
f ₅	-0.1230	0.3946	-0.001 0.382	0.0026	-0.001 0.593	-0.0015	0.0041 0.771	0.0007 0.040	0.0001
] =									
P ₂	0.0846	-0.0656	0.2542 0	-0.0053	0.0075 0	-0.0053	0.0075 0	0.0075 0	-0.0053
P ₃	0.0846	-0.0656	0.2542 0	-0.0053	0.0075 0	-9.0053	0.0075 0	0.0075 0	-0.0053
P ₄	0.0846	-0.0656	0.2542 0	-0.0053	0.0075 0	-0.0053	0.0075 0	0 0075 0	-0.0053
P ₅	0.0846	-0.0656	0.2542 0	-0.0053	0.0075 0	-0.0053	0.0075 0	0.0075 0	-0.0053
Q ₃	0.0915	-0.0586	0.2467 0	0.0018	-0.0025 0	0.0018	-0.0025 0	-0.0025 0	0.0018
Q ₄	0.0915	-0.0586	0.2467 0	0.0018	-0.0025 0	0.0018	-0.0025 0	-0.0025 0	0.0018
	0.0915	-0.0586	0.2467 0	0.0018	-0.0025 0	0.0018	-0.0025 0	-0.0025 0	0.0018
V_{2}^{2}	0.6878	0.6973	-0.748 0	0.7071	-0.9999 0	0.7071	-0.9999 0	-0.9999 0	0.7071
V_{1}^{2} V_{1}^{2}	0.6878	0.6973	0 1	0.7071	0 1	0.7071	0 1	0 1	0.7071
<u> </u>	<u></u>								

4.7.3.2 Nullity of the Singular Jacobian

The simulations reveal that when the solution of (4.21) produces distinct eigenvalues, the eigenvectors, x_s , associated with N of the (2N-1) eigenvalues, including λ_{max} and λ_{min} , define jacobian matrices with nullity one.

4.7.3.3 Observations on the Right and Left Eigenvectors

It can be seen that the right eigenvector, \mathbf{r} , of each matrix, $L(\mathbf{x}_s)$, with nullity one has the component corresponding to the slack bus, $\mathbf{e_i}$, equal to zero. This observation will become significant in a later discussion on multiple load flow solutions. Another observation is that the \mathbf{x}_s 's corresponding to eigenvalues of similar magnitudes and their associated \mathbf{r} 's are orthogonal to each other.

Note that there are only four distinct left eigenvectors (not including the trivial one which has only one non-zero element). This implies that the nine injections described by the vectors \mathbf{x}_s can lie on only four different hyperplanes. Also, the matrices, $\mathbf{L}(\mathbf{x}_s)^T$, with nullity greater than one are the ones with two vectors, \mathbf{l} , spanning their null space. One of these vectors is on the plane $\mathbf{V}_s^2 = 0$ and the other is perpendicular to it.

4.8 Singular Surfaces of R.

Each of the singular surfaces in the x-space is mapped by the function: z = L(x)x, to a corresponding surface in the injection space. These surfaces in the z-space are referred to in the literature as bifurcation surfaces and may demonstrate different types of bifurcation phenomena [20]. In general, though, they are classified as saddle-node bifurcation surfaces [60,61].

So, although the precise geometric characteristics of R_z for a general power network have not been proven, R_z is known to contain these singular surfaces and their intersections. The approach used in this work provides a means of locating arbitrary points on these singular surfaces in R_z .

4.8.1 Boundary of R,

The boundary of R_z has been defined as a hypersurface separating the injection space into regions of feasible and infeasible injections and it is therefore regarded as the outermost surface of the feasibility region. Injections on that surface are denoted by z_b and are obtained from eigenvectors, x_b , associated with the maximum and minimum eigenvalues.

As mentioned in Section 4.6.2, the angle between the two vectors, \mathbf{a} , which are perpendicular to the supporting hyperplanes of \mathbf{R}_z (and consequently, to the boundary injections \mathbf{z}_b) in a given direction \mathbf{z}_1 , is a measure of the "width" of \mathbf{R}_z in that direction. Figure 4.8 shows the relative positions of \mathbf{a} and the boundary injections. Note that the smaller the angle between the two vectors, \mathbf{a} , the "wider" is \mathbf{R}_z in that direction, \mathbf{z}_1 .

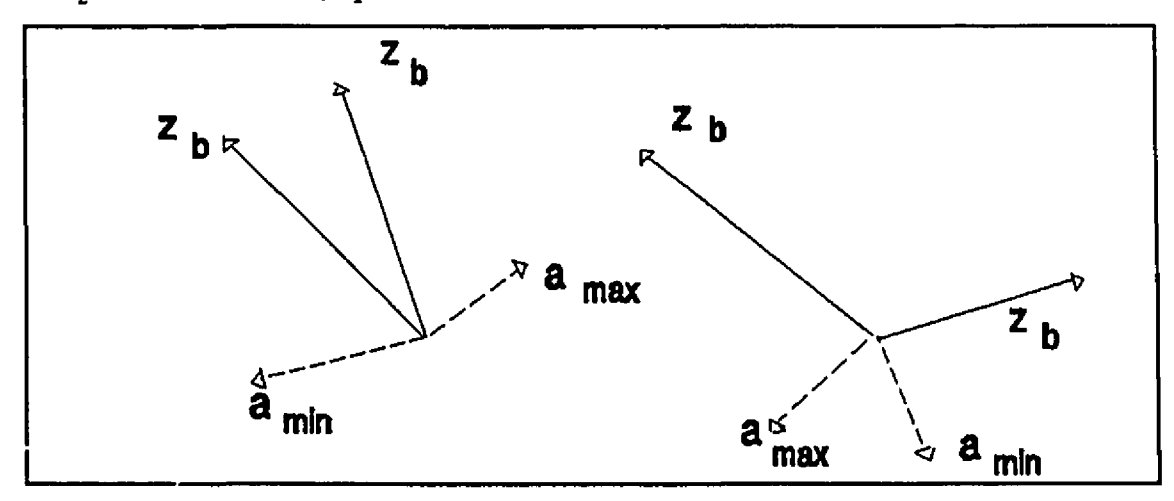


Figure 4.8. Boundary Injections of R_z and the Vectors Perpendicular to them

Eigenvectors associated with some of the *intermediate* eigenvalues may also define points on the boundary of R_z . Simulations on two simple systems, whose feasibility conditions can be derived analytically and for which the shape of R_z is known, show that when this situation occurs, the points z_b are on the boundary portion of R_z described by the hyperplanes $V_i^2 = 0$.

4.8.2 Experimental Results

Table 4.4 shows the angle (θ_z) between the two extreme boundary injections obtained from the eigenvectors associated with the maximum and minimum eigenvalues for the search directions, z_1 , defined in Table 4.2. The network is shown in Figure 4.6.

Table 4.4. Angle Between Extreme Boundary Injections of R_z for a Variety of Directions z_1 : 5-Bus Network

z ₁	Α	В	С	D	E	F	G	Н	I
θ _z	99.3	100	80.4	99.3	96.8	102	81.1	101	100

Note that all the angles are less than 180° . The angle is largest when $\mathbf{z_1}$ is in the direction (F) of only reactive power demand. The smallest angle occurs when $\mathbf{z_1}$ is in the direction (C) of real power generation and increasing voltage magnitude.

The simple two-bus example of Figure 4.3 is used to show that intermediate eigenvalues may also define injections on the boundary of R_z . Solving the generalised eigenvalue problem for this network produces *three* eigenvalues for any z_1 and z_0 . Table 4.5 shows the case where two of the three eigenvalues are identical for a particular choice of z_1 and z_0 . Both injections lie on the boundary of

 R_z . However, for a different choice of z_0 , the eigenvalues are distinct but the three different injections also lie on the boundary of R_z .

Table 4.5. Eigenvalues, Eigenvectors and Boundary Injections of 2-Bus Network for Two Different Values of z_0

λ	0.1038	-1	-1	0.0944	-1.0451	-1
$x_s = e_1$	0.8165	0	0	0.8280	-0.0897	0
e ₂	0.4082	0.7071	0.4557	0.4141	-0.0448	1
$\mathbf{f_2}$	-0.4082	-0.7071	0.8901	-0.3783	-0.9950	0
$z_b = P_2$	-0.6267	0	0	-0.5880	0.1677	0
Q_2	0	1.88	1.88	-0.0532	1.8573	1.88
V ₁ ²	0.6667	0	0.6855	0.0080	0	
$\mathbf{z_1} = [-0.1]$	-0.1 0] ^T ;	$z_0 = [0.1]$	z _o	= [0 0.1	1] ^T	

Note that, for $z_0 = [0 \ 0.1 \ 1]^T$, the injection corresponding to the intermediate eigenvalue, -1, has two components equal to zero and lies on the Q_2 -axis, but also on the plane $V_1^2 = 0$. Observe, also, that there are *three* different x_s for this injection even though this is a two bus system.

4.8.3 Interior Surfaces of R₂

Some of the eigenvectors associated with the intermediate eigenvalues define injections, \mathbf{z}_s , on surfaces which are within the boundary of the feasibility region. These surfaces will be referred to as *interior singular surfaces* of \mathbf{R}_z . Hyperplanes which are tangent to these surfaces can be found in an analogous manner to that used for the boundary of \mathbf{R}_z , i.e. by replacing λ_{max} or λ_{min} in expression (4.19) with the intermediate eigenvalues, λ_k .

4.8.4 Experimental Results

4.8.4.1 5-Bus Network

Results are now presented for the search directions defined in Table 4.2 and the network in Figure 4.6. Table 4.6a shows the angle (θ_{zk}) between the boundary injection associated with λ_{min} (z_{min}) and the injection (z_k) associated with the other eight λ_k 's found from a given search direction. In Table 4.6b the angle between the boundary injection associated with λ_{max} (z_{max}) and the other z_k 's are given. In Table 4.7a, the angle between a_{min} $(z_1 - \lambda_{min} z_0)$ and a_k $(z_1 - \lambda_k z_0)$ is shown. Similarly, Table 4.7b gives the angle between a_{max} $(z_1 - \lambda_{max} z_0)$ and a_k $(z_1 - \lambda_k z_0)$. Recall that a_i is orthogonal to z_i .

For all the search directions studied, the $\mathbf{z_k}$'s associated with the eigenvalues of similar magnitude always lie on at least one of these hyperplanes $V_2^2 = 0$ and $V_1^2 = 0$. The injection $\mathbf{z_{min}}$ also lies on these hyperplanes except when $\mathbf{z_1}$ includes the direction of real power generation (C,D,G). In these three directions, $\mathbf{z_{max}}$ lies on these two hyperplanes. For some of the directions, the angle between $\mathbf{z_{max}}$ and $\mathbf{z_{min}}$ is smaller than the angle between $\mathbf{z_{max/min}}$ and some of the other $\mathbf{z_k}$'s. In such cases, those $\mathbf{z_k}$'s also lie on one of the two hyperplanes mentioned above.

The multiple occurrence of some numbers in each row of Table 4.7a and 4.7b indicates that in every search direction, there are more than one $\mathbf{z_k}$ which lie in the same plane. Of course, this has already been shown by considering the left eigenvectors (Section 4.7.3.3). When "0" occurs more than once, it means that the injections lie on the same plane as $\mathbf{z_{min}}$ or $\mathbf{z_{max}}$. When a different number is repeated, this implies the $\mathbf{z_k}$'s lie on a plane which is different from the one containing $\mathbf{z_{min}}$ or $\mathbf{z_{max}}$. The maximum number of hyperplanes found in any direction is five (Direction I).

Chapter IV: Experimental Studies on the Load Flow Feasibility Region $\begin{tabular}{l} \textbf{Table 4.6a.} Angle Between Boundary Injection, z_{min} and Injections on Other Singular Surfaces of R_Z \\ \end{tabular}$

		θ_{z1}	θ_{z2}	θ_{z3}	θ_{z4}	θ_{z5}	θ_{z6}	θ _{z,7}	θ ₂₈	θ_{z9}
	Α	99.3	94.4	105	0	24.2	49.9	44.3	28.2	47.6
	В	83.9	100	100	114	114	0.96	0.00	21.3	22.3
	С	0	147	161	80.4	85.3	79.8	85.5	90.3	79.7
	D	0	160	145	99.3	99.8	98.3	99.0	97.2	96.1
z ₁	E	88.2	96.8	96.5	0.04	0	115	115	92.2	92.2
	F	89.8	102	92.2	99.6	92.2	0	0	90.0	90.0
	G	0	162	150	81.1	85.9	80.1	86.1	90.5	80.5
	н	0	92.3	101	100	97.7	94.1	12.4	77.9	49.7
	I	83.7	100	100	114	114	96.8	0	21.3	22.3

Table 4.6b. Angle Between Boundary Injection, \mathbf{z}_{max} and Injections on Other Singular Surfaces of R_{Z}

		θ_{z1}	θ_{z2}	θ_{z3}	θ _{z4}	θ _{zS}	θ_{z6}	θ _{z7}	θ,,8	θ_{z9}
	Α	0	160	144	99.3	99.8	98.3	99.1	97.22	96.1
	В	125	0	3.49	73.4	73.4	100	100	88.8	88.6
	С	80.4	78.9	88.6	0	18.3	31.7	25.0	55.7	37.5
	D	99.2	94.5	105	0	24.3	49.9	44.3	28.3	47.6
z ₁	E	63.8	0	96.8	96.8	96.8	91.4	91.4	97.4	97.4
	F	40.7	0	106	9.46	106	103	103	102	102
	G	81.1	89.5	81.1	0	19.0	31.7	25.8	55.8	37.1
	н	101	44.2	0	107	6.82	108	101	106	104
	I	125	0	3.49	73.4	73.4	100	101	88.8	88.6

Chapter IV: Experimental Studies on the Load Flow Feasibility Region

Table 4.7a. Angle Between the Vector \mathbf{a}_{min} and Other Vectors Perpendicular to Hyperplanes which are Tangent to the Singular Surfaces of R_z

		θ_{a1}	θ_{a2}	θ_{a3}	θ_{a4}	θ_{aS}	θ_{a6}	θ_{a7}	θ_{a8}	θ_{a9}
	A	166	9.19	31.8	0	0	0	0	0	0
	В	83.0	174	174	1.2	1.2	0.00	0.00	0	0
	С	0	155	162	166	166	166	166	166	166
	D	0	157	135	166	166	166	166	166	166
z ₁	E	50.3	157	157	0.0	0	0.33	0.33	1.20	1.20
	F	94.6	163	0.64	162	0.64	0	0	0	0
	G	0	163	155	167	166	166	166	166	166
	н	0	95.3	164	0	163	0	0	0	0
	I	83.1	174	174	1.20	1.20	0	0	0.20	0.20

Table 4.7b. Angle Between the Vector \mathbf{a}_{max} and Other Vectors Perpendicular to Hyperplanes which are Tangent to the Singular Surfaces of R_z

		θ_{a1}	θ_{a2}	θ_{a3}	θ_{a4}	θ _{a5}	θ _{a6}	θ _{a7}	θ_{a8}	θ_{a9}
	Α	0	157	134	166	166	166	166	166	166
	В	91.4	0	0.21	173	173	174	174	174	174
	С	166	11.2	4.06	0	0.01	0.11	0.14	0.15	0.15
	D	166	9.12	31.3	0	0.01	0.00	0.00	0.00	0.00
z ₁	E	107	0	0.27	157	157	157	0.33	156	156
]	F	68.0	0	162	0.94	162	163	163	163	163
	G	167	4.11	11.2	0	0.01	0.11	0.13	0.14	0.14
	Н	164	68.7	0	164	0.56	164	164	164	164
	I	91.5	0	0	173	173	174	174	174	174

From Table 4.7b it is seen that in directions A, E, F and H, the hyperplane containing \mathbf{z}_{max} does not contain any other injection (There is only one zero in each of those rows). This implies that those injections, \mathbf{z}_{max} , are on the boundary portion of $\mathbf{R}_{\mathbf{z}}$ which is not planar.

The results in Tables 4.7a and 4.7b may be combined to give an indication of how close the hyperplanes which are tangent to the singular surfaces of R_z are, in the chosen directions. This is illustrated in Figure 4.9 for $z_1 = E$ and I.

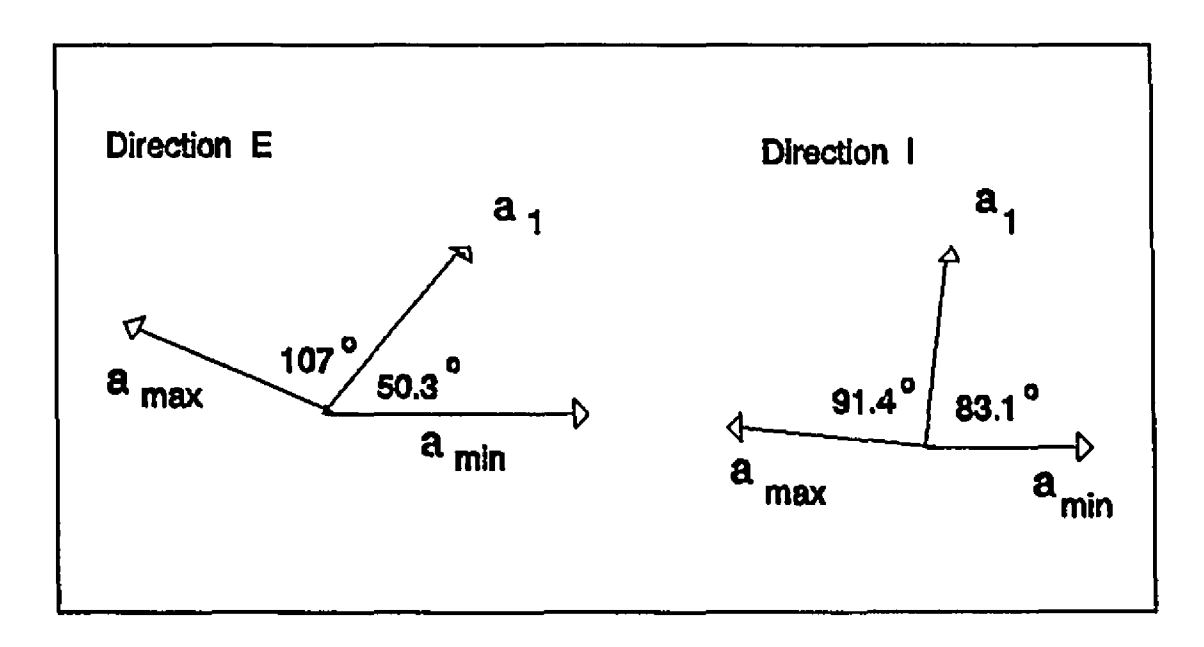
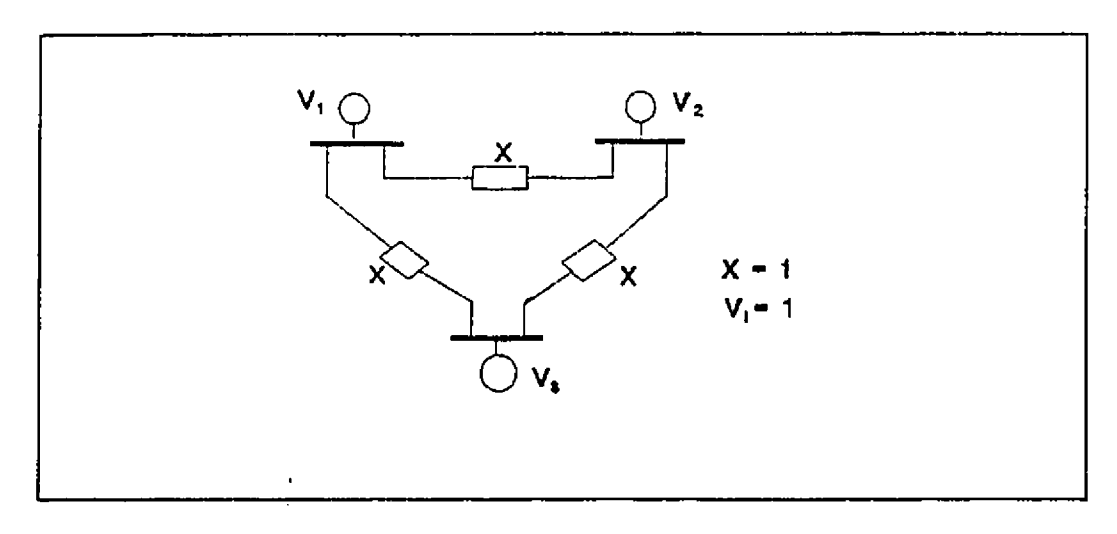


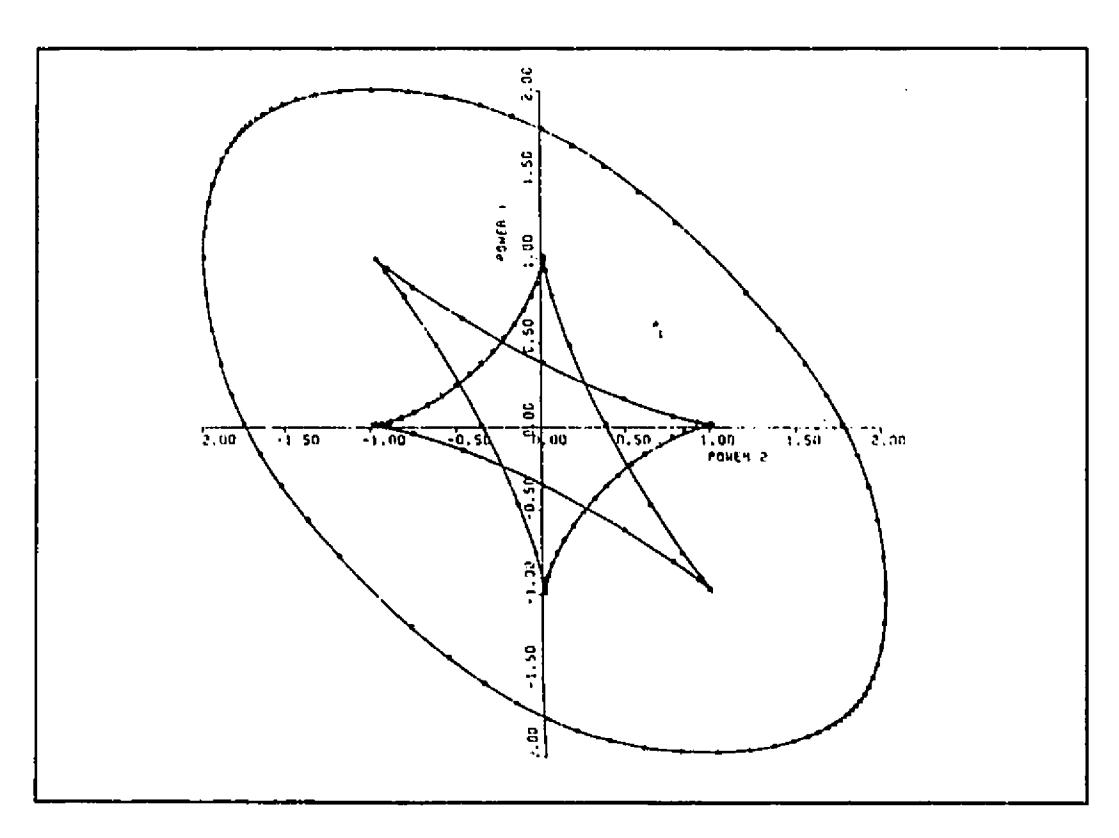
Figure 4.9. Positions of the Hyperplanes Tangent to the Singular Surfaces of R₂

4.8.4.2 2-Bus and 3-Bus Examples

Due to the generally high dimension of the problem, it is impossible to obtain a visualisation of these concepts except for very small systems. Two such systems are now presented.



(a) 3-Bus Network



(b) Feasibility Region of a Lossless 3-Bus Network

Figure 4.10. Feasibility Region of a 3-Bus AC Network

One of the clearest example of these interior surfaces of R_z is provided in the example presented by Tavora and Smith [19] and is reproduced in Figure 4.10b. Note that this feasibility region is defined in the space of real powers only and is a subset of the more general feasibility region considered in this work [26].

A general 3-dimensional feasibility region with an interior surface can be illustrated for a purely resistive 3-bus network. The system in Figure 4.11 will be used. In this simple example, the singular surfaces in the voltage space can be derived explicitly by solving for all the conditions which make the jacobian matrix singular. These conditions are

$$V_{1} = \frac{V_{2} + V_{3}}{4}$$

$$V_{2} = 0$$

$$V_{3} = 0$$
(4.25)

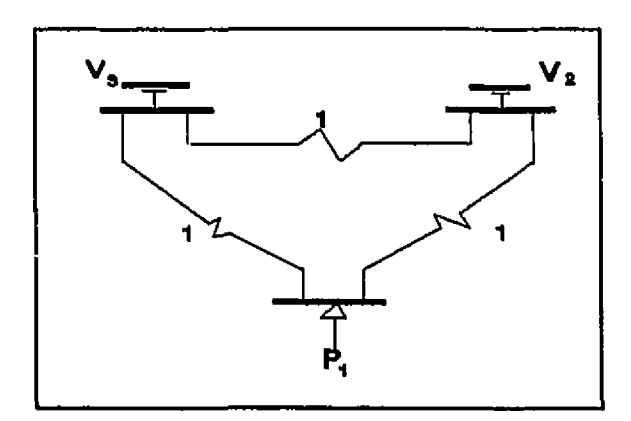


Figure 4.11. 3-Bus Resistive Network

The mapping of these singular surfaces in the injection space is given by

$$P_{1} = -\frac{1}{8} (V_{2}^{2} + 2\sqrt{V_{2}^{2}V_{3}^{2}} + V_{3}^{2})$$

$$V_{2}^{2} = 0$$

$$V_{3}^{2} = 0$$
(4.26)

The three equations in (4.26) define the boundary of the feasibility region. Note that because of the square root in the first equation, the following expression is also valid

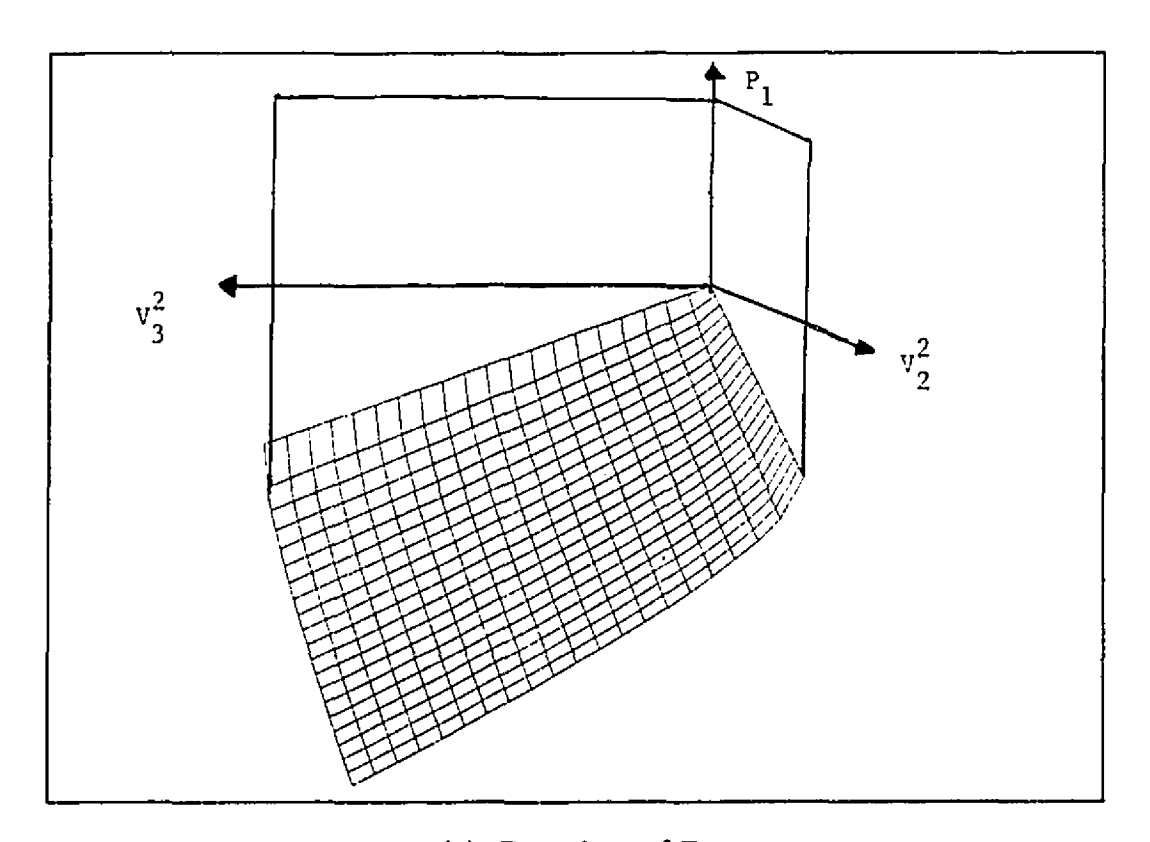
$$P_1 = -\frac{1}{8} \left(V_2^2 - 2\sqrt{V_2^2 V_3^2} + V_3^2 \right) \tag{4.27}$$

Equation (4.27) defines the interior surface of R_z.

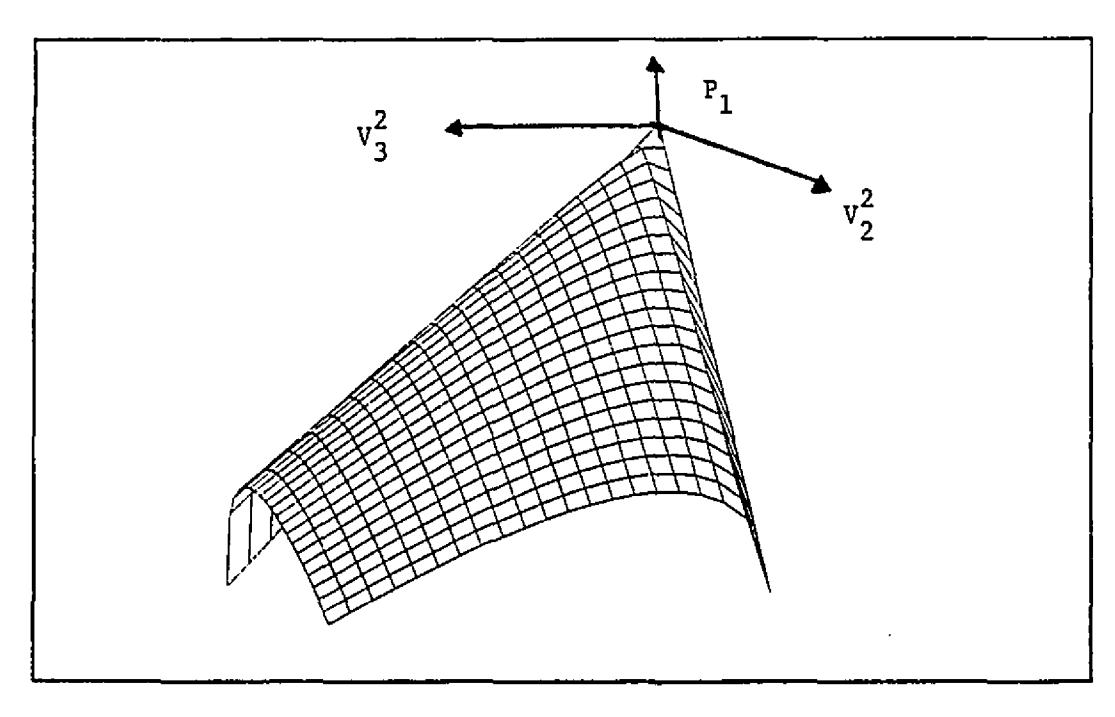
The boundary and interior surface are shown in Figure 4.12. The complete feasibility region is illustrated in Figure 4.13. Note that the feasibility region is in only one quadrant of the injection space and the conical portion lies entirely below the plane $P_1 = 0$. This means that feasibility constraints become active only if bus 1 is a load bus.

The interior surface of R_z can be seen more clearly by examining the feasibility surface, Pz_0 . Taking $z = [P_1 \ V_2^2 \ V_3^2]^T$, $z_0 = [1 \ 1 \ 1]^T$ and changing to a co-ordinate system with z_0 as one of the axes, Pz_0 is shown in the plane $z_0 = 1$ (Figure 4.14).

A projection of R_z onto the V_2^2 - V_3^2 plane (Figure 4.15) also shows the interior surface quite clearly.



(a) Boundary of R₂



(b) Interior Surface of R_z

Figure 4.12. Surfaces of the Feasibility Region of a 3-Bus Resistive Network

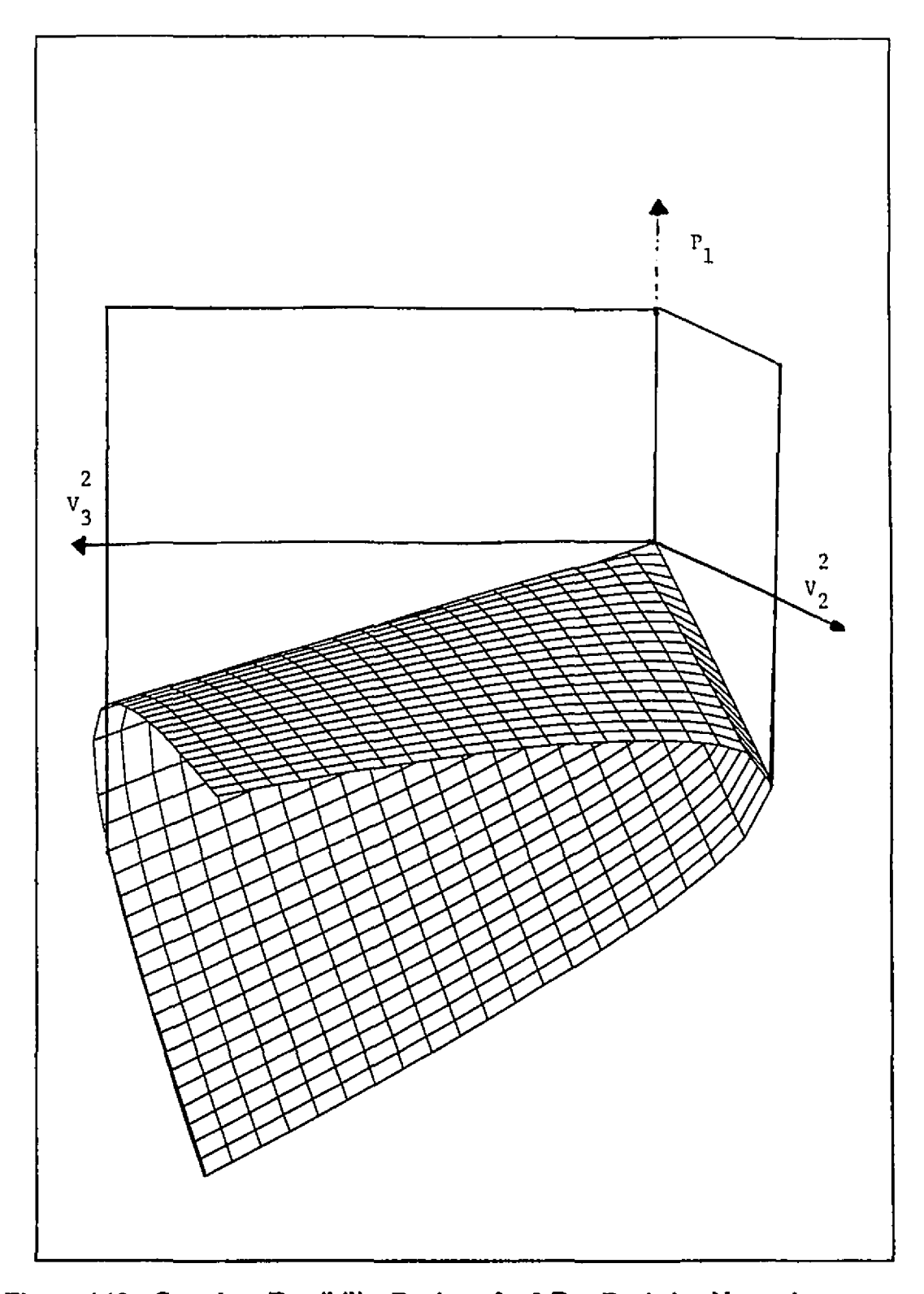


Figure 4.13. Complete Feasibility Region of a 3-Bus Resistive Network

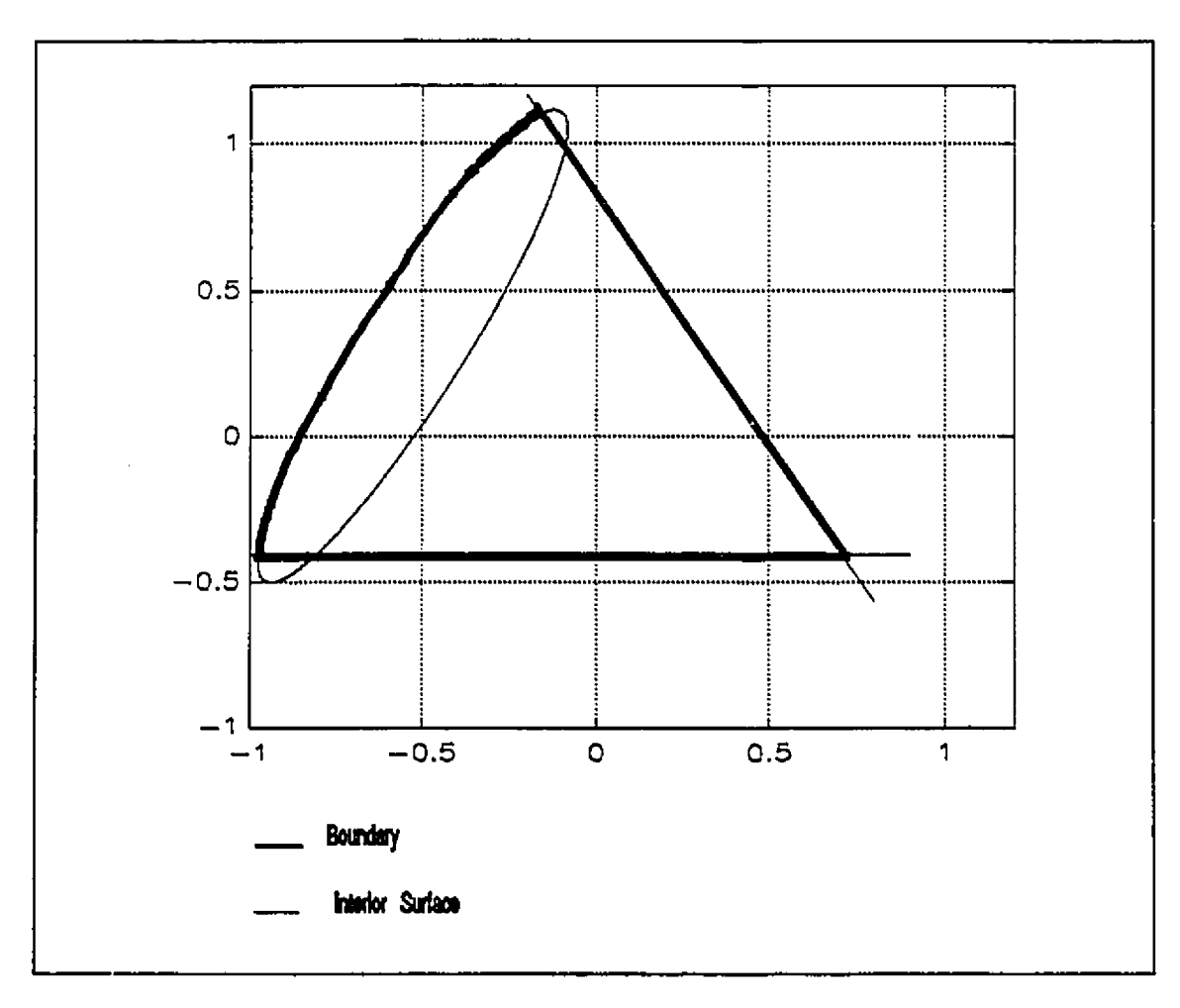


Figure 4.14. Feasibility Surface, P_{20} , of a 3-Bus Resistive Network

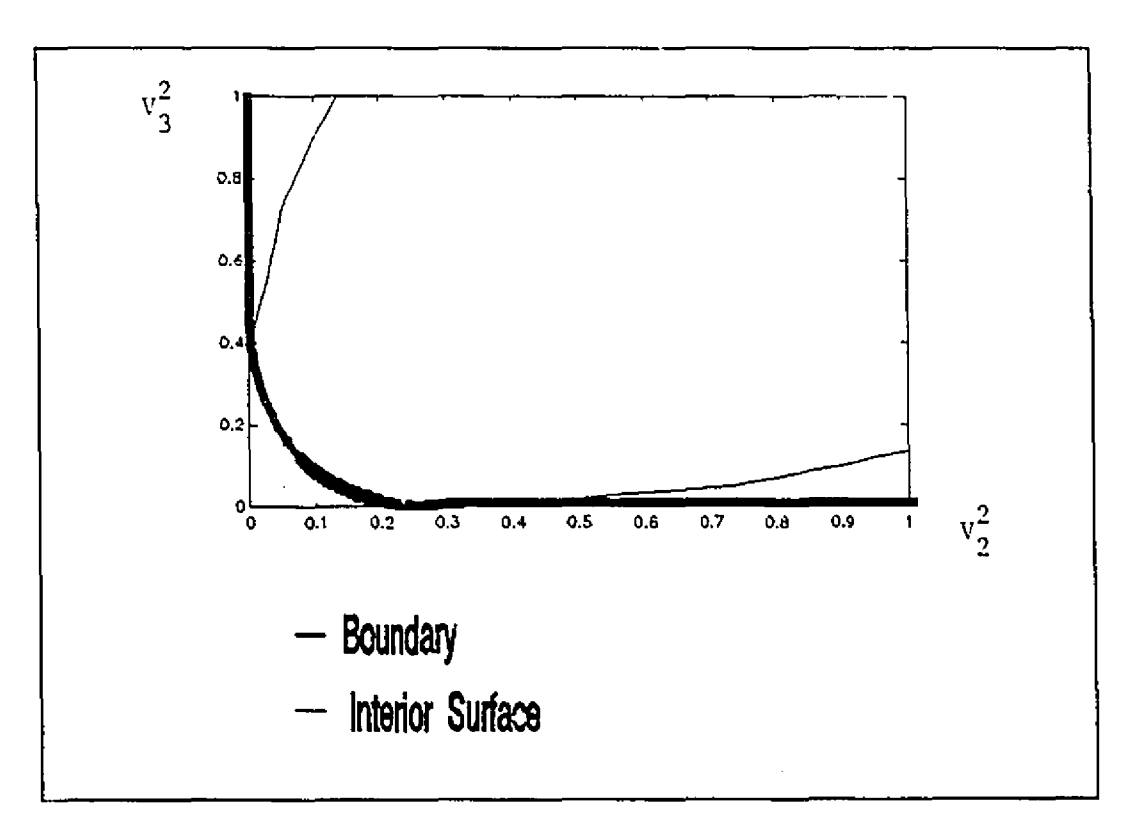


Figure 4.15. Projection of Feasibility Region in the V_2^2 - V_3^2 Plane

Table 4.8. Summary of the Eigenvalue Analysis of a 3-Bus Resistive Network

z _i	$\lambda = [\lambda_1 \lambda_2 \lambda_3]^{\mathrm{T}}$	$x_s = [V_1]$	V ₂ V ₃]	Z _b :	$= [P_1 \ V_2^2]$	V ₃ ²]	Surface
-0.2	-0.2	1 (319 0.8437	2	0	0	B
0.5	0.9097	0.3189 0.43		-0.2034	0.1865	0.7118	B
0.7	0.5569	-0.1385 -0.92		-0.0383	0.8466	0.1342	I
10.2	10.2	1 0	558 0.9209	2	0	0	В
1.5	-10.2695	0.2942 0.25		-0.1731	0.0654	0.848	В
-7	0.4528	-0.2081 -0.96		-0.0866	0.9382	0.0185	І
-6	-6	1 0	967 0.9596	2	0	0	В
-8.2	0.0297	0.2641 0.09		-0.1395	0.0094	0.9209	В
-0.8	-0.5297	-0.2520 -0.96		-0.1270	0.9348	0.0017	В
-0.2	-0.2	1 0	0.9856	2	0	0	В
-0.5	0.8446	0.2654 0.10		-0.1409	0.0106	0,9189	В
0.7	-0.5446	-0.2505 -0.96		-0.1255	0.9360	0.0012	В
0	0	1 0	0	2	0	0	B
0	0	0 1		0	1	0	B
1	1.1667	0.2722 0.13		-0.1481	0.0185	0.9074	B
0	0	1 0	526 0.1361	2	0	0	B
1	1.1667	0.2722 0.95		-0.1481	0.9074	0.0185	B
0	0	0.7001 0		0.4805	0	0.5098	B
1 0 0	1 -0.3333 0	1 0 0.3333 0.66 0 -0.70	667 0.6667	-0.2222 0	0 0.4444 0.5000	0 0.4444 0.5000	B B I
0	0	1 0		2	0	0	B
1	1	0 0.70		0	0.5000	0.5000	I
1	1.3333	0.3333 0.6		-0.2222	0.4444	0.4444	B

Table 4.8 gives a summary of the eigenvalue analysis of the system in Figure 4.11 for a variety of directions, z_1 . It is seen in this case that intermediate eigenvalues also define an injection on the boundary of R_z . This injection is $z_b = [2\ 0\ 0]^T$ which is on the intersection of the planes $V_2^2 = 0$ and $V_3^2 = 0$.

The "Surface" column in Table 4.8 indicates whether z_s lies on the boundary (B) or the interior surface (I) of R_z .

4.8.5 Classification of Singular Points in R,

As mentioned before, all the points on the singular surfaces in the x-space may be regarded as singular points, x_s , and their associated right eigenvectors, r. Their mapping to the singular surfaces of R_z can also be considered as all the pairs of injections z_s and z_r where $z_r = L(r)r$. This classification of the points on the singular surfaces of R_z is significant for examining the nature of multiple load flow solutions.

4.9 Convexity of R_z

A hypothesis is made in [26] that the interior of R_z is convex. The case is made by showing that the interior of R_z cannot be concave. Figure (4.16) shows the feasibility surface, P_{z0} for a 3-dimensional load flow feasibility region.

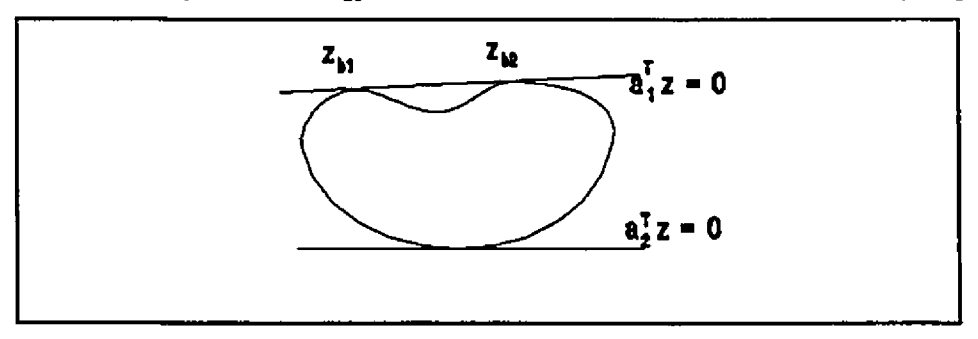


Figure 4.16. Illustration of the Convexity Argument

Chapter IV: Experimental Studies on the Load Flow Feasibility Region This situation is possible if there is a search direction z_1 such that the solution of the generalised eigenvalue problem produces multiple eigenvalues.

However, it is shown that if there are multiple eigenvalues, then the points z_{b1} and z_{b2} , on P_{z0} , must lie in a straight line. This implies that in R_z , these points lie on a plane or the intersection of two planes.

This argument is supported by the results from the three examples presented in the previous section. In the case of the 2-bus system, when there are multiple eigenvalues, the corresponding injections lie on an axis in the z-space and on the plane $V_1^2 = 0$. In the resistive 3-bus and the 5-bus examples, the multiple eigenvalues have corresponding injections on the planes $V_i^2 = 0$. These planes form part of the boundary of R_z . Furthermore, in the 3-bus network, these boundary portions of R_z are parallel to the planes defined by the search direction: $z_1^T z = c$.

4.10 Multiple Load Flow Solutions and Singular Surfaces of R,

4.10.1 Nature of Multiple Solutions

The multiple load flow solutions may be examined in the context of the load flow feasibility region.

Let the load flow equations be z = F(x) = L(x)x. Now assume that two vectors x^* and $(x^* + \delta x)$ satisfy this set of equations. Then

$$z = L(x^*)(x^*) = L(x^* + \delta x)(x^* + \delta x)$$
 (4.27)

which implies that

$$L(2x^* + \delta x)\delta x = 0 (4.28)$$

The definition L() is given in (3.32). From equation (4.28), it can be deduced that the vector $(2x^{\bullet} + \delta x)$ is a singular point, x_s , and δx is its associated right eigenvector, r [9]:

$$2x^* + \delta x = x_s$$

$$\delta x = r$$
(4.29)

From (4.29), the two solutions are therefore

$$x^* = \frac{1}{2} (x_s - r)$$

$$x^* + \delta x = \frac{1}{2} (x_s + r)$$
(4.30)

From the foregoing discussion, it is seen that any two load flow solutions x^* , $x^* + \delta x$ must be of the form [9]

$$x^*, x^* + \delta x = \frac{x_s \pm r}{2}$$
 (4.31)

This means that the sum and difference of any two solutions make the jacobian singular. Also, since the voltage at the slack bus must be identical for the two

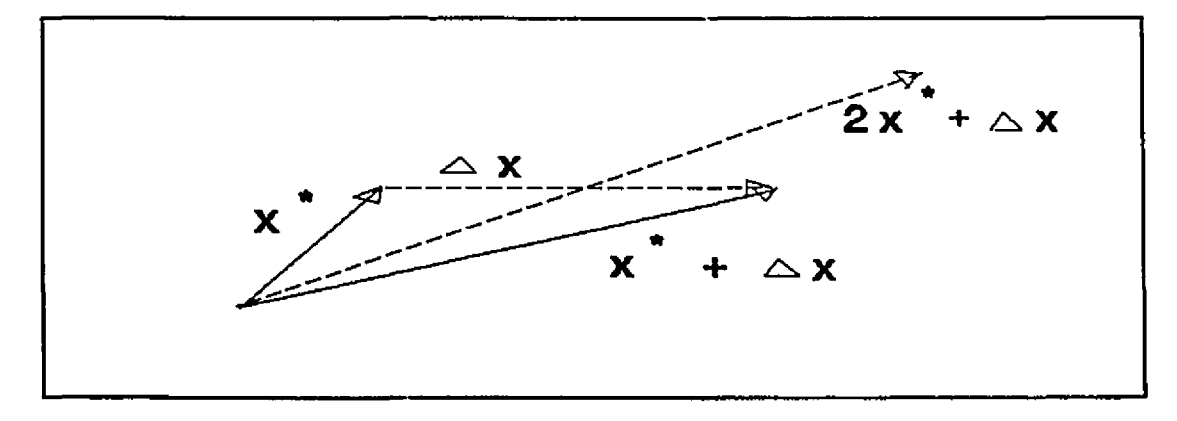


Figure 4.17. Relationship between Multiple Load Flow Solutions

Chapter IV: Experimental Studies on the Load Flow Feasibility Region solutions, the component of either r or x_s corresponding to the slack bus must be equal to zero. Numerical experience has supported this contention (See Table 4.3). These results were also derived in [3] but by first assuming that the solutions are of the form $x_1 + x_2$.

The injection defined by the two solutions in (4.31) is

$$z = \frac{1}{4}L(x_s)x_s \pm \frac{1}{2}L(x_s)r + \frac{1}{4}L(r)r$$

$$= \frac{1}{4}L(x_s)x_s + \frac{1}{4}L(r)r$$

$$= \frac{z_s + z_r}{4}$$
(4.32)

where \mathbf{z}_s and \mathbf{z}_r are as previously defined. Again, due to the specification of the slack bus voltage, the components of either \mathbf{z}_r or \mathbf{z}_s corresponding to the square of the voltage magnitude of the slack bus should be equal to zero. From this it can be concluded that at least one of the injections, \mathbf{z}_s or \mathbf{z}_r , in (4.32), must be a boundary injection, \mathbf{z}_b , which lies on the hyperplane $V_s^2 = 0$. Consequently, any injection \mathbf{z} having multiple solutions must be of the form

$$z = \frac{z_b + z_r}{a} \tag{4.33}$$

4.10.2 Numerical Results

Numerical simulations support the reasoning of the previous section. In Table 4.9, the various pairs of injections, z_s and z_r , found from a particular direction z_1 are given. The network is shown in Figure 4.6.

Note that the injection, z_s , associated with the eigenvalues of similar magnitudes all lie on the hyperplanes $V_1^2 = V_2^2 = 0$. This supports the hypothesis

75

Table 4.9. Injections on the Singular Surfaces of R_z

	,		,		,		,	كالمستحد المنسجا		
λ	0.8126	-1.0637	-0.2941	-13.4058	-13.3927	-13.3511	-13.34	-13.3360	-13.3372	
z, =					1			}		
P.	-4.0171	8.5445	3.1891	-0.0018	0.0006	0.0008	0.0000	0.0000	0.0001	
P ₃	-0.3208	0.2964	0.1056	1.2289	0.7271	1.2487	0.9152	11.1822	4.0736	
P ₄	0.1156	0.0343	0.1129	0.6655	0.7925	-0.0404	0.7001	11.7259	13.5531	
P _s	0.1348	0.1233	0.1964	0.5775	0.9251	3.2278	2.6414	0.0422	0.7137	
Q,	-0.3529	-0.4495	-0.5274	3.5540	2.1216	3.7148	2.7378	33.5194	12.1978	
Q	-0.3563	-0.3756	-0.5635	1.9307	2.3132	-0.1171	2.0947	35.1501	40.6099	
Qs	-0.5498	-0.7406	-0.9861	1.6680	2.6921	9.6128	7.8893	0.1265	2.1401	
V ₂ 2	0.2819	0.4275	0.5399	0.0002	0.0002	0.0000	0.0000	0.0000	0.0000	
V_1^2	0.3886	0.2869	0.0000	0.0001	0.0000	0.0000	0.0000	0.0000	0.0000	
$\mathbf{z_r} = \mathbf{z_r}$	4.6700	1 7142	-2.20 7.2060	0.0002	0 0.0011	0.0002	0 -0.0002	0 0.000	0.0000	
P ₂	4.6709	-1.7143	0.562 -0.2310	1.2149	-0.058 0.7232	0.0002 1.2361	-0.113 0.908		0.0000	
P ₃	-0.6610	1.8649 1.3603	0.302 -0.2310	0.6601	-0.036 0.7232	-0.0398	0.059 0.690	0.034 11.115 -0.017 11.741	4.0643 13.5572	
P ₄	-0.4736	0.9376	0.269 0.0168	0.5764	-0.014 0.7923	3.2299	-0.002 2,642	0.000 0.0421	0.7137	
P ₅	-0.3947 0.3868	2.0836	0.510 -0.4038	3.5591	-0.142 2.1230	3.7192	-0.137 2.740	-0.109 33.530	12.2013	
Q ₃	-0.3709	0.3621	0.412 -0.3648	1.9327	-0.066 2.3140	-0.1174	-0.061 2.096	0.009 35.131	40.6097	
O ₄	-0.3709 -0.7944	-0.1182	0.171 -1.0663	1.6685	-0.003 2.6922	9.6125	-0.001 2.090	0.009 35.131		
Q ₅	0.4752	0.1957	0.017 0.5323	0.0002	0 0.0002	0.0000	0.000 7.889	0 33.132	2,1402	
V ₂ ²	0.4732	0.1937	0.596 0.0595	0.0002	0.969 0.0002	0.0000	0.982 0	1	0.0000	
V _I ²	0.000	0.0000	כפכטים ספכים	ν.νυζυ	0.909 0.0002	0.000	0.962 0	0.998 0	0.0000	
	$z_1 = \begin{bmatrix} -0.1 & -0.1 & -0.1 & -0.1 & -0.1 & 0 & 0 \end{bmatrix}^T$									

in Section 4.9 that when there are repeated eigenvalues, the injections associated with them lie on the hyperplanes which form part of the boundary of R_z . It is assumed that the injections, z_s , in Table 4.9 which do not lie on the hyperplanes $V_i^2 = 0$, lie on the conical portion of R_z . This is the part of R_z that describes the constraints on the real and reactive power injections as well as the square of the voltage magnitudes. These injections would be more similar to a "typical" operating point.

Note that for the x_s and r which are orthogonal (Section 4.7.3.3), z_s and z_r are almost identical. This indicates that an injection formed by the sum of two such injection has double solutions.

The ten known solutions [8] of the 5-bus system in Figure 4.18 are used to verify some of the various relations presented in 4.10.1.

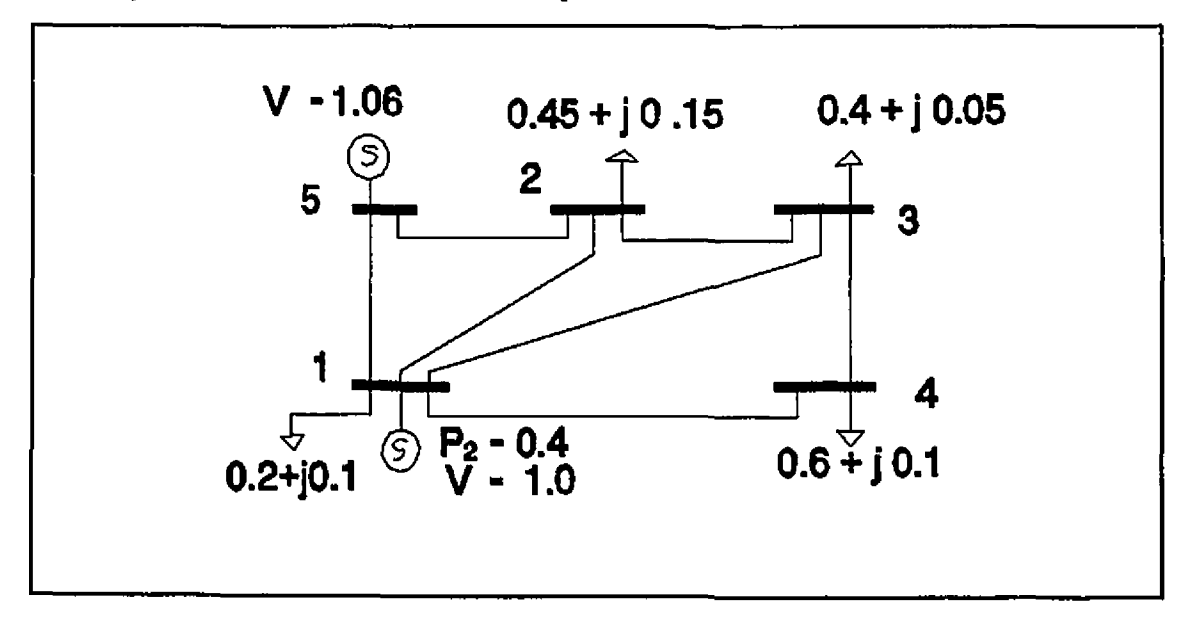


Figure 4.18. 5-Bus Network

Chapter IV: Experimental Studies on the Load Flow Feasibility Region Note that this network is the same as the one given in Figure 4.6 but the buses are numbered differently and the bus types are specified differently. Bus #5 is now the slack bus and bus #2, the voltage control bus.

Solution #1 in Table 4.10 is the "valid" solution. This solution was first added to each of the other nine solutions and the resulting vectors were used to form nine jacobian matrices. Similarly, the difference of the "valid" solution and each of the other nine solutions were used in the formation of nine jacobian matrices. These eighteen jacobian matrices were checked for singularity since from the results in Section 4.10.1, the sum and difference of any two load flow solutions should make the jacobian singular.

Table 4.10. The Ten Solutions of the 5-Bus System

х			Solutions		
	1	2	3	4	5
e ₁	0.9994	-0.7543	-0.6237	0.9776	-0.5966
e ₂	0.9767	-0.3210	-0.1702	0.7736	-0.0581
e ₃	0.9735	-0.4140	-0.2303	0.7184	-0.1756
e ₄	0.9612	-0.6518	-0.0656	0.0181	-0.4799
e _s	1.06	1.06	1.06	1.06	1.06
f ₁	-0.0360	-0.6565	-0.7817	-0.2104	-0.8025
f ₂	-0.0798	-0.3846	-0.3364	-0.1740	-0.0217
f ₃	-0.0850	-0.4161	-0.3392	-0.1775	-0.1239
f ₄	-0.0958	-0.5155	-0.0066	-0.0540	-0.5068
f ₅	0	0	0	0	0

Chapter IV: Experimental Studies on the Load Flow Feasibility Region

Table 4.10 c'td. The Ten Solutions of the 5-Bus System

	Solutions						
х	6	7	8	9	10		
e ₁	0.9587	0.9505	0.9567	0.9237	-0.4982		
e ₂	0.1767	0.0270	0.0121	0.1685	-0.0691		
e ₃	0.0042	0.0079	0.1454	0.0025	-0.1347		
e ₄	0.5761	0.5707	0.6273	0.0149	-0.0749		
e ₅	1.06	1.06	1.06	1.06	1.06		
$\mathbf{f_1}$	-0.2841	-0.3106	-0.2908	-0.3830	-0.8670		
f ₂	-0.0865	-0.0490	-0.0317	-0.1000	-0.0543		
f ₃	-0.0297	-0.0483	-0.1127	-0.0359	-0.0952		
f ₄	-0.2499	-0.2715	-0.2776	-0.0796	-0.0020		
f ₅	0	0	0	0	0		

In the case of the nine jacobian matrices formed from the sum of the load flow solutions, the determinant of the jacobian was not equal to zero. However, at least one of the nine eigenvalues of each matrix was equal to or very close to zero. These results are shown in Table 4.11. It was reported in [3] that the determinant of the jacobian is extremely sensitive around the singular points. Therefore it is assumed that numerical inaccuracies are responsible for the determinant and some of the eigenvalues not being equal to zero.

From equations (4.28) and (4.29), the difference of any two load flow solutions should be in the null space of the jacobian matrix formed from the sum of the two solutions. The simulations reveal that the difference of Solution #1 and the other nine solutions were scalar multiples of the eigenvectors corresponding to the

5

Table 4.11. Real Part of the Eigenvalues and the Determinants of the Jacobian Matrices formed from the Sum of Two Load Flow Solutions

Solu- tion	1+2	1+3	1+4	1+5	1+6	1+7	1+8	1+9	1+10
	22.735	24.914	35.353	16.270	28.348	27.628	29.212	29.060	21.044
	-5.257	-12.28	13.013	8.323	10.563	10.501	11.377	9.995	-13.00
	-5.257	7.284	13.013	8.323	10.563	10.501	11.377	9.995	6.249
Eigen	6.921	7.284	-16.09	-7.507	-14.11	-14.79	-16.34	-12.43	6.249
value	6.921	3.440	3.471	-7.507	-7.308	3,818	3.766	-4.911	3.342
	3.958	3.440	3.471	3.853	3.958	3.818	3.766	3.047	3.342
	3.958	-1.022	-3.329	3.853	3.958	-6.147	-1.249	3.047	-2.553
1	-1.806	-1.022	-3.329	0.000	-0.896	-0.996	-5.535	-0.823	0.002
	0.000	0.001	-0.008	-0.495	0.001	-0.008	-0.008	-0.004	-0.096
			 	_		<u> </u>			
Det	0.7772	-978	1.223 x 10 ⁶	-156	-5.101 x 10 ⁴	2.449 x 10 ⁵	4.081 x 10 ⁵	3.742 x 10 ⁴	-487.931

Chapter IV: Experimental Studies on the Load Flow Feasibility Region

smallest eigenvalue of the jacobian formed from the sum of those solutions. Recall from the previous paragraph that the smallest eigenvalues were equal to or very closeto zero so it is assumed that their associated eigenvectors are in the null space of the jacobian. For the jacobian matrices found formed from the difference of the load flow solutions, both the determinant and one of eigenvalues of each matrix were exactly equal to zero.

Allowing for numerical inaccuracies, the given injection, z_g , also satisfied equation (4.33) for a number of different pairs, z_b and z_r . Results are shown in Table 4.12 for the pairs defined by the sum and difference, respectively, of the "valid solution" and Solutions 2-5 of Table 4.10.

Table 4.12. Specified Injection as the Sum of two Injections on Singular Surfaces of R,

	$(\mathbf{z_b} + \mathbf{z_r})/4$					
z _g	Sol (1 <u>+</u> 2)	Sol (1 <u>+</u> 3)	Sol (1 <u>+</u> 4)	Sol (1 <u>+</u> 5)		
0.20	0.20	0.20	0.20	0.20		
-0.45	-0.45	-0.45	-0.45	-0.45		
-0.40	-0.40	-0.40	-0.40	-0.40		
-0.60	-0.60	-0.60	-0.60	-0.60		
-0.15	-0.15	-0.15	-0.16	-0.16		
-0.05	-0.05	-0.05	-0.04	-0.04		
-0.10	-0.10	-0.10	-0.10	-0.10		
1.00	1.00	1.00	1.00	1.00		
1.1236	1.1236	1.1236	1.1236	1.1236		

4.10.3 Number of Solutions and Singular Surfaces of R,

It is known that the number of load flow solutions depends on the topology of the network and the location of the given injection in the injection space. It is also known that injections close to the zero injection vector have the most solutions [15,19] and those close to the maximum power transfer capacity have a very small number of solutions. These factors are now discussed in terms of the ideas presented in the preceding sections.

4.10.3.1 Position of Injection in R.

Based on the above considerations, one can surmise that the number of solutions to a given set of load flow equations z = F(x) depends on the number of pairs z_b and z_r that satisfy equation (4.33). If there are n solutions, there will be ${}^{n}C_2$ such pairs of vectors. This also suggests that the number of multiple solutions should be even except when at least one of the solutions is a singular point.

One can attempt to explain the number of solutions in terms of the relative positions, in R_z , of the various pairs z_b and z_r . If the given injection is in a portion of R_z where the sum of many different pairs, z_b and z_r intersect, then it is expected that there is a good chance that many of them will satisfy (4.33). On the other hand, if the injection is in a section of R_z where there are not many such intersections, then there will be fewer pairs satisfying (4.33) and consequently, fewer solutions.

4.10.3.2 Example

Figure 4.19 shows a "cross-section" of R_z for the network of Figure 4.11 and the relative positions of the pairs z_b and z_r .

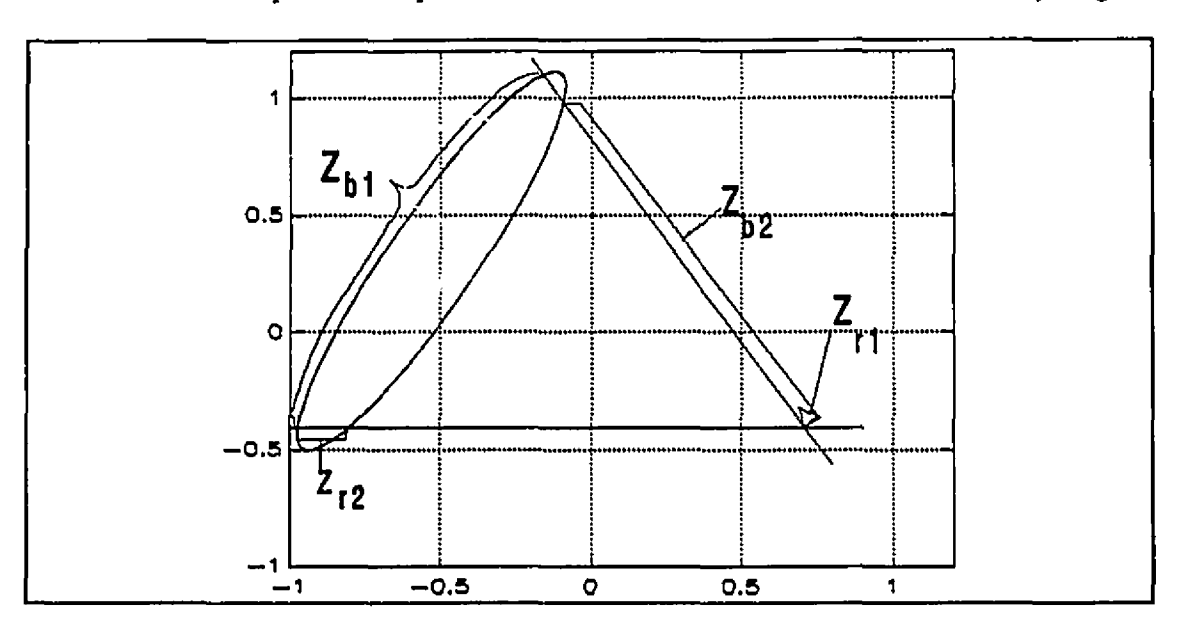


Figure 4.19. Feasibility Surface P_{z0} Showing the Pairs z_b and z_r

Numerical tests on this simple network indicate that if z_b lies on the plane $V_2^2 = 0$, then its z_r lies on the hyperplane $V_3^2 = 0$ and vice versa. On the other hand, if z_b is on the boundary portion of R_z representing the constraints on the power injection, its z_r is on the intersection of the hyperplanes $V_i^2 = 0$. It means, therefore, that in the region of R_z close to the origin of the z-space, in the vicinity of the hyperplanes $V_i^2 = 0$, there are several pairs, z_b and z_r , and consequently, the sum of these pairs will also be in that region. Thus the likelihood of the sum of these pairs intersecting is greater in that area of R_z . There are less pairs, z_b and z_r , close to the boundary portion of R_z representing the constraints on the power injections. As a result, there is less chance that the sum of this small number of pairs will intersect in this area.

For this small system, it can be seen that the injections close to the boundary portion of R_z describing the conditions on the square of the voltage

Chapter IV: Experimental Studies on the Load Flow Feasibility Region magnitude would have more solutions than injections close to the boundary portion of R_z representing the constraints on the power injections.

4.10.3.3 Structure of R₂

The relationship between the multiple load flow solutions and the singular surfaces of R_z can be examined using a different approach. In reference [5], it was shown that any injection, z, which is "close" to a singular injection, z, has two close solutions in the voltage space. These two solutions are in the neighbourhood of a singular point, x_s , which defines a jacobian matrix with nullity one. This fact will be used to determine how the number of singular surfaces in R_z is related to the number of load flow solutions.

The generalised eigenvalue approach used to characterise R_z finds N (where N is the number of buses in the system) singular points in the x-space, for every direction z_1 , which define jacobian matrices with nullity one. These singular points define corresponding injections on singular surfaces in R_z . Assume that these N injections lie on m different surfaces in R_z . Recall that at least two of the injections lie on the boundary of R_z so $m \le N-1$.

Consider any injection, z, which is not feasible and therefore has no real solutions. If z is moved in a direction such that it crosses the boundary of R_z , at least two solutions will appear. As z approaches any interior singular surface, every existing solution "separates" into two new solutions. Therefore when z has moved across the m distinct interior surfaces there will be 2^m solutions. Since $m \le N-1$, the maximum number of load flow solutions must be at least $2^{(N-1)}$.

CHAPTER V

CONCLUSIONS AND

RECOMMENDATIONS FOR FURTHER

RESEARCH

5.1 Conclusions

An analytical study of the load flow problem was undertaken in this thesis. In particular, the quadratic nature of the load flow equations in rectangular co-ordinates was examined in detail. The importance of this formulation of the load equations to the understanding of the nature of multiple load flow solutions as well as the nature of the load flow feasibility region was emphasised. Experimental studies were done which confirm and expand on these concepts.

The main results and conclusions of this work are:

- (i) The load flow equations of an N-bus system describe (2N-1) fully quadratic hypersurfaces in a (2N-1)-dimensional space or alternatively, 2N quadratic hypersurfaces and one hyperplane in a 2N-dimensional space.
- (ii) The hypersurfaces defined by the real and reactive power injections are hyperbolic. Furthermore, the surfaces defined by the reactive power injections are "narrower" than those defined by the real power injections.
- (iii) The matrices describing the real and reactive power injections have four non-zero eigenvalues. The matrices describing the 2N-dimensional

Chapter V: Conclusions and Recommendations for Further Research

hypersurfaces have two identical pairs of eigenvalues. The matrices describing the (2N-1)-dimensional hypersurfaces also have two pairs of eigenvalues but the two pairs are identical only when the matrix defines an injection at a bus which is not connected to the reference bus. The matrices describing the square of the voltage magnitudes have two non-zero eigenvalues.

- (iv) The eigenvectors of the matrices defining the (2N-1)-dimensional hypersurfaces depend on the quantity G_{is} / B_{is} . This indicates that the position of the reference bus, as well as the admittance to susceptance ratio of the line between the bus at which the injection is specified and the reference bus, determines the orientation of these hypersurfaces in the voltage space and consequently, the nature of the intersection of these hypersurfaces.
- (v) If a set of load flow equations has multiple solutions, the solutions can be expressed as the sum and difference of a vector that makes the load flow jacobian singular and another vector in the null space of that singular jacobian matrix.
- (vi) The sum and difference of any two of the multiple load flow solutions make the load flow jacobian matrix singular.
- (vii) Singular points in the voltage space may be obtained by finding the eigenvectors of the generalised eigenvalue problem, $[J(z_1) \lambda J(z_0)] x = 0$. The matrices $J(z_1)$ and $J(z_0)$ are linear combinations of the matrices describing the specified injections and z_0 is a vector which is perpendicular to a hyperplane that intersects all the boundary points of the load flow feasibility region.
- (viii) The load flow feasibility region, R_z , consists of a convex cone lying on or above a set of hyperplanes. The cone and hyperplanes define surfaces in R_z . The

Chapter V: Conclusions and Recommendations for Further Research injections on these surfaces are defined by vectors which make the load flow jacobian singular.

(ix) Any feasible injection can be expressed as the sum of two injections on singular surfaces of R_z . At least one of these two injections must lie on the hyperplane $V_i^2=0$ where bus i is the slack bus.

5.2 Recommendations for Further Research

The work in this thesis demonstrated that the rectangular form of the load flow equations highlights the relationship between, as well as the properties of, the multiple load flow solutions. The following are suggestions for further research in this area:

- (i) It was established that the solutions of the load flow equations may be obtained by finding the intersection of (2N-1) quadratic surfaces, some of which quadratic surfaces are hyperboloids. If (2N-1) linearly independent vectors, $\mathbf{z_0}$, can be found such that the linear combinations $\mathbf{z_0}^T \mathbf{z}$ are positive, then the solutions of the load flow may be obtained by finding the intersection of (2N-1) ellipsoids. It may also be possible to use algorithms designed for positive definite matrices in this approach.
- (ii) The fact that any given injection can be expressed as the sum of two injections on singular surfaces of R_z can also be used to find the load flow solutions. If a systematic method can be devised to find all such pairs for a given injection, then the solutions of the load flow are simply the sum and difference of the vectors which define these pairs of injections.

SELECTED BIBLIOGRAPHY

- [1] Klos, A., Mikolajczyk, S., "Non-Uniqueness and Stability of Load Flows", Proceedings of the Sixth Power System Computation Conference, Vol. 2, pp.704-710.
- [2] Iba, K., Suzuki, H., Egawa, M., Watanabe, T., "A Method for Finding a Pair of Multiple Load Flow Solutions in Bulk Power Systems", IEEE Transaction on Power Systems, Vol. 5, No. 2, May 1990, pp.582-591.
- [3] Tamura, Y., Nakanishi, Y., Iwamoto, S., "On the Multiple Solution Structure, Singular Point and Existence Conditions of the Multiple Load Flow Solutions", Paper A 80 044-8, IEEE Power Engineering Society Winter Meeting, New York, February 1980.
- [4] Tamura, Y., Iba, K., Iwamoto, S., "A Method for Finding Multiple Load-Flow Solutions for General Power Systems", Paper A 80 043-0, IEEE Power Engineering Society Winter Meeting, New York, February 1980.
- [5] Galiana, F.D., Zeng, Z.C., "Analysis of the Load Flow Behaviour near a Jacobian Singularity", IEEE Transactions on Power Systems, Vol. 7, No. 3, August 1992, pp.1362-1369.
- [6] Overbye, T.J., DeMarco, C.L., "Improved Techniques for Power System Voltage Stability Assessment using Energy Methods", IEEE Transactions on Power Systems, Vol. 6, No. 4, November 1991, pp.1446-1452.
- [7] Iwamoto, S., Tamura, Y., "A Load Flow Calculation Method for Illconditioned Power Systems", IEEE Transactions on Power Apparatus and

- Systems, Vol PAS-100, No. 4, April 1981, pp.1736-1743.
- [8] Thorp, J.S., Ma, W., "An Efficient Algorithm to Locate all the Load Flow Solutions", IEEE Transactions on Power Systems, Vol 8, No. 3, August 1993, pp.1077-1083.
- [9] Galiana, F.D., Lee, K., "On the Steady State Stability of Power Systems", Proceedings of the Power Industry and Computer Applications (PICA), May 1977, pp.201-210.
- [10] Guo, S., Salam, F., "The Real Homotopy-Based Method for Computing Solutions of Electric Power Systems", Proceedings of the IEEE International Symposium on Circuits and Systems, May 1992, pp.2737-2740.
- [11] Thomas, R.J., Barnard, R.D., Meisel, J., "The Generation of Quasi Steady-State Load Flow Trajectories and Multiple Singular Point Solutions", IEEE Transactions on Power Apparatus and Systems, Vol. PAS-90, No. 5, September/October 1971, pp.1967-1974.
- [12] Klopfenstein, R.W., "Zeros of Non-Linear Functions", Journal of the Association for Computing Machinery, Vol. 8, 1961, pp.366-373.
- [13] El-Abiad, A.H., Nagappan, K., "Transient Stability Regions of Multimachine Power Sytems", IEEE Transactions on Power Apparatus and Systems, Vol. PAS-89, February 1970, pp.233-239.
- [14] Korsac, K., "On the Question of Stable Load-Flow Solutions", IEEE Transactions on Power Apparatus and Systems, Vol. PAS-91, May/June 1972,

- pp.1093-1100.
- [15] Baillieul, J., Byrnes, C.I., "Geometric Critical Point Analysis of Lossless Power System Models", IEEE Transactions on Circuits and Systems, Vol. CAS-29, No. 11, November 1982, pp.724-737.
- [16] Johnson, B.K., "Extraneous and False Load Flow Solutions", IEEE Transactions on Power Apparatus and Systems, Vol. PAS-96, March/April 1977, pp.524-534.
- [17] Price, G.B., "A Generalised Circle Diagram Approach for Global Analysis of Transmission System Performance", IEEE Transactions on Power Apparatus and Systems, Vol. PAS-103, No. 10, October 1984, pp.2881-2890.
- [18] Tinney, W.F., "Discussion of [Price 1984]", IEEE Transactions on Power Apparatus and Systems, Vol. PAS-103, No. 10, October 1984, p.2888.
- [19] Tavora, C.J., Smith, O.J.M., "Equilibrium Analysis of Power Systems", IEEE Transactions on Power Apparatus and Systems, Vol. PAS-91, May/June 1972, pp.131-1137.
- [20] Arapostathis, A., Sastry, S., Varaiys, P., "Bifurcation Analysis of the Load Flow Equations", Paper TP3-2:30, Proceedings 19th Conference on Decision and Control including the Symposium on Adaptive Processes, Vol. 1, December 1980, pp.641-644.
- [21] Sauer, P., Pai, M.A., "Power System Steady State and the Load Flow Jacobian", IEEE Transactions on Power Systems, Vol. 5, November 1990,

- pp.1374-1383.
- [22] Dobson, I., "Observations on the Geometry of Saddle Node Bifurcation and Voltage Collapse in Electrical Power Systems", IEEE Transactions on Circuits and Systems Part 1: Fundamental Theory and Applications, Vol. 39, No. 3, March 1992, pp.240-243.
- [23] Dobson, I., "An Iterative Method to Compute the Closest Saddle-Node or Hopf Bifurcation in Multi-Dimensional Space", IEEE International Symposium on Circuits and Systems, May 1992, pp.2513-2516.
- [24] Kwatny, H.G., Pasrija, A.K., Bahar, L.Y., "Static Bifurcations in Electric Power Networks: Loss of Steady-State Stability and Voltage Collapse", IEEE Transactions on Circuits and Systems, Vol. CAS-33, October 1986, pp.981-991.
- [25] Galiana, F.D., "Power-Voltage Limitations imposed by the Network Structure of a Power System", Proceedings of the Power Industry and Computer Applications (PICA), June 1975, pp.356-363.
- [26] Jarjis, J., "Load Flow Feasibility Conditions in Power Networks", PH.D. thesis, Dept. of Electrical Engineering, McGill University, Montreal, Canada, March 1980.
- [27] Dobson, I., "An Iterative Method to Compute the Closest Saddle Node or Hopf Bifurcation in Multidimensional Space", Proceedings of the IEEE International Symposium on Circuits and Systems, May 1992, pp.2513-2516.

- [28] Wallach, Y., <u>Calculations & Programs for Power System Networks</u>, Prentice-Hall Inc., New Jersey, 1986, pp.14-27.
- [29] Abe, S., Hamada, N., Isono, A., Okuda, K., "Load Flow Convergence in the Vicinity of a Voltage Stability Limit", IEEE Transactions on Power Apparatus and Systems, Vol. PAS-97, No. 6, November/December 1978, pp.1983-1993.
- [30] Jeger, M., Eckmann, B., <u>Vector Geometry and Linear Algebra for Engineers</u> and Scientists, John Wiley & Sons Ltd., England, 1967.
- [31] Olmsted, J.M.H., Solid Analytical Geometry, D. Appleton-Century Co. Inc., U.S.A., 1947.
- [32] Love, C.E., Analytical Geometry, The Mcmillan Co., New York, 1926.
- [33] Rachtschaffen, E.E.M., "Algebraic Properties of Bus and Line Power Equations with Applications in Network Planning and Analysis", **Proceedings** of the Sixth Power System Computation Conference, August 1978, pp.184-187.
- [34] Ilic, M., "Network Theoretic Conditions for Existence and Uniqueness of Steady State Solutions to Electric Power Circuits", Proceedings of the IEEE International Symposium on Circuits and Systems, May 1992, pp.2821-2828.
- [35] Stott, B., "Review of Load Flow Calculation Methods", **Proceedings of IEEE**, Vol. 62, No. 7, July 1974, pp.916-929.
- [36] Elgerd, O., Electric Energy Systems Theory: An Introduction, McGraw Hill Inc., Singapore, 1983, p.242.

- [37] Dunstan, J.B., "Digital Load Flow Studies", AIEE Transactions, Part 3A, Vol. 73, 1954, pp.825-831.
- [38] Ward, J.B., Hale, H.W., "Digital Computer Solution of Power Flow Problem", AIEE Transactions on Power Apparatus Systems, Vol. 75, June 1956, pp.398-404.
- [39] Brameller A., Denmead, J.K., "Some Improved Methods of Digital Network Analysis", Proceedings of IEE, Part A, Vol. 109, 1962, pp.109-116.
- [40] Van Ness, J.E., "Iteration Method for Digital Load Flow Studies", AIEE Transactions on Power Apparatus Systems, Vol. 80, August 1959, pp.583-588.
- [41] Tinney, W.F., Walker, J.W., "Direct Solutions of Sparse Network Equations by Optimally Ordered Triangular Factorisation", Proceedings of IEE, Vol. 55, November 1967, pp.1801-1809.
- [42] Sasson, A.M., "Nonlinear Programming Solutions for the Load-Flow, Minimum-Loss, and Economic Dispatching Problems", IEEE Transactions on Power Apparatus Systems, Vol. 88, April 1969, pp.399-409.
- [43] Stott B., Alsac, O., "Fast Decoupled Load Flow", IEEE Transactions on Power Apparatus Systems, Vol. 93, May/June 1974, pp.859-867.
- [44] Sauer, P., "Explicit Load Flow Series and Function", IEEE Transactions on Power Apparatus and Systems, Vol. PAS-100, No. 8, August 1981, pp.3754-3761.

- [45] Rajicic, D., Bose, A., "A Modification to the Fast Decoupled Power Flow for Networks with High R/X Ratios", IEEE Transactions on Power Apparatus Systems, Vol. 3, No. 2, May 1988, pp.743-747.
- [46] Haley, P.H., Ayres, M., "Super Decoupled Loadflow with Distributed Slack Bus", IEEE Transactions on Power Apparatus and Systems, Vol. PAS-104, No. 1, January 1985, pp.104-113.
- [47] Behnam-Guilani, K., "Fast Decoupled Load Flow: The Hybrid Model", IEEE Transactions on Power Apparatus Systems, Vol. 3, No. 2, May 1988, pp.734-742.
- [48] Chang, S., Brandwajn, V., "Adjusted Solutions in Fast Decoupled Load Flow".

 IEEE Transactions on Power Apparatus and Systems, Vol. 3, No. 2, May 1988, pp.726-733.
- [49] Bacher, R., Tinney, W.F., "Faster Local Power Flow Solutions: The Zero Mismatch Approach", IEEE Transactions on Power Systems, Vol. 4, No. 4, October 1989, pp.1345-1354.
- [50] Wu, F.F., "Theoretical Study of the Fast Decoupled Load Flow", IEEE Transactions on Power Apparatus Systems, Vol. PAS-96, January/February 1977, pp.268-275.
- [51] Nagendra Rao, P.S., Praska Rao., K.S., Nanda, J., "An Empirical Criterion for the Convergence of the Fast Decoupled Load Flow Method", IEEE Transactions on Power Apparatus and Systems, Vol PAS-103, No. 5, May 1984, pp.974-987.

- [52] Sachdev, M.S., Medicherla K.P.T., "A Second Order Load Flow Technique", IEEE Transactions on Power Apparatus Systems, Vol. PAS-96, No. 1, January/February 1977, pp.189-197.
- [53] Iwamoto, S., Tamura, Y., "A Fast Load Flow Method Retaining Nonlinearity", IEEE Transactions on Power Apparatus and Systems, Vol. PAS-97, No. 5, September/October 1978, pp.1586-1599.
- [54] El-Hawary, M.E., Wellon, O.K., "The Alpha-Modified Quasi-Second Order Newton Raphson Method for Load Flow Solutions in Rectangular Form", IEEE Transactions on Power Apapratus Systems, Vol. PAS-101, No. 4, April 1982, pp.854-866.
- [55] Nagendra Rao, P.S., Praska Rao, K.S., Nanda, J., "An Exact Fast Load Flow Method Including Second Order Terms in Rectangular Coordinates", IEEE Transactions on Power Apparatus Systems, Vol. PAS-101, No. 9, 1982, pp.3261-3268.
- [56] Fan, L., "Solution of the Ill-Conditioned Load Flow Problem by the Tensor Method", Master's Thesis, Department of Electrical Engineering, McGill University, Montreal, Canada, June 1989.
- [57] Semlyen, A., "Calculation of the Extreme Loading Condition of a Power System for the Assessment of Voltage Stability", IEEE Transactions on Power Systems, Vol. 6, No. 1, February 1991, pp.307-315.
- [58] Kataoka, Y., "An Approach for the Regularisation of a Power Flow Solution around the Maximum Loading Point", IEEE Transactions on Power Systems,

- Vol. 7, No. 3, August 1992, pp.1068-1077.
- [59] Iba, K., Suziki, H., Egawa, M., Watanabe, T., "Calculation of Critical Loading Condition with Nose Curve Using Homotopy Continuation Method", IEEE Transactions on Power Systems, Vol. 6, May 1991, pp.584-589.
- [60] Venkatasubramanian, V., Schattler, H., Zaborsky, J., "A Stability Theory of Diferential Algebraic Systems Such as the Power System", Proceedings of the IEEE International Symposium on Circuits and Systems, May 1992, pp.2517-2520.
- [61] Dobson, I., Lu, L., "New Methods for Computing a Closest Saddle Node Bifurcation and Worst Case Load Power Margin for Voltage Collapse", IEEE Transactions on Power Systems, Vol. 8, No. 3, August 1993, pp.905-913.
- [62] Gottfried, B.G., Weissman, J., <u>Introduction to Optimisation Theory</u>, Prentice-Hall, Englewood Cliffs, N.J., 1973.
- [63] Wilkinson, J.H., <u>The Algebraic Eigenvalue Problem</u>, Clarendon Press, Oxford, 1964.
- [64] Crow, M.L., Lesieutre, B.C., "Voltage Collapse: An Enginering Challenge", IEEE Potentials, April 1994, p.18.
- [65] Banakar, M.H., "Analysis and Characterization of General Security Regions in Power Networks", Ph.D. Thesis, Department of Electrical Engineering, McGill University, Montreal, Canada, September 1980.

APPENDIX A

REVIEW OF LOAD FLOW CALCULATION METHODS

A.1 Introductory Remarks

The complexity of the load flow problem may be assessed by the fact that after more than three decades of research, new results are still being presented. One of the result of the tremendous amount of work that has been done in this area is that the numerical tools for solving this problem have been very well developed and documented [2]. The main considerations in the development of the numerical techniques have been improving the rate of convergence, robustness of the algorithm, storage requirements and computing time.

A.2 Numerical Methods for Load Flow Calculation

Load flow calculations were done by analog simulation techniques [36] until the advent of digital computers in the 1950's [37,38]. This provided the motivation for developing iterative numerical techniques and fuelled indepth research into all aspects of the load flow problem.

The first digital methods were based on the Y-matrix approach and the Gauss-Siedel algorithm is a typical example. Its main feature is a low storage requirement due to the sparsity of the admittance matrix. However, it is not very robust and the number of iterations required for convergence increases with network size. The convergence problems of the Y-matrix approach gave way to the Z-matrix

methods [39]. These methods have better convergence properties but require a large amount of memory because the impedance matrix is full.

The draw-backs of these early iterative techniques led to the implementation of the Newton-Raphson method [40]. This method is based on the solution of simultaneous non-linear equations and exhibits quadratic convergence. The number of iterations is almost independent of the size of the network but the iteration time is longer than that of the Gauss-Seidel algorithm. This is due to the fact that the jacobian matrix has to be inverted. The introduction of optimally ordered sparsity programming [41] made this task more efficient and the Newton-Raphson method has now become the method of choice in the power industry.

The load flow equations may be expressed in either polar or rectangular co-ordinates for use in the Newton-Raphson algorithm and the convergence characteristics are different for each of the two forms. In reference [29], Abe et al showed that the region of convergence of the rectangular form is larger but less stable than that of the polar form. The rectangular version also requires more storage.

There are other variations of the iterative load flow technique. One of them formulates the problem as a nonlinear optimisation scheme with the square of the power mismatches as the objective function [42]. Another approach solves for the voltage variables as an explicit power series of the specified injections [44]. This latter method utilises the rectangular form of the load flow equations.

There has been considerable modification of the original Newton-Rapson algorithm and some variations was due, in part, to the analytical work that was done on the load flow problem.

Most notable of these improvements was the development of the fast decoupled load flow method by Stott [43]. It neglects the weak coupling between the real power and the voltage magnitude as well as between the reactive power and the voltage angle. This method is fast, relatively simple and requires considerably less memory than the full Newton-Raphson method. It is used extensively in steady state security analysis where speed is one of the most essential considerations.

The fast decoupled load flow is not as reliable as the full Newton-Raphson because some of the simplifying assumptions made in developing the model do not always hold true. In particular, it is prone to failure when used on systems in which the ratio of line resistance to reactance is large. There have been some proposals to overcome this difficulty [45,46]. One such scheme introduces a fictitious node in the middle of the offending line while another uses the concept of the distributed slack bus. There have also been some variations to improve the performance of the basic algorithm [47-49]. The theoretical foundation for analysing the performance of the method is provided in [50] and expanded in [51].

The Newton-Raphson algorithm utilises a linearised version of the load flow equation. A more accurate model including a second-order term has been employed in load flow calculations [20]. In fact, the load flow equations in rectangular form may be expressed exactly by the sum of the first three terms of the Taylor series [21-23]. The objective is to improve convergence and reduce computation time.

The second-order model has also been used to solve the ill-conditioned load flow when the jacobian matrix is close to singularity [55,56]. Other recent approaches to overcome the problems associated with the jacobian singularity include using a different load model [57,58] and homotopy methods [59].

Appendix A

The numerical load flow is an indispensable tool in the planning and operation of power systems. Nonetheless, there are problems associated with it that are inherent to all numerical procedures and it should be complemented by other analytical approaches to the load flow.

APPENDIX B

DERIVATION OF THE EIGENVALUES AND EIGENVECTORS OF THE J_i MATRICES

B.1 Introductory Remarks

The J_i matrices describing the power injections are symmetric and very sparse - containing only two non-zero rows and columns. This allows their eigenvalues and eigenvectors to be determined explicitly. The dimensions of the matrices may be either 2N x 2N or (2N-1) x (2N-1) where N is the number of buses in the system.

B.2 The 2N x 2N Matrix

Any linear combination of real power injections can be written as

$$\sum_{i=1}^{N} \gamma_i P_i = \gamma^T P = X_r^T J_{\gamma^T P} X_r$$
 (B.1)

where

$$J_{\gamma^{T_p}} = \frac{1}{2} \begin{bmatrix} diag(\gamma) G + Gdiag(\gamma) & -diag(\gamma) B + Bdiag(\gamma) \\ diag(\gamma) B - Bdiag(\gamma) & diag(\gamma) G + Gdiag(\gamma) \end{bmatrix}$$

 γ is an arbitrary N x 1 vector, **P** is an N x 1 vector of real power injections, \mathbf{x}_r is the 2N x 1 vector $[\mathbf{e}^T \mathbf{f}^T]$ and \mathbf{e} and \mathbf{f} are the real and imaginary parts respectively, of the complex voltage. G and B are the real and imaginary parts of the bus admittance matrix.

If γ consists of zeroes everywhere except for a one in the ith position, this particular vector will be denoted by α . Then, $\alpha^T P$ is equal to P_i and $\operatorname{diag}(\alpha)G$ is equal to αg^T where g is the ith column of the matrix G. Similarly, $\operatorname{diag}(\alpha)B$ is equal to αb^T where b is the ith column of the matrix B. Therefore J_{P_i} can be written as

$$J_{\alpha^{T_{P}}} = \frac{1}{2} \begin{bmatrix} \alpha g^{T} + g \alpha^{T} & -\alpha b^{T} + b \alpha^{T} \\ \alpha b^{T} - b \alpha^{T} & \alpha g^{T} + g \alpha^{T} \end{bmatrix}$$
(B.2)

The search for the eigenvalues and eigenvectors of J_{Pi} requires the solution of

$$J_{\alpha r_P} x_r = \lambda x_r \tag{B.3}$$

or

$$\frac{1}{2} \begin{bmatrix} \alpha g^T + g \alpha^T & -\alpha b^T + b \alpha^T \\ \alpha b^T - b \alpha^T & \alpha g^T + g \alpha^T \end{bmatrix} \begin{bmatrix} e \\ f \end{bmatrix} = \lambda \begin{bmatrix} e \\ f \end{bmatrix}$$
(B.4)

Simplifying (B.4) results in

$$\frac{1}{2} \begin{bmatrix} \alpha (g^T e - b^T f) + g \alpha^T e + b \alpha^T f \\ \alpha (b^T e + g^T f) + g \alpha^T f - b \alpha^T e \end{bmatrix} = \lambda \begin{bmatrix} e \\ f \end{bmatrix}$$
 (B.5)

Both sides of equation (B.5) are pre-multiplied by $[\alpha^T \ 0^T]$ where 0 is an N x 1 vector of zeros to give

$$\frac{1}{2}\left[\alpha^{T}\alpha\left(g^{T}e-bf\right)+\alpha^{T}g\alpha^{T}e+\alpha^{T}b\alpha^{T}f\right] = \lambda\alpha^{T}e$$
 (B.6)

Since $\alpha^T \alpha = 1$, (B.6) may be simplified to

Appendix B

$$(g^T e - b^T f) + (\alpha^T g - 2\lambda) \alpha^T e + \alpha^T b \alpha^T f = 0$$
(B.7)

Also pre-multiplying (B.5) by $[0^T \alpha]$ results in

$$\frac{1}{2} \left[\alpha^T \alpha (b^T e + g^T f) + \alpha^T g \alpha^T f - \alpha^T b \alpha^T e \right] = \lambda \alpha^T f$$
 (B.8)

Equation (B.8) may be simplified to produce the following result

$$(b^T e + g^T f) + (\alpha^T g - 2\lambda) \alpha^T f - \alpha^T b \alpha^T e = 0$$
(B.9)

Pre-multiplying (B.5) by [g^T -b^T] results in

$$\frac{1}{2}[g^{T}\alpha(g^{T}e-b^{T}f)+g^{T}g\alpha^{T}e+g^{T}b\alpha^{T}f-b^{T}\alpha(b^{T}e+g^{T}f)-b^{T}g\alpha^{T}f+b^{T}b\alpha^{T}e]=\lambda(g^{T}e-b^{T}f)$$
(B.10)

Re-arranging and simplifying (B.10) gives

$$(g^{T}\alpha - 2\lambda)(g^{T}e - b^{T}f) + (g^{T}g + b^{T}b)\alpha^{T}e - (b^{T}\alpha(b^{T}e + g^{T}f) = 0$$
(B.11)

Pre-multiply (B.5) by [b^T g^T] to get the following

$$\frac{1}{2}\left[b^T\alpha(g^Te-b^Tf)+b^Tg\alpha^Te+b^Tb\alpha^Tf+g^T\alpha(b^Te+g^Tf)+g^Tg\alpha^Tf-g^Tb\alpha^Te\right]=\lambda\left(b^Te+g^Tf\right) \tag{B.12}$$

Again, simplifying (B.12) gives

$$b^{T}\alpha(g^{T}e - b^{T}f) + (b^{T}b + g^{T}g)\alpha^{T}f + (g^{T}\alpha - \lambda)(b^{T}\alpha + g^{T}f) = 0$$
 (B.13)

Equations (B.7), (B.9), (B.11) and (B.13) can be put in matrix form as follows

$$\begin{bmatrix} (\alpha^{T}g - 2\lambda) & \alpha^{T}b & 1 & 0 \\ -\alpha^{T}b & (\alpha^{T}g - 2\lambda) & 0 & 1 \\ (g^{T}g + b^{T}b) & 0 & (g^{T}\alpha - 2\lambda) & -b^{T}\alpha \\ 0 & (g^{T}g + b^{T}b) & b^{T}\alpha & (g^{T}\alpha - 2\lambda) \end{bmatrix} \begin{bmatrix} \alpha^{T}e \\ \alpha^{T}f \\ g^{T}e - b^{T}f \\ b^{T}e + g^{T}f \end{bmatrix} = \begin{bmatrix} 0 \\ 0 \\ 0 \\ 0 \end{bmatrix}$$
(B.14)

The following expression can be derived from the first two equations of (B.14)

$$\begin{bmatrix} g^T e - b^T f \\ b^T e + g^T f \end{bmatrix} = - \begin{bmatrix} (\alpha^T g - 2\lambda) & \alpha^T b \\ -\alpha^T b & (\alpha^T g - 2\lambda) \end{bmatrix} \begin{bmatrix} \alpha^T e \\ \alpha^T f \end{bmatrix}$$
(B.15)

Substituting the right-hand side of (B.15) into the third and fourth equations of (B.14) produces the following

$$(g^{T}g + b^{T}b)\begin{bmatrix} \alpha^{T}e \\ \alpha^{T}f \end{bmatrix} + \begin{bmatrix} (g^{T}\alpha - 2\lambda) & -b^{T}\alpha \\ b^{T}\alpha & (g^{T}\alpha - 2\lambda) \end{bmatrix} \left(-\begin{bmatrix} (\alpha^{T}g - 2\lambda) & \alpha^{T}b \\ -\alpha^{T}b & (\alpha^{T}g - 2\lambda) \end{bmatrix} \begin{bmatrix} \alpha^{T}e \\ \alpha^{T}f \end{bmatrix} \right) = \begin{bmatrix} 0 \\ 0 \end{bmatrix}$$
 (B.16)

Simplifying (B.16) results in

$$\begin{bmatrix} (g^T g + b^T b)I - \begin{bmatrix} (g^T \alpha - 2\lambda)^2 + (\alpha^T b)^2 & 0 \\ 0 & (g^T \alpha - 2 - \lambda)^2 + (\alpha^T b)^2 \end{bmatrix} \end{bmatrix} \begin{bmatrix} \alpha^T e \\ \alpha^T f \end{bmatrix} = \begin{bmatrix} 0 \\ 0 \end{bmatrix}$$
(B.17)

and "I" in (B.17) is the 2 x 2 identity matrix. Finally, the determinant of equation (B.17) can be set to zero and the resulting equation

$$g^Tg + b^Tb - (g^T\alpha - 2\lambda)^2 - (\alpha^Tb)^2 = 0$$
 (B.18)

solved for λ . The roots are repeated. Each pair of the repeated roots is equal to

$$\lambda = \frac{g^T \alpha \pm \sqrt{-(\alpha^T b)^2 + (g^T g + b^T b)}}{2}$$
 (B.19)

From (B.18), it is evident that all the elements of the matrix in (B.17) must be equal to zero. This means that $\alpha^T e$ and $\alpha^T f$ are completely arbitrary. This fact can be used in (B.5) to derive the eigenvectors of the matrix defining the real power injections. Note that $\alpha^T e$ and $\alpha^T f$ represent the real and imaginary components, respectively of the voltage at the bus under consideration. Choosing $[\alpha^T e \alpha^T f]$ equal to [1 0] for the first pair of eigenvalues and [0 1] for the second pair and substituting them in (B.5) gives two eigenvectors for each pair of the non-zero eigenvalues. The general expressions are

$$v = \begin{bmatrix} g + (2\lambda - \alpha^T g)\alpha \\ -b + (\alpha^T b)\alpha \end{bmatrix}$$
 (B.20)

for the first pair λ_1 , λ_2 and

$$v = \begin{bmatrix} b - (\alpha^T b) \alpha \\ g + (2\lambda - \alpha^T g) \alpha \end{bmatrix}$$
 (B.21)

for the second pair λ_1 , λ_2 . It can be easily verified that the four vectors are mutually orthogonal.

The eigenvalues and vectors of the J_i matrix describing the reactive power can be derived following the same procedure. This amounts to replacing g and g in the expressions for the real power with g and g respectively.

B.2 The $(2N-1) \times (2N-1)$ Matrix

In most load flow studies, the reference angle is set to zero. This can be done without loss of generality. In this case, the dimension of the J_i matrix may be reduced to (2N-1) x (2N-1) by deleting the (N+s)th row and column from the 2N x 2N matrix. The reference bus is taken to be bus s. Recall that the slack bus is also assumed to be the reference bus. The eigenvalues and eigenvectors of this smaller matrix are now derived.

Once again, assuming that α consists of zeroes everywhere except a one in the ith position, the J_i matrix describing the real power injection now becomes

$$J_{\alpha^{T_p}} = \frac{1}{2} \begin{bmatrix} \alpha g^T + g \alpha^T & (b \alpha^T - \alpha b^T) - ((b \alpha^T - \alpha b^T)\beta)b^T \\ (\alpha b^T - b \alpha^T) - \beta(\beta^T (\alpha b^T - b \alpha^T)) & (\alpha g^T + g \alpha^T) - ((\alpha g^T + g \alpha^T)\beta)\beta^T - \beta(\beta^T (\alpha g^T + g \alpha^T)) \end{bmatrix}$$
(B.22)

where β is N x 1 vector containing zeros everywhere except a "1" at the sth position and bus s is the slack bus.

The system of equations to be solved is again

$$J_{a^{T}P}x = \lambda x \tag{B.23}$$

Using the fact that $\boldsymbol{\beta}^T \mathbf{f}$ is equal to zero since \mathbf{f}_s is equal to zero and also that $\boldsymbol{\alpha}^T \boldsymbol{\beta}$ is equal to zero since power injections are specified for buses other than the slack bus, equation (B.23) may be written as

$$\frac{1}{2} \begin{bmatrix} \alpha (g^T e - b^T f) + g \alpha^T e + \alpha^T f \\ \alpha (b^T e + g^T f) - b \alpha^T e + g \alpha^T f + \beta (\beta^T b \alpha^T e - \beta^T g \alpha^T f) \end{bmatrix} = \lambda \begin{bmatrix} e \\ f \end{bmatrix}$$
(B.24)

Pre-multiplying (B.24) by $[\alpha^T \ 0^T]$, the following expression is obtained

$$g^{T}e - b^{T}f + (\alpha^{T}g - 2\lambda)\alpha^{T}e + \alpha^{T}b\alpha^{T}f = 0$$
 (B.25)

Pre-multiplying (B.24) by $[0^T \ \alpha^T]$ and simplifying gives

$$b^T e + g^T f - (\alpha^T g - 2\lambda)\alpha^T f - \alpha^T b \alpha^T e = 0$$
 (B.26)

Again, pre-multiplying (B.24) by [g^T -b^T] and simplifying results in

$$(g^{T}a-2\lambda)(g^{T}e-b^{T}f)-b^{T}a(b^{T}e+g^{T}f)+(g^{T}g+b^{T}b-(b^{T}\beta)^{2})a^{T}e+(b^{T}\beta g^{T}\beta)a^{T}f=0$$
(B.27)

Pre-multiplying (B.24) by [b^T g^T] and simplifying gives

$$b^{T}\alpha(g^{T}e - b^{T}f) + (g^{T}\alpha - 2\lambda)(b^{T}e + g^{T}f) + (g^{T}\beta b^{T}\beta)\alpha^{T}e + (b^{T}b + g^{T}g - (\beta^{T}g)^{2})\alpha^{T}f = 0$$
(B.28)

Equations (B.25) - (B.28) can be put into matrix form as follows

$$\begin{bmatrix} (\alpha^{T}g-2\lambda) & \alpha^{T}b & 1 & 0 \\ -\alpha^{T}b & (\alpha^{T}g-2\lambda) & 0 & 1 \\ g^{T}g+b^{T}b-(\beta^{T}b)^{2} & \beta^{T}b\beta^{T}g & (\alpha^{T}g-2\lambda) & -\alpha^{T}b \\ \beta^{T}b\beta^{T}g & b^{T}b+g^{T}g-(\beta^{T}g)^{2} & \alpha^{T}b & (\alpha^{T}g-2\lambda) \end{bmatrix} \begin{bmatrix} \alpha^{T}e \\ \alpha^{T}f \\ g^{T}e-b^{T}f \\ b^{T}e+g^{T}f \end{bmatrix} = \begin{bmatrix} 0 \\ 0 \\ 0 \\ 0 \end{bmatrix}$$
(B.29)

The first two equations in (B.29) are identical to those in (B.14). Again, they are used to find the expression given in (B.15). This expression is substituted into the last two equations of (B.29) to get

$$\begin{bmatrix} g^{T}g + b^{T}b - (\beta^{T}b)^{2} - (\alpha^{T}b)^{2} - (\alpha^{T}g - 2\lambda)^{2}) & \beta^{T}g\beta^{T}b \\ \beta^{T}g\beta^{T}b & g^{T}g + b^{T}b - (\beta^{T}g)^{2} - (\alpha^{T}b)^{2} - (\alpha^{T}g - 2\lambda)^{2} \end{bmatrix} \begin{bmatrix} \alpha^{T}e \\ \alpha^{T}f \end{bmatrix} = \begin{bmatrix} 0 \\ 0 \end{bmatrix}$$
 (B.30)

Finally, the determinant of the matrix in (B.30) can be set to zero to solve for the eigenvalues. There are two pairs, one of which is identical to the expression in (B.19). The other pair is given by

$$\lambda = \frac{\varepsilon^{T_{\alpha}} \pm \sqrt{\varepsilon^{T} g + b^{T} b - (\alpha^{T} b)^{2} - (\beta^{T} g)^{2} - (\beta^{T} b)^{2}}}{2}$$
(B.31)

In this case, $\alpha^T e$ and $\alpha^T f$ are no longer arbitrary. For the pair of eigenvalues in (B.19), the relationship between them is

$$\alpha^T e = \frac{\beta^T g}{\beta^T b} \alpha^T f \tag{B.32}$$

Choosing $\alpha^T f$ equal to "1" and substituting (B.32) in (B.24), the following expression is obtained for the eigenvector corresponding to those eigenvalues

$$v = \begin{bmatrix} (2\lambda - \alpha^{T}g + \alpha^{T} \left(\frac{\beta^{T}g}{\beta^{T}b}\right)b)\alpha + g - \left(\frac{\beta^{T}g}{\beta^{T}b}\right)b \\ (\alpha^{T}b + \alpha^{T} \left(\frac{\beta^{T}g}{\beta^{T}b}\right)g - 2\lambda \left(\frac{\beta^{T}g}{\beta^{T}b}\right)\alpha - b - \left(\frac{\beta^{T}g}{\beta^{T}b}\right)g \end{bmatrix}$$
(B.33)

For the eigenvalues in (B.31), the relationship between $\alpha^{T}e$ and $\alpha^{T}f$ is

$$\alpha^T f = -\left(\frac{\beta^T g}{\beta^T b}\right) \alpha^T e \tag{B.34}$$

The eigenvector corresponding to these eigenvalues is

$$v = \begin{bmatrix} -(\alpha^{T}b + \alpha^{T} \left(\frac{\beta^{T}g}{\beta^{T}b}\right)g - 2\lambda \left(\frac{\beta^{T}g}{\beta^{T}b}\right)\alpha + b + \left(\frac{\beta^{T}g}{\beta^{T}b}\right)g \\ (2\lambda - \alpha^{T}g + \alpha^{T} \left(\frac{\beta^{T}g}{\beta^{T}b}\right)b)\alpha + g - \left(\frac{\beta^{T}g}{\beta^{T}b}\right)b \end{bmatrix}$$
(B.35)

As in the first instance, the eigenvalues and eigenvectors of the J_i matrix describing the reactive power injection may be obtained from those of the real power injections by replacing g and b in the expressions for the real power with -b and g, respectively. The derivation is identical.

Appendix B

These expressions were checked against the Matlab function used to obtain the eigenvalues and eigenvectors of a matrix. The derived eigenvalues were identical for both the $2N \times 2N$ and the $(2N-1) \times (2N-1)$ matrices were identical to those found by the Matlab routine. The eigenvectors with only one arbitrary component (smaller matrix) were also the same.

APPENDIX C

EXAMPLES OF THE (2N-1) X (2N-1) MATRICES DESCRIBING SPECIFIED INJECTIONS

Some examples of the symmetric matrices describing the specified injections of an arbitrary 3-bus system are now presented.

With N being the number of buses in the system, the 2N x 2N matrices (J_{Pi}) describing the real power injections are:

$$J_{P_{1}} = \begin{bmatrix} 2G_{11} & G_{21} & G_{31} & 0 & -B_{21} & -B_{31} \\ G_{21} & 0 & 0 & B_{21} & 0 & 0 \\ G_{31} & 0 & 0 & -B_{31} & 0 & 0 \\ 0 & B_{21} & B_{31} & 2G_{11} & G_{21} & G_{31} \\ -B_{21} & 0 & 0 & G_{21} & 0 & 0 \\ -B_{31} & 0 & 0 & G_{31} & 0 & 0 \end{bmatrix}$$
(C.1)

and

$$J_{P_2} = \begin{bmatrix} 0 & G_{21} & 0 & 0 & -B_{21} & 0 \\ G_{21} & 2G_{22} & G_{23} & -B_{21} & 0 & -B_{23} \\ 0 & G_{23} & 0 & 0 & B_{23} & 0 \\ 0 & -B_{21} & 0 & 0 & G_{21} & 0 \\ B_{21} & 0 & B_{23} & G_{21} & G_{22} & G_{23} \\ 0 & -B_{23} & 0 & 0 & G_{23} & 0 \end{bmatrix}$$
(C.2)

and

Appendix C

$$J_{P_3} = \begin{bmatrix} 0 & 0 & G_{31} & 0 & 0 & B_{31} \\ 0 & 0 & G_{23} & 0 & 0 & B_{32} \\ G_{31} & G_{32} & 2G_{33} & -B_{31} & -B_{32} & 0 \\ 0 & 0 & -B_{31} & 0 & 0 & G_{31} \\ 0 & 0 & -B_{32} & 0 & 0 & G_{23} \\ B_{31} & B_{32} & 0 & G_{31} & G_{32} & 2G_{33} \end{bmatrix}$$
(C.3)

If bus s is chosen as the reference bus, the (2N-1) x (2N-1) matrix may be obtained from the 2N x 2N matrix by deleting the (N+s)th row and column of the matrix Js_i which is defined as

$$Js_{i} = (M^{-1})^{T} Js_{i} M^{-1}$$
 (C.4)

For a 3-bus system with bus 1 as the reference bus and the reference angle equal to δ_s , the matrix M is given by

$$M = \begin{bmatrix} 1 & 0 & 0 & 0 & 0 & 0 \\ 0 & 1 & 0 & 0 & 0 & 0 \\ 0 & 0 & 1 & 0 & 0 & 0 \\ \tan \delta_s & 0 & 0 & -1 & 0 & 0 \\ 0 & 0 & 0 & 0 & 1 & 0 \\ 0 & 0 & 0 & 0 & 0 & 0 \end{bmatrix}$$
(C.5)

The inverse of the matrix M is equal to M so for P_2 , Js_i as defined in equation (C.4) is

$$J_{S_{P_{2}}} = \begin{bmatrix} 0 & G_{21} - B_{21} \tan \delta_{s} & 0 & 0 & B_{21} + g_{21} \tan \delta_{s} & 0 \\ G_{12} - B_{21} \tan \delta_{s} & 2G_{22} & G_{23} & B_{21} & 0 & -B_{23} \\ 0 & G_{23} & 0 & 0 & B_{23} & 0 \\ 0 & B_{12} & 0 & 0 & -G_{21} & 0 \\ B_{21} + G_{21} \tan \delta_{s} & 0 & B_{23} - G_{21} & 2G_{22} & G_{23} \\ 0 & -B_{23} & 0 & 0 & G_{23} & 0 \end{bmatrix}$$
 (C.6)

Similarly, the matrix describing P₃ is

$$J_{S_{P_{2}}} = \begin{bmatrix} 0 & 0 & G_{31} - B_{31} \tan \delta_{s} & 0 & 0 & B_{31} + G_{31} \tan \delta_{s} \\ 0 & 0 & G_{32} & 0 & 0 & B_{32} \\ G_{31} - B_{31} \tan \delta_{s} & G_{32} & 2G_{33} & B_{31} & -B_{32} & 0 \\ 0 & 0 & B_{31} & 0 & 0 & -G_{31} \\ 0 & 0 & -B_{32} & 0 & 0 & G_{32} \\ B_{31} + G_{31} \tan \delta_{s} & B_{32} & 0 & G_{31} & G_{32} & 2G_{33} \end{bmatrix}$$
(C.7)

The (2N-1) x (2N-1) matrix is obtained by deleting the 4th row and column of Js_{Pi} . Note that only four elements of this matrix which are different from the original J_i matrix with its (N+s)th row and column deleted: the (s,i)th, (i,s)th and the (s,N+i)th and (N+i,s)th elements, where i is the bus at which the injection is specified. The matrix for the reactive power may be obtained by replacing G and B with -B and G respectively.